NATIONAL TECHNICAL UNIVERSITY OF ATHENS

SCHOOL OF ELECTRICAL AND COMPUTER ENGINEERING

DIVISION OF ELECTRIC POWER

System Identification and Validation of Aggregate Models of Renewable Resources

Diploma Thesis

of

KRYSTALLIDIS APOSTOLOS

Supervisors : Nikolaos Hatziargyriou, Proffesor in NTUA, Athens
Luigi Vanfretti, Associate Professor KTH, Sweden

Athens, October 2015

Abstract

The process of arriving to a dynamical model (difference or differential equations) from observed data is called System Identification and is of great importance in the area of control theory. The complexity of modern power systems, which is augmented by the increasing penetration of renewable resources along with the necessity to secure power system's reliability, has been a strong motivation for extensive research in control and system identification area in particular.

The objective of the thesis is two-fold: 1) provide an insight to different identification methods by presenting the mandatory related theoretical background and 2) apply them to synthetic time domain data derived from simulations using PSAT software in order to identify dynamic systems.

The first study is based on a 24-state space representation of Kundur power system and is an introductory and illustrative example for the better understanding of the identification techniques. ARX, ARMAX and ERA methods are applied, identified models are extracted while for validation purposes different input signals are introduced and finally a comparison between the eigenvalues of the identified and the original model is conducted.

The second test case corresponds to a wind farm model in a 14-bus system. After selecting the proper input-output signals for the identification, the three aforementioned methods are applied and the identified models are constructed. Validation with completely different wind speed time series present accurate estimates and Hankel Singular Value Decomposition (a mode truncating technique) is applied for the reduction of the model order and consequently, for the additional simplification of the system. As a final step for the assessment of the results, measurement noise is introduced to the output signals, the methods are applied and residual tests are conducted for every identification procedure.

Acknowledgements

First of all, I would like to express my deep gratitude to my supervisor Prof. Nikolaos Hatziargyriou for giving me the opportunity to undertake a part of my Thesis in Royal Institute of Technology and for all the assistance he willingly provided during my studies. I would also like to thank Prof. Luigi Vanfretti, for accepting me in KTH and in SmarTS lab in particular and for giving valuable orientation and advice during our cooperation. Furthermore, many thanks should be addressed to Rafael Segundo and Tetiana Bogodorova for their help and all the time they dedicated to me, as well.

Finally and more importantly, I would like to thank my family - my father, Konstantinos, my mother, Ioanna, my little sisters, Konstantina and Alkyoni, my grandmother, Evdoxia and my grandfather, Apostolos- for the inexhaustible love, support, encouragement and faith they keep showing in me.

Contents

Notation

PCC	Point of Common Coupling
PSAT	Power System Analysis Toolbox
GUI	Graphical User Interface
SVD	Singular Value Decomposition
HSVD	Hankel Singular Value Decomposition
MOR	Model Order Reduction
ARX	AutoRegressive with eXternal Input
ARMAX	AutoRegressive Moving Average with eXternal input
ERA	Eigensystem Realization Algorithm
WT	Wind Turbine
SSSA	Small Signal Stability Analysis
SISO	Single Input Single Output
MIMO	Multi Input Multi Output
PMU	Phasor Measurement Unit
PSS	Power System Stabilizer
SNR	Signal to Noise Ratio

List of Figures

1 Introduction

1.1 Problem Definition

Power systems continuously undergo changes especially due to the stochastic nature of the loads. Each change in load leads to an oscillatory response of the power system, a logical fact considering the dynamic nature of power generation systems. These responses of the system are observable in most of the measured variables like bus voltages, injected active and reactive powers, transmission line currents and in the frequencies as well [7],[15].

Besides the stochastic evolution of loads that affect the system operating conditions there is another factor which plays a significant role in modern power grid operating scenarios determination: the growing use of non-conventional and renewable energy technologies. Wind power as well as solar energy are always associated with a degree of uncertainty given that wind velocities and sunlight often present big variations. These variations can potentially cause disturbances between the load and generation balance which consequently may cause instabilities, rendering the system insecure and unreliable.

In order to maintain the balance between the electric power produced and the power consumed, modern control theory techniques are being applied. The modern control theory results require that the models of the processes in terms of state equations are available. The necessity of obtaining such models has led to the extensive research in the area of system identification theory.

The aim of this thesis is the identification of aggregate models of renewable resources and of wind farms in particular by applying different methods to time domain data obtained from measurements on various components of the power system. A detailed, high order model is not only not required but also not desirable given that it is impractical to be processed even by advance modern control tools. Consequently, the final goal of the thesis is the proper representation of the dynamic modes of the models under identification at the point of common coupling (PCC).

1.2 Objectives

In order to achieve the goal listed above, the following objectives were set:

- Perform a literature review.
- Learn the PSAT software for power system simulations.
- Perform illustrative example of system identification for a pre-known 24 state-space representation of a power system.
- Perform system identification of a wind farm as a part of a power system.
- Validate the results of the various identification processes.

1.3 Thesis Outline

The rest of this thesis is organized as follows. Chapter 2 is a brief description of the software tools that are used. Chapter 3 corresponds to a general introduction to dynamic systems and model identification theory while Chapter 4 provides valuable information regarding the mandatory background in systems theory for the understanding of the various system identification approaches. In Chapter 5 there is a detailed description of the methods used in the context of this thesis and in Chapter 6 wind turbine model and the components that compose it are presented. Identification and model validation of a 24 state-space system using ARX, ARMAX and ERA methods are performed in Chapter 7. Chapter 8 discusses the identification and validation of a wind farm model as a part of a 14 -bus test system. Finally conclusions, future work and the challenges that should be faced are provided in Chapter 9.

2 Software tools used

2.1 Introduction to MATLAB

MATLAB is a high-level language being used in a wide variety of domains, from natural sciences to all disciplines of engineering and beyond.

In this thesis, MATLAB is used for the processing of the results derived from PSAT simulations, for the realization of the identification methods, and finally for the validation of the efficiency of the proposed models.

2.2 Introduction to Power System Analysis Toolbox (PSAT)

Power System Analysis toolbox is a free software Matlab toolbox for electric power system analysis and control. It supports a variety of static and dynamic components in order to perform an accurate power system analysis and includes several features like power flow, continuation power flow, optimal flow, time domain simulation and small signal stability analysis [16].

All operations can be assessed by means of user-friendly Graphical User Interfaces (GUIs) which facilitate the application of PSAT's various features.

PSAT main window is shown in Fig. 2.1:

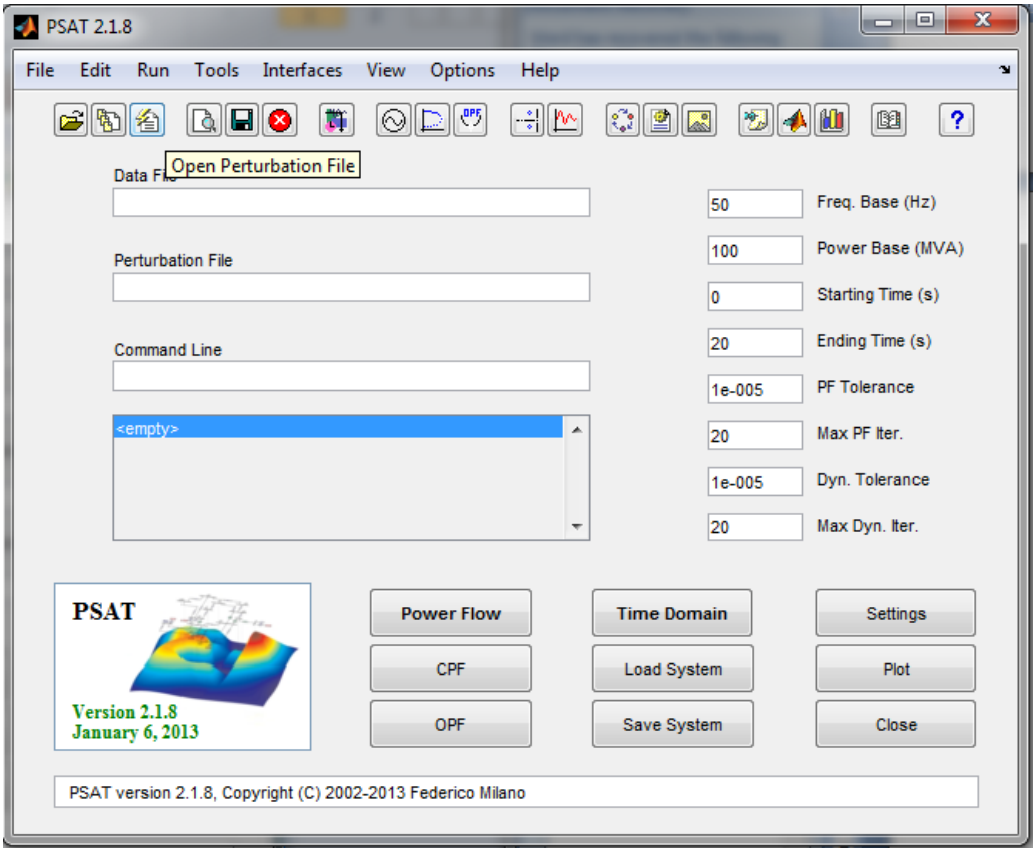

Figure 2.1: Main GUI of PSAT

Finally, PSAT provides a Simulink-based library in order to assist the user in designing the desirable networks.

3. Dynamic Systems

3.1 Introduction to Dynamic Systems

In loose terms a system is an object in which variables of different kinds interact and produce observable signals. The system is also affected by external stimuli, which can be either inputs or disturbances, or both. Inputs are the signals that can be manipulated by the observer whereas the others are the disturbances and can be divided into those that are directly measured and those that are only observed through their influence on the output.

Dynamic Systems are the systems whose current output value depends not only on the current external stimuli but also on their earlier values. Time series are the outputs of dynamical systems whose external stimuli are not observed [3].

A broad definition of a model of a system is the relationship among observed signals; in other words it is the concept of how system's variables relate and interact to each other.

For advanced systems we use models that describe the relationships among the system variables in terms of mathematical expressions such as difference or differential equations. These models are called mathematical or analytical models. Analytical models can be further categorized by a number of adjectives (time continuous or time discrete, deterministic or stochastic linear or nonlinear etc.) signifying the type of difference or differential equation used.

3.2 The System Identification Procedure

The goal of System Identification is a mathematical model of a dynamic system based on experimental data. The model should be compact and adequate with respect to the purpose it is to be used for. The construction of a model from data involves four basic entities:

1. A data set like the recorded inputs and outputs over a time interval:
   $$Z^N = \{\mathrm{u}(1), \mathrm{y}(1), \ldots, \mathrm{u}(\mathrm{N}), \mathrm{y}(\mathrm{N})\} \quad (3.1).$$
   The input-output data are sometimes recorded during a specifically designed identification experiment, where the user may determine which signals to measure and when. The main objective and at the same time a big challenge of the experiment design is to make the "right" choices so that the data become maximally informative.
2. A set of candidate models; a Model Structure. A set of candidate models is obtained by specifying within which collection of models we are going to look for a suitable one. There is no doubt that this step is the most important and the most difficult one. It is here that *a priori* knowledge, engineering intuition and insight play a significant role. Generally speaking, a model structure is a parameterized mapping from past inputs and outputs Z^{t-1} to the space of the model outputs:
   $$\hat{y}(t|\theta) = g(\theta, Z^{t-1}) \quad (3.2)$$
3. Here θ is the finite dimensional vector used to parameterize the mapping and $\hat{y}(t|\theta)$ is the calculated value based on the past data.

4. A rule by which candidate models can be assessed using the data. Determining the "best" model in the set, guided by the data. The assessment of model quality is based on how the models perform when they attempt to reproduce the measured data.
5. Model Validation. At this final step the model that has been chosen is going to be tested in order to conclude whether it is "good enough" or not, that is, whether it is valid for its purpose. Such tests are known as model validation and involve various procedures to assess how the model relates to observed data, to prior knowledge, and to its intended use. A model can never be accepted as a final and true description, thus it can at best be regarded as a good description of certain aspects that are of particular interest to us.

The system identification loop can be understood from the following figure, known as "The System Identification Loop":

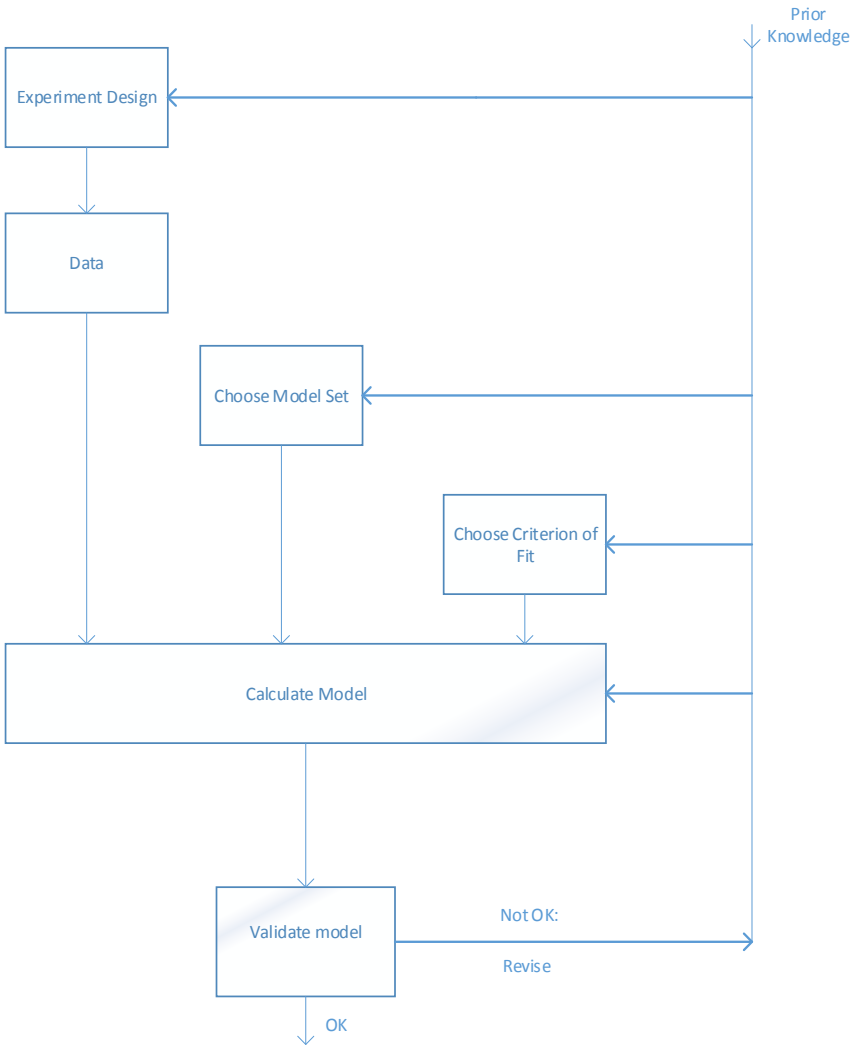

Figure 3.1: General system identification loop

3.3 Categories of Modal Identification Methods

The oscillatory dynamic response of a power system can be divided in two main categories: 1) transient (sometimes termed a ringdown); and 2) ambient. For the ambient case, the power system is excited by low-amplitude random variations typically assumed to be load variations. This leads to a system response that reveals the system dynamics. On the other hand, a sudden switching or a fault is the basic assumption for the transient case which typically is larger in amplitude than the ambient one. The resulting time-domain response is a multi-modal oscillation superimposed on the underlying ambient response. Both categories are shown in the following figures:

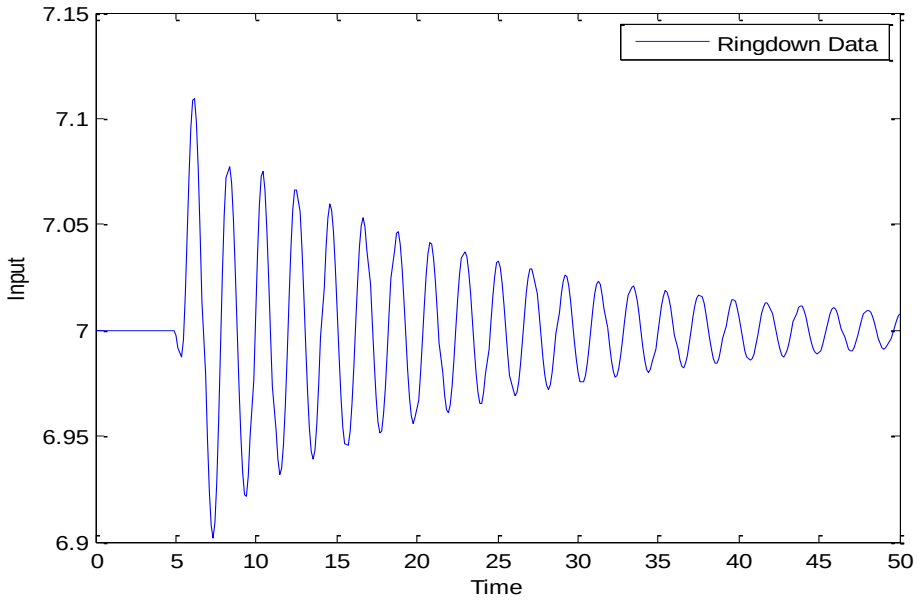

Figure 3.2: Transient reponse of a system

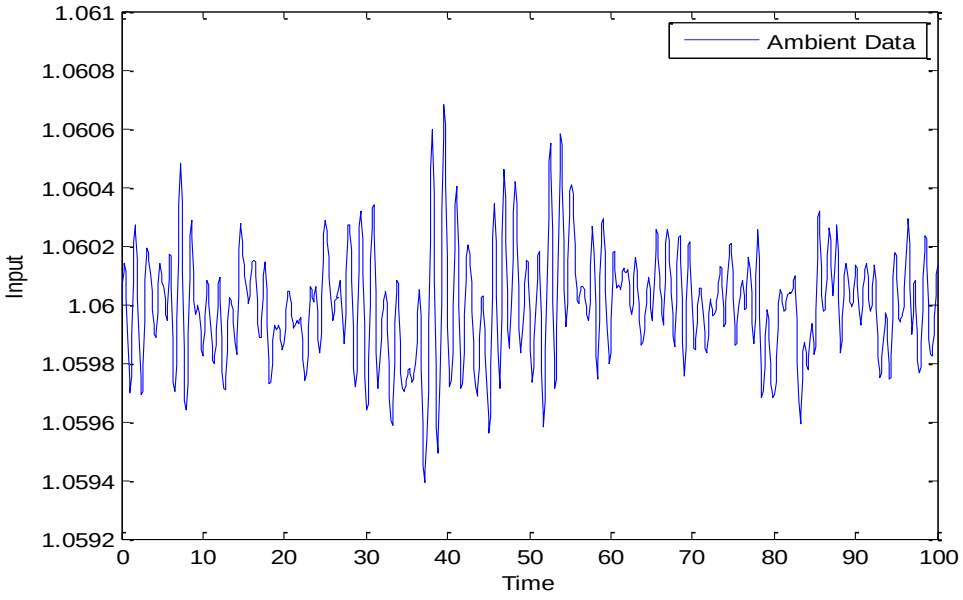

Figure 3.3: Ambient response of a system

In terms of application, we classify modal frequency and damping parameter estimation algorithms into two categories: 1) ringdown analyzers and 2) mode meters. A ringdown analysis tool operates solely on the ringdown portion of the response; typically the first several cycles of the oscillation (between 5 and 20 seconds). On the other hand, a mode meter can be applied in any portion of the response: ambient; transient or a combination of them. Finally, mode meters are automated tools that estimate modal properties continuously and without reference to any exogenous system input [14].

Generally, there is a variety of categories in which the analysis methods can be classified:

- Parametric or non-parametric depending on whether they are based on a basic model or on several assumptions, respectively.
- Time-domain or frequency-domain depending on whether they use time-domain or frequency-domain data.
- Block or Recursive processing algorithms techniques. The block processing algorithms generate modal estimates based on an entire data set. On the other hand, recursive algorithms computes modal estimates using adaptive strategies to ensure that the most accurate model is used for the most recent data.

4. Systems Theory Background

4.1 State-Space Representation

Consider the following linear system:

$$\left.\begin{aligned} \dot{x} &= Ax + Bu, \quad x(t_0) = x_0 \\ y &= Cx + Du \end{aligned}\right\} \quad (4.1)$$

where

- x is a vector of n elements (n is the order of the differential equation) and represents the internal state of the system.
- u is the input of the system.
- y is the output of the system.
- $\dot{x} = \frac{d}{dt}x(t)$ is the differentiation of x with respect to time.
- A is the state or system matrix with dimensions $n \times n$.
- B is the input matrix with dimensions $n \times p$.
- C is the output matrix with dimensions $n \times q$.
- D is the feedthrough or feedforward matrix with dimensions $q \times p$.

The corresponding form of the system (4.1) in discrete time is the following:

$$\begin{aligned} x(k+1) &= Ax(k) + Bu(k), \quad x(t_0) = x_0 \\ y(k) &= Cx(k) + Du(k) \end{aligned} \quad (4.2)$$

The forms (4.1) and (4.2) are called the general state-space representation of a linear system with p inputs, q outputs and n state variables.

The main goal of the modal analysis (the study of dynamic properties under vibration excitation) is to determine the eigenvalues of A. Transfer function identification must, in addition to the poles, determine also the zeros and gains along one or more response paths. More precisely, system's transfer function includes all the matrices in equation (4.1).

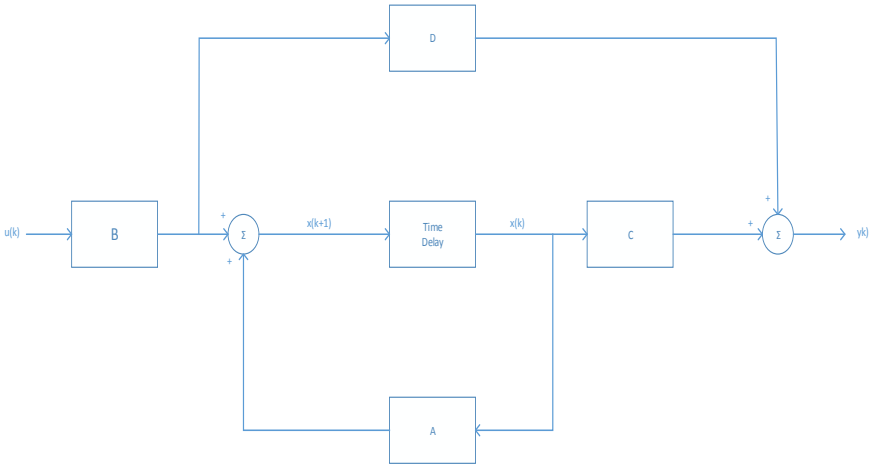

Figure 4.1: Discrete state-space representation block diagram

4.2 Transfer Function Representation

Contrary to the state space representation, which describes the complete internal behavior of the system as well as the input and the output properties, the transfer function representation is related only to the input-output behavior. A prerequisite for the transfer function to be defined is the knowledge of the state-space representation of the system.

Let a dynamic system be described in state-space as in eq. (4.1).

Taking the Laplace Transformation of the equation (4.1) with zero initial condition:

$$\left.\begin{aligned} X(s) &= AX(s) + BU(s) \\ Y(s) &= CX(s) + DU(s) \end{aligned}\right\} \quad (4.3)$$

The state equation can be placed in the form:

$$(sI - A)X(s) = BU(s) \quad (4.4)$$

and by pre-multiplying both sides by $(sI - A)^{-1}$:

$$X(s) = (sI - A)^{-1}BU(s) \quad (4.5)$$

In the output equation $X(s)$ can be substituted according to (4.5):

$$Y(s) = [C(sI - A)^{-1}B + D]U(s) \quad (4.6)$$

Finally, using (4.6), transfer function can be defined:

$$G(s) = \frac{Y(s)}{U(s)} = C(sI - A)^{-1}B + D \quad (4.7)$$

The poles of $G(s)$ are given by the eigenvalues of the state matrix A previously defined in section 4.1.

4.3 Eigenproperties of the state matrix

A power system typically comprises a large number of components that are described through differential-algebraic equations. Hence, just as every other dynamic system, the behavior of a power system can be described by a set of n first order nonlinear ordinary differential equations denominated as state equations, together with a set of algebraic equations, developed on the basis of the system model [11].

Even though power systems are highly nonlinear, they can be expressed in the linearized state space representation form around an initial operating point:

$$\left.\begin{aligned} \Delta\dot{x}(t) &= A\Delta x(t) + B\Delta u(t) \\ \Delta y(t) &= C\Delta x(t) + D\Delta u(t) \end{aligned}\right\} \quad (4.8)$$

Where the matrices A,B,C,D have been described in the equation (4.1)

The eigenvalues of the state matrix A determine the time domain response of the system and provide valuable information for the dynamic behavior of the system, such as information regarding the stability characteristics of the system:

- A real eigenvalue corresponds to a non-oscillatory mode. A negative real eigenvalue represents a decaying mode whereas a positive real eigenvalue represents aperiodic instability.
- Complex eigenvalues occur in conjugate pairs, and each pair corresponds to an oscillatory mode. The real component of the eigenvalues gives the damping and the imaginary component gives the frequency of oscillation. A negative real party corresponds to a damped oscillation whereas a positive real part represents oscillation of increasing amplitude. Thus, for a complex pair of eigenvalues:

  $$\lambda = \sigma \pm j\omega \quad (4.9)$$

  The frequency of oscillation in Hz is given by

  $$f = \frac{\omega}{2\pi} \quad (4.10)$$

  The natural frequency ω_n of the eigenvalue can be computed:

  $$\omega_n = |\lambda| = \sqrt{\sigma^2 + \omega^2} \quad (4.11)$$

  The damping ratio is given by:

  $$\zeta = -\frac{\sigma}{\sqrt{\sigma^2+\omega^2}} \quad (4.12)$$

  The damping ratio ζ determines the rate of decay of the amplitude of the oscillation.

4.4 Model Order Reduction Methods

4.4.1 Introduction to Model Order Reduction (MOR)

Although power systems are high order, the grid dynamic behavior can be described and understood by constructing suitable reduced order models. The Model Order Reduction (MOR) is an established field of study in linear control theory and its aim is to arrive at reduced models of system that retain selected aspects of the dynamic behavior [2]. The techniques that are used within the frameworks of this thesis are 1) the magnitude of the residues of the transfer function model, 2) the Singular Value Decomposition (SVD) and 3) the Hankel Singular Value Decomposition (HSVD).

4.4.2 Residues

As already stated, a physical problem description can be utilized by the state space representation:

$$\left.\begin{matrix}\dot{X} = AX + BU, \\ Y = CX\end{matrix}\right\} \quad (4.13)$$

which input-output relationship can be given by the transfer function:

$$G(s) = C(sI - A)^{-1}B = K * \frac{N(s)}{D(s)} \quad (4.14)$$

If $N(s)$ and $D(s)$ can be factored, $G(s)$ can be rewritten:

$$G(s) = K * \frac{(s-z_1)(s-z_2)\dots(s-z_l)}{(s-p_1)(s-p_2)\dots(s-p_n)} \quad (4.15)$$

Where,

the n values of p are called poles of G(s)

and

the l values of z are called zeros of G(s).

Now, $G(s)$ can be expanded in partial fractions as:

$$G(s) = \sum_1^n \frac{R_i}{(s-p_i)} = \frac{R_1}{(s-p_1)} + \frac{R_2}{(s-p_2)} + \dots + \frac{R_n}{(s-p_n)} \quad (4.16)$$

The general form of the equation above can contain potential multiplicities m_i of the eigenvalues $\lambda_i,\ \iota = 1, \dots, n$:

$$G(s) = \sum_{i=1}^{n} \sum_{j=1}^{m_i} \frac{R_i}{(s-p_i)} \quad (4.17)$$

Residues can be described also in terms of the eigenvectors, according to the following equation:

$$R_i = C * \Phi_i * \Psi_i * B \quad (4.18)$$

where

- Φ_i is the normalized right eigenvector
- Ψ_i is the normalized left eigenvector
- B is the nxp input matrix
- C is the qxn output

It is necessary to mention that Φ_i and Ψ_i are the normalized eigenvectors with

$$\Phi_i * \Psi_i = 1 \quad (4.19)$$

In addition, we can define the new matrices C' and B' such that:

$$B' = \Phi^{-1} B = \Psi B \quad (4.20)$$

$$C' = C\Phi \quad (4.21)$$

The nxr matrix B' is referred to as the mode controllability matrix, while the mxn matrix C' as the mode observability matrix.

The equation (4.18) can be rewritten:

$$R_i = B'C' \quad (4.22)$$

The importance of residues knowledge is highly reflected in model order reduction problems. A pole λ_j that corresponds to a residue $R_j$with large magnitude $|R_j|$ is called a dominant pole, i.e. a pole that is "well" observable and controllable in the transfer function. This can also be observed from the corresponding Bode Magnitude plot of H(s), where peaks occur at frequencies close to the imaginary parts of the dominant poles of the $G(s)$. The transfer function can be approximated by a new transfer function consisting of $k < n$ terms with $|R_j|$ above a specified value [9].

4.4.3 Singular Value Decomposition (SVD)

Let A be a $n \times m$ matrix. The singular values of A are the square roots of the eigenvalues of $m \times m$ matrix $A^T A$ listed according to their algebraic multiplicity [13]. The eigenvalues of the matrix $A^T A$ will always be positive numbers so it makes sense to take the square root. The singular values are denoted in a descending order (regarding their magnitude) by $\sigma_1, \dots, \sigma_N$ with:

$$\sigma_1 \geq \sigma_2 \geq \dots \geq \sigma_N \quad (4.23)$$

Every $n \times m$ matrix A can be written in the form $A = U\Sigma V^T$ where:

- Σ is an $n \times m$ matrix whose r first diagonals entries are the non zero singular values $\sigma_1, \dots, \sigma_r$ of A and whose other entries are all zeros.
- U, V are unitary matrices (orthogonal for real numbers) such that $U \in C^{n \times n}, V \in C^{m \times m}$ (A complex matrix B is unitary when $BB^* = I$ where B^* is the conjugate transpose of B).

The expression $U\Sigma V^T$ is known as the Singular Value Decomposition of the matrix A and it is a useful tool for determining an appropriate order of the model. The determination of the order of the model is based on the ratio of the singular values in Σ [6]. Matrix Σ can be decomposed into two parts Σ_n and Σ_z regarding the relative size of the singular values such that:

- Σ_n will contain in the diagonal entries all the singular values σ_ι , $\iota \leq n \; with \; \frac{\sigma_\iota}{\sigma_{max}} \geq 10^{-p}$ (4.24) where 10^{-p} is called threshold value and p is the number of significant decimal digits.
- Σ_z will contain in the diagonal entries all the singular values σ_ι , $n + 1 \leq \iota \leq N$

Finally matrix A can be now factorized as following:

$$A = |U_n \quad U_z| \begin{bmatrix} \Sigma_n & 0 \\ 0 & \Sigma_z \end{bmatrix} \begin{vmatrix} V_n^T \\ V_z^T \end{vmatrix} \quad (4.25)$$

4.4.4 Hankel Singular Value Decomposition (HSVD)

For simplification purposes a mode truncation can be applied on the original system by using the Hankel Singular Value Decomposition (HSVD) in order to construct a new state space model by retaining only the dominant poles. In order to truncate the order of the system, the contribution of the modes in the transfer function can be examined by using the State Energy indicator. High energy states are retained while lower energy states are discarded in order to preserve most of its characteristics in terms of stability, frequency, and time responses [8].

In order to explore the energy intuition, the energy interpretation of the following norm is the key:

$$\|G\|_{2-induced} = \sup_{u \in L_2} \left\{ \frac{\|y(t)\|_{L_2}}{\|u(t)\|_{L_2}} \right\} \; |y(t) = \sup_{\omega} \left(\sigma_{max}(G(j\omega)) \right) \quad (4.26)$$

The value $\|u(t)\|_{L_2}$ measures the amount of energy received by the system G and the value $\|y(t)\|_{L_2}$ measures the amount of energy produced by G, given the received energy

$\|u(t)\|_{L_2}$. This norm provides an estimate of how much energy can be produced by a system to an arbitrary input signal u and based on this norm, modes that are least involved in the energy transfer from input to output are deleted.

L_2 is the space of square-summable functions with 2- norm, or energy:

$$\|x(t)\|_2 = \sqrt{\int_{-\infty}^{+\infty} \|x(t)\|_2^{\,2}}\, dt = \sqrt{\int_{-\infty}^{+\infty} x(t)^T * x(t) dt} = \sqrt{x_1 + x_{2.} + \cdots + x_n} \quad (4.27)$$

where

x is a random vector with n elements

$$x = (x_1, x_2, \dots, x_n) \quad (4.28)$$

To some extent, the amount of received and induced energy can be measured by two energy functions. These functions are known as L_c and L_O and can be computed with the use of the following Gramians:

$$L_O = \sum_{t=0}^{\infty} y(t)^T y(t) \quad (4.29)$$

and

$$L_C = \sum_{t=-\infty}^{0} u(t)^T u(t) \quad (4.30)$$

In a similar manner the two functions can be computed:

$$L_c = \langle x, {W_C}^{-1} x \rangle \quad (4.31)$$

and

$$L_O = \langle x, W_O x \rangle \quad (4.32)$$

Where,

W_C, W_O are the controllability and observability matrices respectively,

and

operator $\langle a, b \rangle$ corresponds to the inner product of the two vectors a, b.

The HSVD method is based on finding an appropriate coordinate system for the state-space in which the chosen Gramian matrices of the system are diagonal and equal. In the simplest case, the controllability and observability Gramians W_C and W_O can be equal diagonal matrices:

$$W_c = W_O = \begin{bmatrix} \sigma_1 & 0 & 0 & 0 \\ 0 & \ddots & 0 & 0 \\ 0 & 0 & \sigma_{n-1} & 0 \\ 0 & 0 & 0 & \sigma_n \end{bmatrix} \Rightarrow {W_C}_{ii} = {W_O}_{ii} = \sigma_i. \quad (4.33)$$

The matrices Wc and W_o can be computed by solving the next equations, which are called Lyapunov equations and are defined as:

$$AW_C + W_C A^T = -BB^T \quad (4.34)$$

$$A^T W_O + W_O A = -C^T C \quad (4.35)$$

The two Gramians can be computed according to [1]:

$$W_C(t_0, t_1) = \int_{t_0}^{t_1} e^{A(t_0-\tau)} BB^T e^{A^T(t_0-\tau)} d\tau \quad (4.36)$$

$$W_0(t_0, t_1) = \int_{t_0}^{t_1} e^{A^T(t_0-\tau)} C^T C e^{A(t_0-\tau)} d\tau \quad (4.37)$$

where t_0 , t_1 correspond to zero and infinity respectively if the system is universally stable [12].

Finally, the energy transfer from past inputs to future outputs by considering the output energy resulting from an initial state x^0 (L_O) and the minimal energy needed to reach x^0 (L_C) can be computed according to [12]:

$$E = \frac{L_O}{L_C} = \frac{(\bar{x}^0)^T W_C^{\frac{1}{2}} W_O W_C^{\frac{1}{2}} \bar{x}^0}{(\bar{x}^0)^T \bar{x}^0} \quad (4.38)$$

where

$$\bar{x}^0 = W_C^{\frac{1}{2}} x^0 \quad (4.39)$$

Note that:

$$(\Lambda(W_C W_O))^{\frac{1}{2}} = (\Lambda\left(W_C^{\frac{1}{2}} W_O W_C^{\frac{1}{2}}\right))^{\frac{1}{2}} \quad (4.40)$$

Thus, according to eq. (4.38) and eq. (4.40), the HSVs measure how much the states are involved in the energy transfer from inputs to outputs.

In summary, it seems reasonable to obtain a new reduced-order model by removing the least controllable and observable states, keeping states containing the major part of the system energy as these are the ones which are most involved in the energy transfer from inputs to outputs. That is, keeping the states corresponding to largest HSVs and therefore two matrices Ψ_1, Ψ_2 can be created, where:

- Ψ_1 is the diagonal matrix that contains all the singular values σ_i in descending order. The SVs $\sigma_i,\ 1 \le i \le k$ correspond to states x_i "much more" observable and controllable than $\sigma_{j,}\ k+1 \le j \le n$. That means that the magnitude of σ_i is significantly bigger than of σ_j , $\sigma_i \gg \sigma_j \quad \forall i, j$
- Ψ_2 is the diagonal matrix that contains all the singular values σ_j in descending order. The SVs σ_j correspond to states x_j that are less important due to low observability and controllability.

$$\Psi = \begin{bmatrix} \Psi_1 & 0 \\ 0 & \Psi_2 \end{bmatrix} \quad (4.40)$$

The reduction of the model is based on the truncation of the less important states according to the process described and the matrices A, B, C, D can be partitioned respectively:

$$\left.\begin{aligned} A &= \begin{bmatrix} A_{11} & A_{12} \\ A_{21} & A_{22} \end{bmatrix} \\ B &= \begin{bmatrix} B_1 \\ B_2 \end{bmatrix} \\ C &= \begin{bmatrix} C_1 & C_2 \end{bmatrix} \end{aligned}\right\} \quad (4.41)$$

Finally, the reduced model is described by the new matrices formed from the truncation A_{11}, B_1, C_1.

5. System Identification Methods

5.1 Introduction to the Identification Methods

In the context of this thesis three different methods are used for the identification of the dynamic systems: 1) Autoregressive with external input (ARX), 2) Autoregressive moving average with exernal input (ARMAX) and 3) Eigensystem realization algorithm (ERA). The first two methods, which are going to be described and applied in the next chapters, belong to the family of transfer function models while the third one belongs to the family of state-space models. The ARX and ARMAX methods are considered mode meters according to the definition given in Chapter 3.4 and use input and output data for the identification process, a fact that classify these methods in the family of I/O methods. On the other hand, ERA is a ringdown analyzer according to the definition given also in Chapter 3.4 and requests only output data, which renders it an output-only identification technique. Finally, it is of great importance to emphasize that all of the three aforementioned model structures are black-box models, i.e. they are used for identifying a system without any knowledge of its internal workings.

5.2 AutoRegressive with eXternal input (ARX) Model Description

The system's input and output at time t can be denoted by $u(t)$ and $y(t)$ respectively. The most basic relationship between the input and output is the linear difference equation:

$$y(t) + \mathrm{a_1 y(t-1)} + \cdots + \mathrm{a_n y(t-n)} = \mathrm{b_1 u(t-1)} + .. \mathrm{b_m u(t-m)} \quad (5.1)$$

The system is in discrete time, primarily because observed data are always collected by sampling and therefore it is more straightforward to relate observed data to time discrete models.

Equation (5.1) can be reconstructed in order to provide a way of determining the next output value given previous observations:

$$y(t) = -\mathrm{a_1 y(t-1)} - \ldots - \mathrm{a_n y(t-n)} + \mathrm{b_1 u(t-1)} + .. \mathrm{b_m u(t-m)} \quad (5.2)$$

We introduce the following vectors:

$$\theta = [a_1 \ldots a_n \;\; b_1 \ldots b_m]^T \quad (5.3)$$

$$\varphi(t) = [-y(t-1) \ldots -y(t-n) \;\; u(t-1) \ldots u(t-m)]^T \quad (5.4)$$

With the previous, (5.2) can be rewritten as:

$$y(t) = \varphi^T(t)\theta \quad (5.5)$$

To emphasize that the calculation of y(t) from past data depends on the parameters of θ we will use the following notation:

$$\hat{y}(t|\theta) = \varphi^T(t)\theta \quad (5.6)$$

From the equation (5.5) we conclude that the predictor $\hat{y}$ is the scalar product between a known vector φ(t) and the parameter vector θ. In statistics such a model is called linear regression and the vector φ(t) is known as the regression vectors.

At this point we will introduce the forward shift operator q by :

$$qu(t) = u(t+1) \quad (5.7)$$

and the backward shift operator q^{-1} by:

$$q^{-1}u(t) = u(t-1) \quad (5.8)$$

In the equation (5.1) we will introduce a white-noise term $e(t)$ as a direct error and we will call the new model an *equation error* model (structure):

$$y(t) + \mathrm{a_1 y(t-1)} + \ldots + \mathrm{a_n y(t-n)} = \mathrm{b_1 u(t-1)} + \ldots \mathrm{b_m u(t-m)} + \mathrm{e(t)} \quad (5.9)$$

We introduce the following polynomials:

$$A(q) = 1 + \mathrm{a_1} q^{-1} + \ldots \mathrm{a_{n_a}} q^{-n_a} \quad (5.10)$$

$$B(q) = \mathrm{b_1} q^{-1} + \ldots \mathrm{b_{n_b}} q^{-n_b} \quad (5.11)$$

and we see that (5.9) can be written as :

$$A(q)y(t) = B(q)u(t) + e(t) \Rightarrow y(t) = \frac{B(q)}{A(q)}u(t) + \frac{1}{A(q)}e(t) \quad (5.12)$$

Finally if we set:

$$G(q,\theta) = \frac{B(q)}{A(q)} \quad (5.13)$$

$$H(q,\theta) = \frac{1}{A(q)} \quad (5.14)$$

then (5.12) takes its final form:

$$\hat{y}(t|\theta) = G(q,\theta)u(t) + H(q,\theta)e(t) \quad (5.15)$$

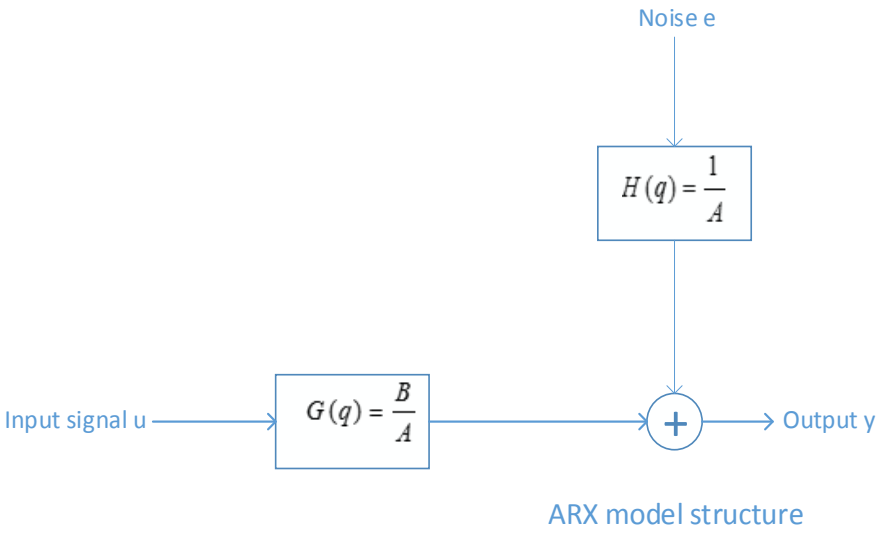

Figure 5.1: ARX model structure block diagram

5.3 AutoRegressive Moving Average with eXternal input (ARMAX) Model Description

The ARX model (5.9) lacks adequate freedom in describing the properties of the disturbance $e(t)$. This disadvantage could be counterbalanced by describing the equation error as a moving average of noise. This gives the following model:

$$y(t) + \mathrm{a_1 y(t-1)} + \cdots + \mathrm{a_{n_a} y(t-t_{n_a})} = \mathrm{b_1 u(t-1)} + \cdots \mathrm{b_{n_b} u(t-t_{n_b})} + \mathrm{e(t)} + \mathrm{c_1 e(t-1)} + \cdots \mathrm{c_{n_c} e(t-t_{n_c})} \quad (5.16)$$

Let $C(q) = 1 + \mathrm{c_1} q^{-1} + \ldots \mathrm{c_{n_c}} q^{-n_c}$ (5.17)

Then the eq. (5.16) can be rewritten:

$$A(q)y(t) = B(q)u(t) + C(q)e(t) \Rightarrow y(t) = \frac{B(q)}{A(q)}u(t) + \frac{C(q)}{A(q)}e(t) \quad (5.18)$$

and clearly corresponds to (5.15) with

$$G(q,\theta) = \frac{B(q)}{A(q)} \quad (5.19)$$

$$H(q,\theta) = \frac{C(q)}{A(q)} \quad (5.20)$$

$$\theta = [a_1 \ldots a_{n_a} \;\; b_1 \ldots b_{n_b} \, c_1 \ldots \, c_{n_c}]^T \quad (5.21)$$

The involvement of the moving average (MA) part $C(q)e(t)$ leads to the model (5.18) known as ARMAX. The ARMAX model is widely used a tool in control theory for both system description and control design.

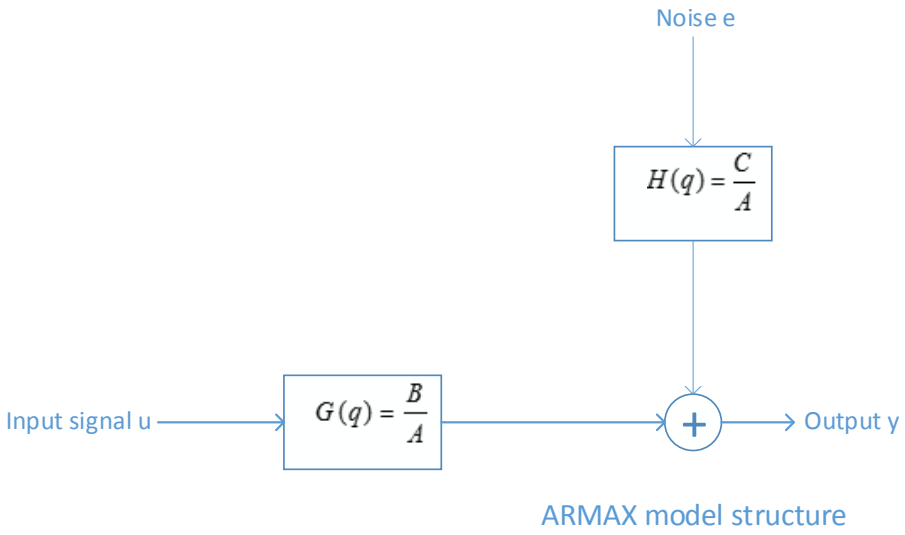

Figure 5.2: ARMAX model structure block diagram

5.4 Parameter Estimation

In order to construct the ARX and ARMAX transfer function models, the parameters contained in the vector θ have to be estimated.

The prediction error of a proposed method is equal:

$$\varepsilon(t,\theta) = y(t) - \hat{y}(t|\theta) \quad (5.22)$$

When the dataset Z^N defined in equation (3.1) is known, these errors can be computed for $t = 1,2,\ldots,N$.

The main goal of the identification is to select the parameters $\widehat{\theta}_N$ at time $t = N$ so that the prediction error $\varepsilon(t,\theta_N), t = 1,2,\ldots,N$ becomes minimum.

The prediction error sequence is a vector in R^N and can be measured using any norm in R^N. In order to restrict the amount of choices of norms, we let the prediction error sequence to be filtered through a stable linear filter L(q):

$$\varepsilon_F(t,\theta) = L(q)\varepsilon(t,\theta) \quad (5.23)$$

The general type of the norm is the following:

$$V_N = \frac{1}{N}\sum_1^N l(\varepsilon_F(t,\theta)) \quad (5.24)$$

where $l(\cdot)$ is a positive-scalar valued function.

The minimization of the function V_N defines the estimated vector of the parameters (minimizing arguments) $\hat{\theta}_N$:

$\hat{\theta}_N = \arg_{\min} V_N$ (5.25)

For the Linear Regression methods ARX and ARMAX that we are using, we will assume that $L(q) = 1$ (5.26), since the pre-filtering of $\varepsilon(t)$ is done by the corresponding linear functions $H(q, \theta)$as shown in Fig. (5.1), (5.2).

The scalar function $l(\cdot)$ will be equal to a quadratic norm:

$l(\varepsilon) = \frac{1}{2}\varepsilon^2$ (5.27)

Using the equation (5.6) the prediction error becomes:

$\varepsilon(t, \theta) = y(t) - \varphi^T \theta$ (5.28)

and by assuming that L(q)=1 and $l(\varepsilon) = \frac{1}{2}\varepsilon^2$ (5.29) the criterion function V_N

is:

$\mathrm{V_N}(\theta, \mathrm{Z^N}) = \frac{1}{\mathrm{N}}\sum_1^{\mathrm{N}}\frac{1}{2}|\mathrm{y(t)} - \varphi(\mathrm{t})\theta|^2$ (5.30)

The equation (5.30) is known as the *Least-Squares Criterion* for linear regression and it can be minimized analytically given that it is a quadratic function of θ.

The minimizing arguments are being found by setting the derivative of (5.30) to zero:

$$\frac{d}{d\theta}V_N(\theta, Z^N) = 0 => \frac{2}{N}\sum_1^N[\varphi(t)(y(t) - \varphi^T(t)\theta)] = 0 =>$$

$$\frac{1}{\mathrm{N}}\sum_1^{\mathrm{N}}[\varphi(\mathrm{t})\mathrm{y(t)}] = \frac{1}{\mathrm{N}}\sum_1^{\mathrm{N}}[\varphi(\mathrm{t})\varphi^{\mathrm{T}}(\mathrm{t})\theta] \quad (5.31)$$

or

$\hat{\theta}_N^{LS} = \arg_{\min} V_N(\theta, Z^N) = \left[\frac{1}{N}\sum_1^N[\varphi(\mathrm{t})\varphi^{\mathrm{T}}(\mathrm{t})]\right]^{-1}\frac{1}{N}\sum_1^N[\varphi(\mathrm{t})\mathrm{y(t)}]$ (5.32)

$\hat{\theta}_N^{LS}$ is known as the *Least-Squares Estimate* (LSE)

Let

$R(N) = \frac{1}{N}\sum_1^N[\varphi(\mathrm{t})\varphi^{\mathrm{T}}(\mathrm{t})]$ (5.33)

and

$f(N) = \frac{1}{N}\sum_1^N[\varphi(t)y(t)]$ (5.34)

Now, if we suppose that the original data $y(t)$ are generated for some sequence $\{v_0\}$ then they will have the following form:

$y(t) = \varphi^T(t)\theta_0 + v_0$ (5.35)

We may think of θ_0 as a "true value" of the parameter vector.

Then, $y(t)$ can be replaced in the equation (5.32) and using the notations $R(N)$ and $f(N)$:

$\hat{\theta}_N^{LS} = R^{-1}(N)\frac{1}{N}[\sum_1^N[\varphi(t)\varphi^T(t)\theta_0] + \sum_1^N[\varphi(t)v_0(t)]]$ (5.36)

Finally, the deviation of $\hat{\theta}_N^{LS}$ can be computed from the original vector θ_0:

$\lim_{N\to\infty}(\hat{\theta}_N^{LS}) - \theta_0 = \lim_{N\to\infty}(R^{-1}(N)\frac{1}{N}\sum_1^N[\varphi(t)v_0(t)]) = (R^*)^{-1}f^*$ (5.37)

where R^* and f^* are the following mathematical expectations:

$R^* = \bar{E}(\varphi(t)\varphi^T(t))$ (5.38)

$f^* = \bar{E}(\varphi(t)v_0(t))$ (5.39)

5.5 Computation of the Least Square Estimate based on QR Factorization

The prediction-error approach with a quadratic norm gives the least squares method described in Chapter 5.4 and according to equations (5.32), (5.33) and (5.34) the minimizing element $\hat{\theta}_N^{LS}$ can be written as:

$$\hat{\theta}_N^{LS} = R^{-1}(N)f(N) \quad (5.40)$$

An alternative is to view $\hat{\theta}_N^{LS}$ as the solution of:

$$R(N)\hat{\theta}_N^{LS} = f(N) \quad (5.41)$$

The coefficient matrix R(N), particularly if it is of high dimension, can render the computation of $\hat{\theta}_N^{LS}$ inefficient and at some cased unbearable. Instead of forming matrix R(N), a new matrix R can be introduced with the property:

$$R * R^T = R(N) \quad (5.42)$$

For the construction of the matrix R the QR-factorization is being used.

The QR factorization of an $n \times d$ matrix A is a decomposition as the following:

$A = QR$ (5.43)

where

Q is an $n \times n$ orthonormal matrix (i.e $Q^T Q = I$)

R is an $n \times d$ upper triangular matrix

Let's introduce the matrices:

$Y^T = [y^T(1) \cdots y^T(N)]$, Y is a matrix of N*dimensions(y)×1 elements (5.44)

$\Phi^T = [\varphi(1) \cdots \varphi(N)]$, Φ is a matrix of N*dimensions(y)×d elements (5.45)

Then the Least Square Criterion (5.30) can be rewritten as:

$V_N(\theta, Z^N) = |Y - \Phi\theta|^2$ (5.46)

Since Q is an orthonormal matrix, the norm in equation (5.46) is not affected by inserting matrix Q in the norm (orthonormal transformation in the vector of $Y - \Phi\theta$) as shown below:

$V_N(\theta, Z^N) = |Y - \Phi\theta|^2 = |Q(Y - \Phi\theta)|^2 = |Q^T(Y - \Phi\theta)|^2$ (5.47)

The QR factorization of the matrix $[\Phi\ Y]$:

$[\Phi\ Y] = QR \Rightarrow Q^T[\Phi\ Y] = R$, with $R = \begin{bmatrix} R_0 \\ \cdots \\ 0 \end{bmatrix}$ (5.48)

Here R_0 is an upper triangular $(d+1)$ x $(d+1)$ matrix which can be decomposed as:

$$\left.\begin{array}{l} R_0 = \begin{bmatrix} R_1 & R_2 \\ 0 & R_3 \end{bmatrix} \\ R_1 \text{ is } d \times d \text{ matrix} \\ R_2 \text{ is } d \times 1 \\ R_3 \text{ is scalar} \end{array}\right\} \quad (5.49)$$

Using the equation (5.47), (5.48) can be written as:

$$V_N(\theta, Z^N) = |Q^T(Y - \Phi\theta)|^2 = \left|\begin{bmatrix} R_2 \\ R_3 \end{bmatrix} - \begin{bmatrix} R_1\theta \\ 0 \end{bmatrix}\right|^2 = \left|\begin{bmatrix} R_2 - R_1\theta \\ R_3 \end{bmatrix}\right|^2 \Rightarrow$$

$V_N(\theta, Z^N) = |R_2 - R_1\theta|^2 + |R_3|^2$ (5.50)

Thus, the minimizing arguments $\hat{\theta}_N^{LS}$ and the minimum value of the norm are equal to:

$\hat{\theta}_N^{LS} = \arg_{\min} V_N(\theta, Z^N) = {R_1}^{-1} R_2$ (5.51)

$\mathrm{V_N}(\hat{\theta}_N^{LS}, \mathrm{Z^N}) = |R_3|^2$ (5.52)

Equations (5.51) and (5.52) show that for computing the $\hat{\theta}_N^{LS}$ and the loss function $\mathrm{V_N}(\theta, \mathrm{Z^N})$ the matrix Q is never required. Note that there are many algorithms for computing matrix R such as Householder transformations and the Gram-Schmidt procedure. Matlab computes full QR factorization of a matrix A using the Householder algorithm by the matlab command:

$[Q, R] = qr(A)$ (5.53)

Detailed information regarding the algorithm for computing the QR can be found in [5].

5.6 Introduction to Eigensystem Realization Algorithm (ERA)

The main goal of the Eigensystem Realization Algorithm as well as of every modal analysis technique (the study of dynamic properties under vibration excitation) is to determine the eigenvalues of the matrix A in the State-Space description (4.1) of the dynamical system.

The Eigensystem Realization algorithm (ERA) is based on the Singular Value Decomposition (SVD) of the Hankel matrix H_0 of the system's impulse response [4]. A Hankel matrix is a square matrix with constant skew-diagonals. In this method we are computing the two Hankel matrices H_0,H_1 using all the available data $Z^N = [y_1, y_2, \dots, y_N]$:

$$H_0 = \begin{bmatrix} y_0 & \cdots & y_r \\ \vdots & \ddots & \vdots \\ y_r & \cdots & y_{N-1} \end{bmatrix} \quad (5.54)$$

$$H_1 = \begin{bmatrix} y_1 & \cdots & y_{r+1} \\ \vdots & \ddots & \vdots \\ y_{r+1} & \cdots & y_N \end{bmatrix} \quad (5.55)$$

where $r = \frac{N}{2} - 1$ (5.56)

The number of data must be sufficient so that $r > n$.

The singular value decomposition of H_0 is the following:

$$H_0 = |U_n \quad U_z| \begin{bmatrix} \Sigma_n & 0 \\ 0 & \Sigma_z \end{bmatrix} \begin{vmatrix} {V_n}^T \\ {V_z}^T \end{vmatrix} \quad (5.57)$$

where

$\Sigma_n = diag(\sigma_1, \sigma_2, \dots, \sigma_n)$ (5.58)

and

$\Sigma_z = diag(\sigma_{n+1}, \sigma_{n+2}, \dots, \sigma_N)$ (5.59)

The set of singular values to be contained in Σ_n is determined after deciding a value for the threshold according to (4.24)

The Hankel matrix H_0 can be approximated by:

$$H_0 \approx U_n \Sigma_n {V_n}^T \quad (5.60)$$

where it is assumed that:

$$\sigma_n >> \sigma_{n+1} \quad (5.61)$$

Finally, the discrete matrices of the state space representation of the model are computed as follows:

$$\begin{pmatrix} A_{discrete} = {\Sigma_n}^{-1/2} {U_n}^T H_1 V_n \Sigma_n \\ B_{discrete} = {\Sigma_n}^{1/2} {V_n}^T \\ C_{discrete} = U_n {\Sigma_n}^{1/2} \\ D_{discrete} = y_0 \end{pmatrix} \quad (5.62)$$

To calculate the corresponding matrices in continuous time, the discrete matrices above have to be converted by assuming a zero order hold (holding each sample value for one sample interval) and sampling interval Δt:

$$\begin{pmatrix} A_{continuous} = ln\left(\frac{A_{discrete}}{\Delta t}\right) \\ B_{continuous} = \left[\int_0^{\Delta t} e^{A\tau} d\tau\right]^{-1} B_{discrete} \end{pmatrix} \quad (5.63)$$

The identified system response can be computed from the continuous matrices.

A conceptual view of the ERA identification process is shown in the Fig. (5.3)

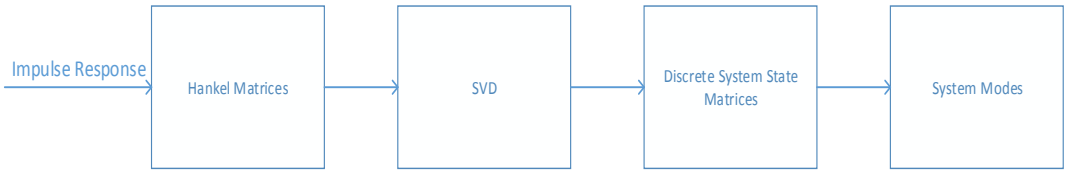

Figure 5.3: ERA process block diagram

6. Wind Turbine Description

6.1 Introduction

The wind turbine (WT) is designed in such a way as to allow the production of electrical energy generated from wind power. Wind generates a twisting force on the blades of the wind turbine and causes the blades to rotate and consequently produce the mechanical energy required for varying speed shafts to generate electricity. There is a variety of components that ensure the smooth operation of the wind turbine. The Fig (6.1) shows the components found within the wind turbine:

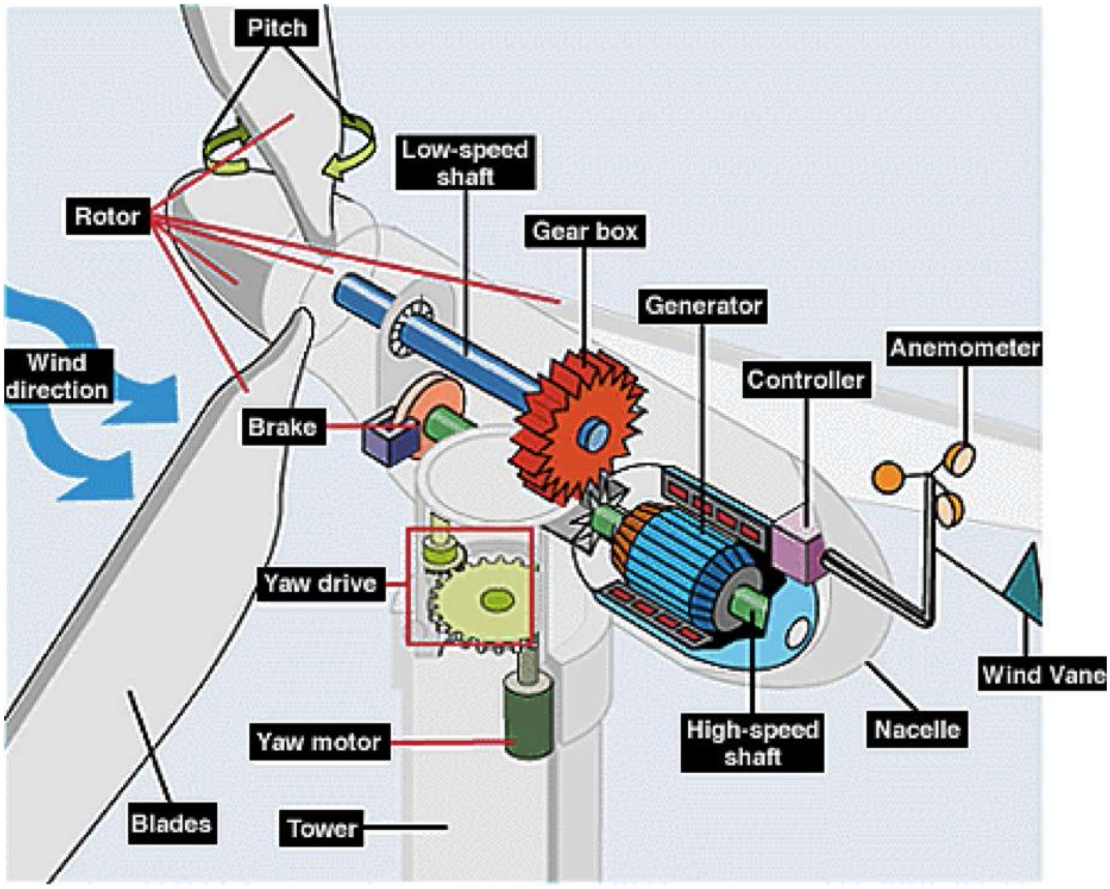

Figure 6.1: Wind Turbine components

The movement of the blades with respect to the direction of the wind is facilitated by a system which consists of a drive and a motor and is called Yaw system. The Yaw system is found on the tower which provides supports to the various components.

A wind turbine can be divided in three functional sub-systems: The mechanical-drive train system, the electrical system and the control system. This division leads to a deep understanding of how wind turbine actually works.

6. 2 Mechanical and Drive Train System

This System is the entry point of the wind turbine system. The wind provides input to the wind turbine, to the blade and pitch system. A hub and three blades make up the blade and pitch system forming the rotor. The blades are designed to optimize the aerodynamic properties of the wind turbine and the pitch corresponds to the angle formed by the blades to an imaginary horizontal axis plane. The Rotor generates torque and rotational force which serves as an input to the drive train system. The drive train system usually consists of a low-speed shaft, a high speed shaft and a gear box. The principle of operation of the drive train is based on a speed transmission mechanism. Firstly, a planetary gear system is used to boost the speed generated by the low speed shaft unto a high-speed shaft. In many cases the drive train system also contains a brake which is used in order to slow down the low speed shaft in cases of extremely high wind speeds. The high-speed shaft is used in order to transmit the adequate torque and rotational speed to the generator for the production of the electrical energy.

6.3 Electrical System

This system consists of the generator and the converter. The generator takes as input the rotational energy transferred from the drive train system and converts it into electrical energy. The converter utilizes the control of the power flow by providing a constant power output from the system.

6.4 Control System

The control system is "responsible" for the monitoring and regulation of the operation of the wind turbine. Monitoring provides knowledge of faults when a component fails to satisfy its original purpose. Regulating the system involves all the necessary processes to ensure that the system delivers the expected output at all times. Control can be applied in both the mechanical and the electrical part of the wind turbine. At the early stages of the development of wind turbines the control was applied only to the mechanical system and satisfied the very basic functions (starting, rated power, shut down), usually with only mechanical devices. In recent years, the development of power electronics not only made possible the control of the wind turbine through the electrical system but also rendered the control more robust, flexible and reliable.

Typically, there are two modes of operation: the partial load mode and the full load mode as shown in the next figure:

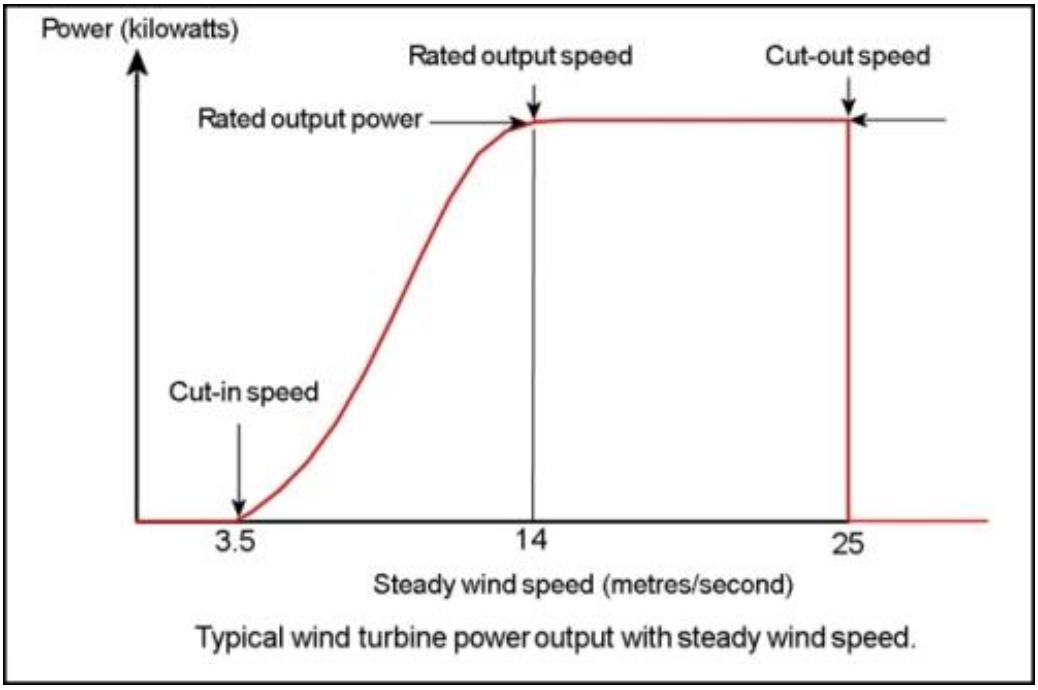

Figure 6.2: Power output of Wind Turbine with steady wind speed

The partial load mode concerns wind velocities from 3.5 m/s to 14 m/s where the control system seeks to secure the maximization of the electric power measured in Watts by capturing the maximum amount of energy of the wind. In the full load region, from 14 m/s to 25m/s, the control system keeps the electric power constant by changing both the pitch angle and the rotational speed of the generator. At wind speeds above 25m/s the wind turbine is shut down to prevent potential structural damages due to adverse wind conditions. To summarize, the main goal of the controller is to follow a reference power output and in some instances, when this cannot be achieved, the controller minimizes the reference error.

The following diagram contains the basic parts of the wind turbine as described above:

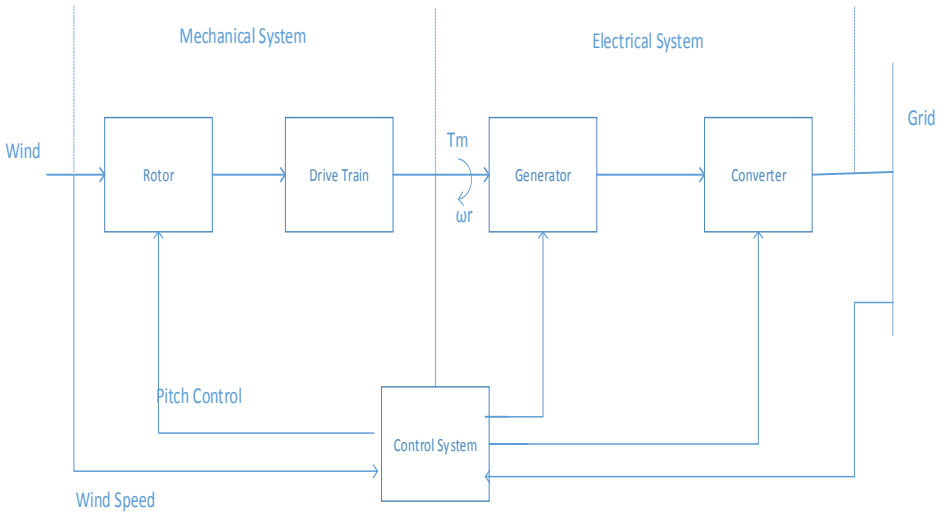

Figure 6.3: Basic parts of the Wind Turbine

Based on the relationship between power and rotor speed the wind turbines can be divided into:

- Constant Speed at Constant Frequency Wind Turbines (CSWT)
- Variable Speed at Constant Frequency Wind Turbines (VSWT)

The Variable Speed WT's superiority comparing to the Constant Speed WT lies on the fact that the rotor can operate in different speeds for which the performance coefficient $C_p(\lambda)$ is optimized and consequently the produced power is maximized. Besides that, another important advantage of the VSWT is that the mechanical torques which are caused due to wind variations are decreased and, consequently, so are the power variations.

The next figure shows the variation of the mechanical power for different values of wind speed.

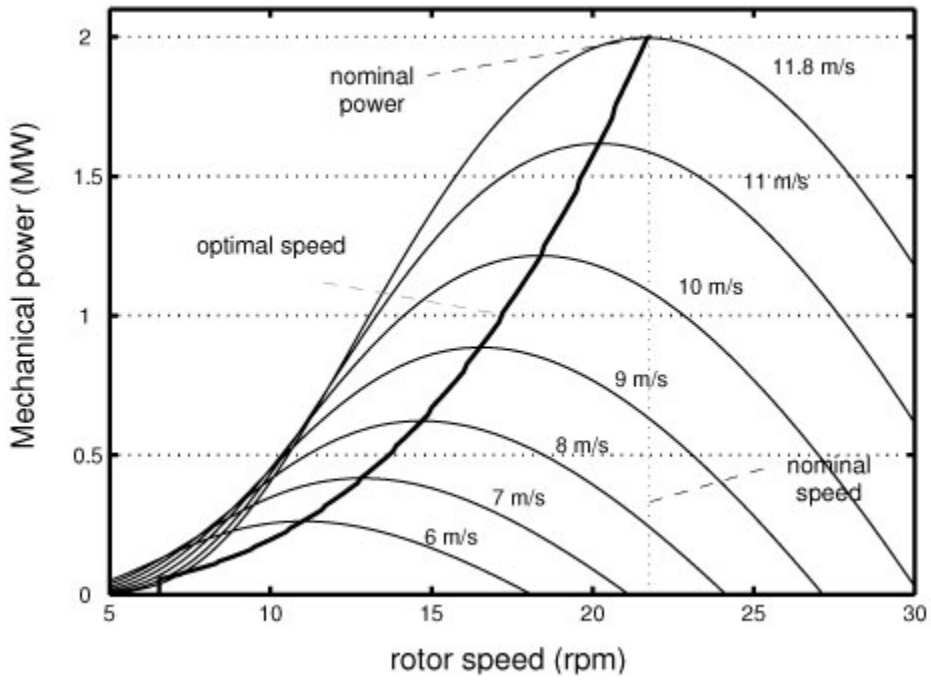

Figure 6.4: Mechanical power for different wind speeds

It is obvious that for a certain wind speed the mechanical power is maximized for a specific rotor speed. In other words, the maximum power is obtained when the WT follows the curve that connects the maximum points of the wind speed curves as shown above. Variable Speed WT's base their operation on that observation while on the other hand, in constant speed WT's the generator output is tied directly to the grid (local ac power network) and, therefore the rotation speed of the generator is fixed (typically it can vary a little given that slip is allowed to vary 2% to 3%). Any fluctuation in wind speed causes the mechanical power at the wind turbine to vary as well and, because the rotation speed is fixed, this causes the torque at the wind turbine to vary accordingly. Whenever a wind gust occurs, this leads to a significant increase of

the torque while the rotor speed varies a little. Wind gust stresses the mechanical components of the WT (especially the gearbox) and causes sudden increase in rotor torque and in the output power. As a result, wind speed variations and gusts render CSWTs a source of instability in the power network to which they are connected.

On the other hand, VSWT cannot be implemented by synchronous generators which operate at a strictly constant speed when they are connected to the grid and by asynchronous generators as the rotation speed of the generator is quasi-constant when its output is tied directly to the grid. Finally, for the case of VSWT power electronics must be introduced as an interface between the wind turbine and the grid.

6.5 Doubly Fed Induction Generator (DFIG) for Wind Turbine

The Doubly Fed Induction generator (DFIG) is a common configuration for large, variable-speed wind turbines that are connected to the grid. This is primarily due to the many advantages that doubly-fed induction generators offer and can be summarized below:

- Reduced inverter cost, because inverter rating is typically low (around 25% of total power system output)
- Reduced cost of the inverter filters because filters are rated for 0.25 p/u of totally system power
- Improved system efficiency given that the system losses are reduced.
- Power-factor can be implemented at lower cost because DFIG system basically operates similar to a synchronous generator. The converter provides only excitation energy.

The implementation scheme of the DFIG WT is shown in the next figure:

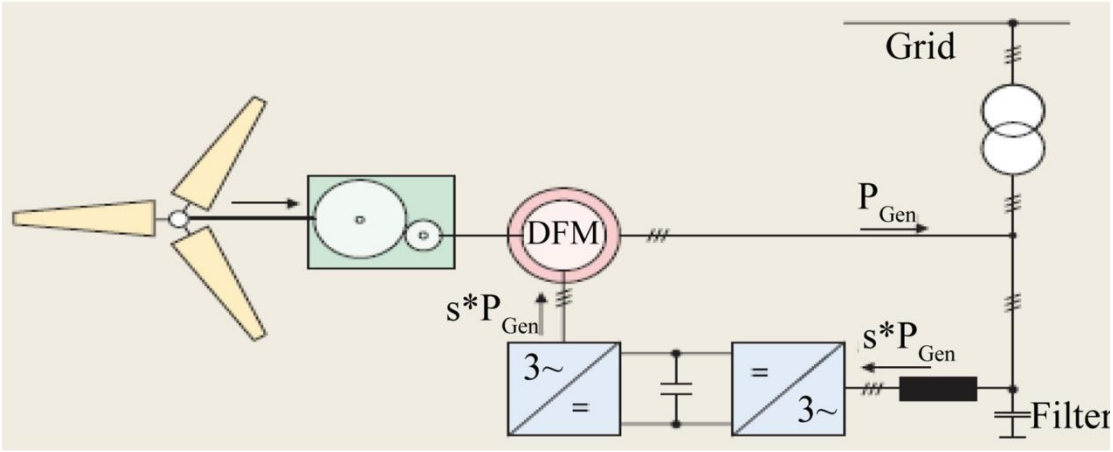

Figure 6.5: DFIG Wind Turbine connected to the grid

6.6 Mathematical Description of the DFIG system

Steady-state electrical equations of the doubly fed induction generator are assumed and the converter controls basically decouple the generator from the grid. As a result, the following equations describe the system:

$$v_{ds} = -r_s i_{ds} + ((x_s + x_\mu) i_{qs} + x_\mu i_{qr}) \quad (6.1)$$

$$v_{qs} = -r_s i_{qs} + ((x_s + x_\mu) i_{ds} + x_\mu i_{dr}) \quad (6.2)$$

$$v_{dr} = -r_s i_{dr} + (1 - \omega_m)((x_s + x_\mu) i_{qr} + x_\mu i_{qs}) \quad (6.3)$$

$$v_{qr} = -r_s i_{qr} + (1 - \omega_m)((x_s + x_\mu) i_{dr} + x_\mu i_{ds}) \quad (6.4)$$

where r_s is the stator resistance, x_s is the stator reactance, x_μ is the magnetizing reactance, ω_m is the rotor angular speed and i_{dr} $i_{qr} i_{ds}$ i_{qs} are the dq axis currents of the rotor and stator respectively.

The stator voltages are functions of the grid voltage magnitude and phase:

$$v_{ds} = -v sin\theta \quad (6.5)$$

$$v_{qs} = v cos\theta \quad (6.6)$$

The generator active and reactive powers depend on the stator and converter currents accordingly as follows:

$$p = v_{ds} i_{ds} + v_{dc} i_{dc} + v_{qc} i_{qc} \quad (6.7)$$

$$q = v_{qs} i_{ds} + v_{qc} i_{dc} - v_{dc} i_{qc} \quad (6.8)$$

where v_{dc}, v_{qc}, i_{dc}, i_{qc} are the voltages and converter's voltages and currents respectively.

The converter powers on the grid side are:

$$p_c = v_{dc} i_{dc} + v_{qc} i_{qc} \quad (6.9)$$

$$q_c = v_{qc} i_{dc} - v_{dc} i_{qc} \quad (6.10)$$

while on the rotor side are:

$$p_r = v_{dr} i_{dr} + v_{qr} i_{qr} \quad (6.11)$$

$$q_c = v_{qr} i_{dr} - v_{dr} i_{qr} \quad (6.12)$$

Assuming a loss-less converter model, the active power of the converter coincides with the rotor active power and, therefore, $p_c = p_r$. In addition, by neglecting stator resistance and assuming the d-axis coincides with the maximum of the stator flux the active and reactive powers injected in the grid are:

$$p = v_{ds}i_{ds} + v_{qs}i_{qs} + v_{dr}i_{dr} + v_{qr}i_{qr} \quad (6.13)$$

$$q = -\frac{x_\mu v i_{dr}}{x_s + x_\mu} - \frac{v^2}{x_\mu} \quad (6.14)$$

Assuming that the converter controls can filter shaft dynamics, the generator motion equation is modeled as single shaft:

$$\dot{\omega_m} = (\tau_m - \tau_e)/2H_m \quad (6.15)$$

$$\tau_e = \psi_{ds}i_{qs} - \psi_{qs}i_{ds} \quad (6.16)$$

where H_m is the rotor inertia, ψ_{ds} , ψ_{ds} are the stator fluxes and τ_m and τ_e are the mechanical and electrical torques.

The link between stator fluxes and generator currents is:

$$\psi_{ds} = -((x_s + x_\mu)i_{ds} + x_\mu i_{dr}) \quad (6.17)$$

$$\psi_{qs} = -((x_s + x_\mu)i_{qs} + x_\mu i_{qr}) \quad (6.18)$$

The simplified electrical torque is approximated as follows:

$$\tau_e = -\frac{x_\mu v i_{qr}}{\omega_{b(}x_s + x_\mu)} \quad (6.19)$$

where ω_b is the system frequency rate.

The mechanical torque is:

$$\tau_m = -\frac{p_w}{\omega_m} \quad (6.20)$$

where p_w is the mechanical power exctracted from the wind and can be computed as follows:

$$p_w = \frac{n_g \rho}{2S_n} C_p(\lambda, \theta_p) A_r {v_w}^3 \quad (6.21)$$

$C_p(\lambda, \theta_p)$ is the performance or power coefficient, λ is the tip speed ration, θ_p is the pitch angle, and A_r is the area swept by the rotor.

C_p and λ can be approximated as follows:

$$C_p = 0.22(\frac{116}{\lambda_i} - 0.4\theta_p - 5)e^{-\frac{12.5}{\lambda_i}} \quad (6.22)$$

$$\frac{1}{\lambda_i} = \frac{1}{\lambda + 0.08\theta_p} - \frac{0.035}{{\theta_p}^3 + 1} \quad (6.23)$$

Converter dynamics are modeled as an ideal current source, where i_{qr} and i_{dr} are state variables and are used for the rotor speed control and voltage control respectively.

Differential and algebraic equations are as follows:

$$i_{qr} = \left(-\frac{\frac{x_s + x_\mu}{x_\mu v} p_w * (\omega_m)}{\omega_m} - i_{qr}\right) \frac{1}{T_e)} \quad (6.24)$$

$$i_{dr} = K_V\left(v - v_{ref}\right) - \frac{v}{x_\mu} - i_{dr} \quad (6.25)$$

where T_e is the power control time constant, v_{ref} is the initial reference signal and $p_w * (\omega_m)$ is the power-speed characteristic which optimizes the wind energy capture and is calculated using the current rotor speed value as:

$$p_w * (\omega_m) = \begin{cases} 0 & if\ \omega_m < 0.5 \\ 2\omega_m - 1 & if\ 0.5 \leq \omega_m \leq 1 \\ 1 & if\ \ \omega_m > 1 \end{cases} \quad (6.26)$$

The following schemes show the rotor speed control and voltage control respectively:

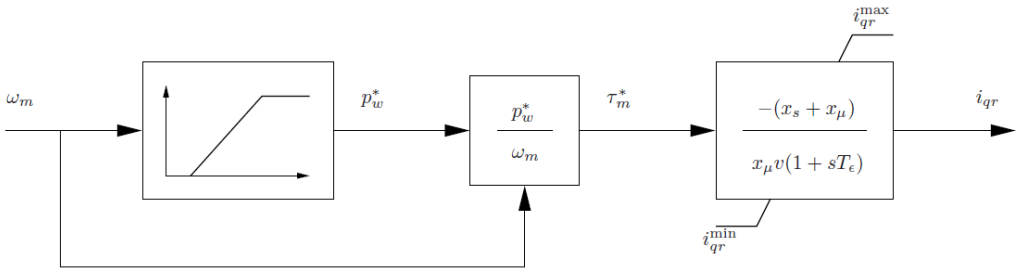

Figure 6.6: Rotor speed control

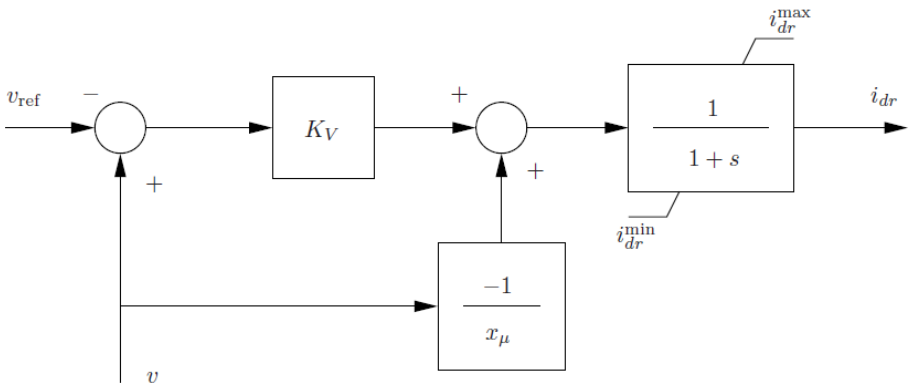

Figure 6.7: Voltage control

Rotor current limits are computed based on active and reactive limits and assuming bus voltage $v \approx 1$ as follows:

$$i_{qr}{}^{max} \approx -\frac{x_s+x_\mu}{x_\mu} p^{min} \quad (6.27)$$

$$i_{qr}{}^{min} \approx -\frac{x_s+x_\mu}{x_\mu} p^{max} \quad (6.28)$$

$$i_{dr}{}^{max} \approx -\frac{x_s+x_\mu}{x_\mu} q^{min} - \frac{x_s+x_\mu}{{x_\mu}^2} \quad (6.29)$$

$$i_{dr}{}^{min} \approx -\frac{x_s+x_\mu}{x_\mu} q^{max} - \frac{x_s+x_\mu}{{x_\mu}^2} \quad (6.30)$$

Finally, the pitch angle control is described by the following differential equation:

$$\dot{\theta_p} = (K_P \varphi(\omega_m - \omega_{ref}) - \theta_V)/T_P \quad (6.31)$$

where $K_P$is the pitch control gain, T_P is the pitch control time constant and φ is a function which allows varying the pitch angle set point only if the difference $(\omega_m - \omega_{ref})$ exceeds a predefined value.

Pitch control is illustrated in the following scheme:

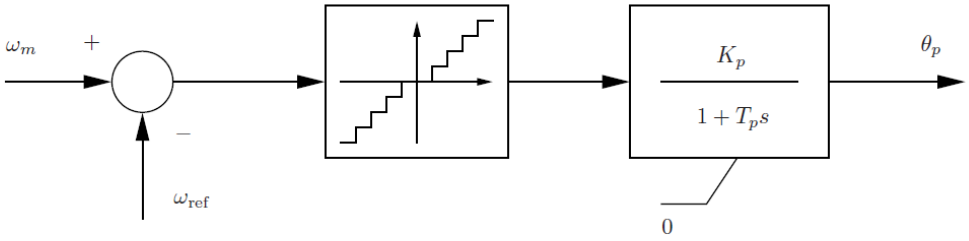

Figure 6.8: Pitch control

7. Identification of a 24 State-Space model

7.1 Introduction to state-space representation of Kundur System

As a first approach on the identification of dynamic models, the three aforementioned identification techniques are going to be applied directly into a 24 state-space system that describes the dynamic behavior of the Kundur System. This system and its respective matrices have been obtained by performing Small Signal Stability Analysis (SSSA) using PSAT after solving the power flow for the Kundur system:

$$A = \begin{bmatrix} A_{1,1} & \cdots & A_{1,44} \\ \vdots & \ddots & \vdots \\ A_{24,1} & \cdots & A_{24,24} \end{bmatrix} = \begin{bmatrix} 0 & 0.3142 & \cdots & 0 \\ \vdots & \vdots & \ddots & \vdots \\ -0.0107 & 0 & \cdots & -5 \end{bmatrix}$$

$$B = \begin{bmatrix} B_1 \\ \vdots \\ B_{24} \end{bmatrix} = \begin{bmatrix} 0 \\ \vdots \\ 363.6364 \\ \vdots \\ 0 \end{bmatrix}$$

$$C = \begin{bmatrix} C_{1,1} & \cdots & C_{1,24} \\ \vdots & \ddots & \vdots \\ C_{11,1} & \cdots & C_{11,24} \end{bmatrix} = \begin{bmatrix} -0.1009 & \cdots & 0 \\ \vdots & \ddots & \vdots \\ -0.0023 & \cdots & 0 \end{bmatrix}$$

$$D = 0 \qquad (7.9)$$

Kundur System is a power system that contains eleven buses and two areas, connected by a weak tie between bus 07 and bus 09. One load and one zip load are connected to the bus 07 while another load along with a second zip load are connected to the bus 09 along. The zip loads are used for retaining the voltage at the buses within acceptable limits by controlling the active and reactive power. Each area of the system consists of two generators, each having a rating of 900 MVA and 20 kV.

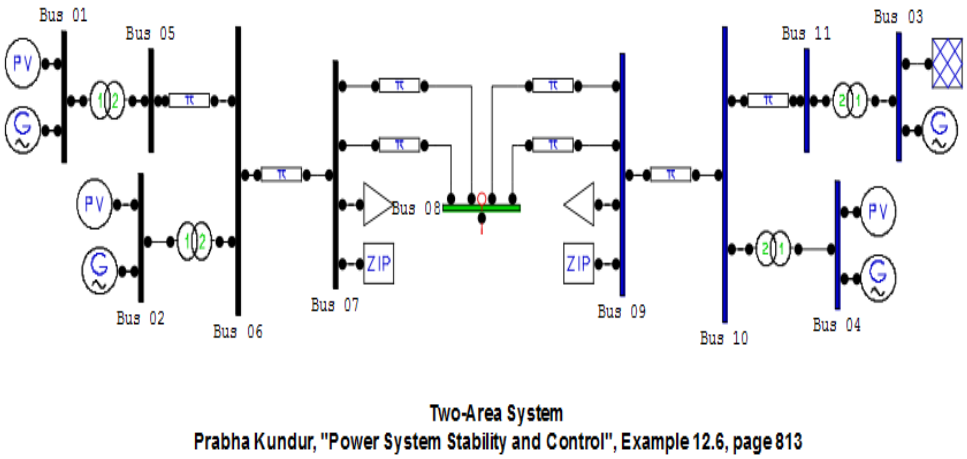

Figure 7.1: Kundur Power System

The original matrix C contains the output of the system measured as the voltage magnitude at the 11 buses comprising the system.

For simplification purposes, the system will be conceptualized as a SISO model where different input signals depending on the identification process are going to be applied. The measured output is the voltage magnitude at the 9th bus. Consequently, the C matrix that is used for the representation of the system (7.9) is replaced by the following:

$$C = [C_{9,1} \quad \cdots \quad C_{9,44}] = [0.1218 \quad \cdots \quad 0] \quad (7.10)$$

7.2 Implementation of ARX Identification technique

ARX is a technique tailored for ambient data, which, as it has been already mentioned corresponds to random low-amplitude variations. For the identification of the 24-state system a signal consisting of random numbers of zero mean value and a standard deviation of 4 is being introduced as input. That input could correspond to the random variations of the load connected to the Buses 07 and 09.

The system is simulated and the response is measured in order to create the estimation data for the identification.

The I/O signals are shown in the next figure:

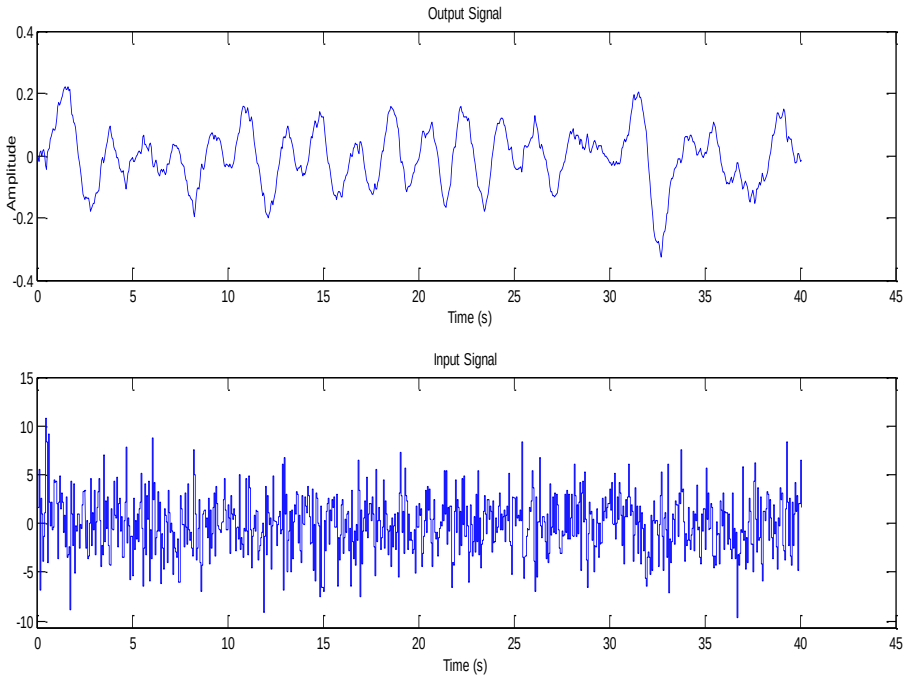

Figure 7.2: Estimation data

The next matrix is used for the construction of the ARX transfer function model as well as for the consideration of the appropriate model order in order to minimize the error between the measured data and the output of the identified model:

$$NN = [n_a\ n_b\ n_k] \quad (7.1)$$

where

- n_a is the order of the polynomial A. In our case, n_a is a vector of values between 1 and 10
- n_b is the order of the polynomial B. In our case, n_a is a vector of values between 1 and 10
- n_k is the input-output delay expressed as fixed leading zeros of the B polynomial.

The input-output delay for our input-output data is zero. This fact is confirmed by the use of *delayest* function in matlab. This command estimates the time delay in a system by estimating a low-order discrete-time ARX model and treating the delay as an unknown parameter.

For validation purposes a completely new signal consisting also of random numbers of a mean value equal to 1 and a standard deviation of 1 is produced.

The I/O validation data are shown in the Fig. 7. 3:

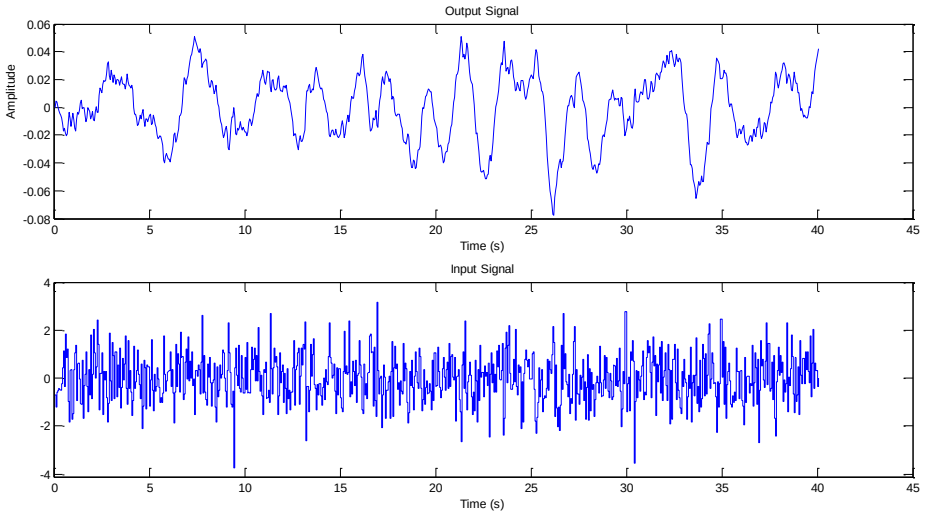

Figure 7.3: Validation data

The Fig. 7.4 shows different ARX models with certain orders and delays.

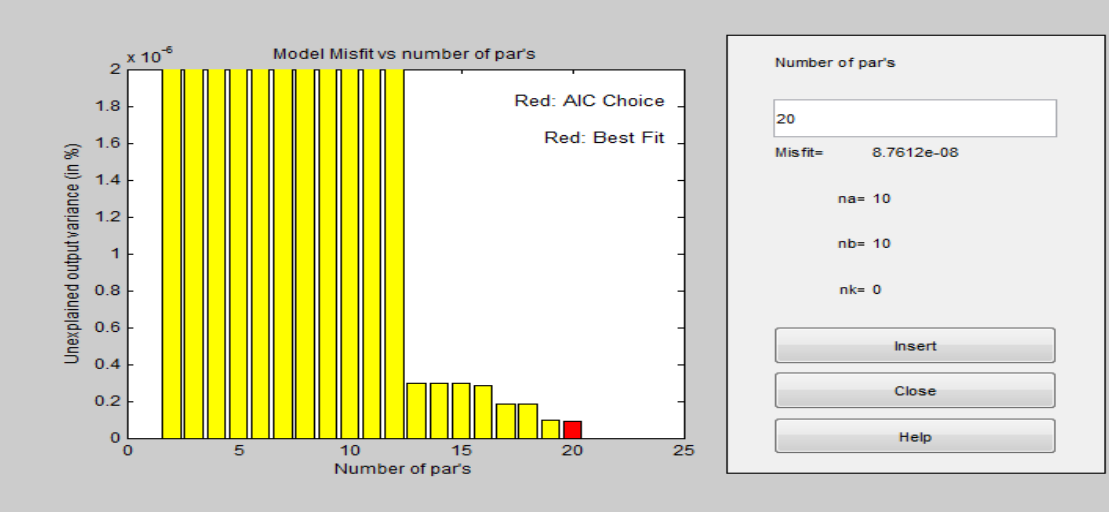

Figure 7.4: ARX model orders

The x-axis shows the total number of parameters in the respective models while the y-axis shows the part of the output variance which is not explained by the model. That is the ratio between the prediction error variance and the output variance in percent:

$$Unexplained\ Ouput\ Variance = \frac{var(Output_{original} - Output_{identified})}{var(Ouput_{original})} \quad (7.3)$$

From Fig. 7.4, the ARX transfer function that corresponds to $n_a = 10,\ n_b = 10$ and $n_k = 0$ minimizes the following two criteria:

- The Best Fit Criterion, which is the Normalized Root Square Mean Error (NRME) and is computed:

:

$$\text{FIT} = 100 * \left(\frac{1 - \|Y - \hat{Y}\|}{\|Y - \bar{Y}\|}\right) \quad (7.4)$$

where

Y is the output of the validation data
$\hat{Y}$ is the identified system output
$\bar{Y}$ is the mean value of the validation data

- The Akaike Information Criterion (AIC), which is defined:

$$AIC = \log V + \frac{2d}{N} \quad (7.5)$$

where

V is the loss function and is defined by the following equation:

$$V = \det\left(\frac{1}{N}\sum_{1}^{N}\varepsilon(t,\widehat{\theta_N})(\varepsilon(t,\widehat{\theta_N}))^T\right) \quad (7.6)$$

and

d is the number of estimated parameters
N is the number of values in the estimation data set

After simulations for sampling time varying from 0.01 sec to 0.125 sec, the optimum sampling time has been computed at 0.05 sec and the optimum order of the transfer function as it is mentioned above is [10 10 0].

The output of the system overlaid with the validation data and their respective Fitness is shown in the Fig. 7.5:

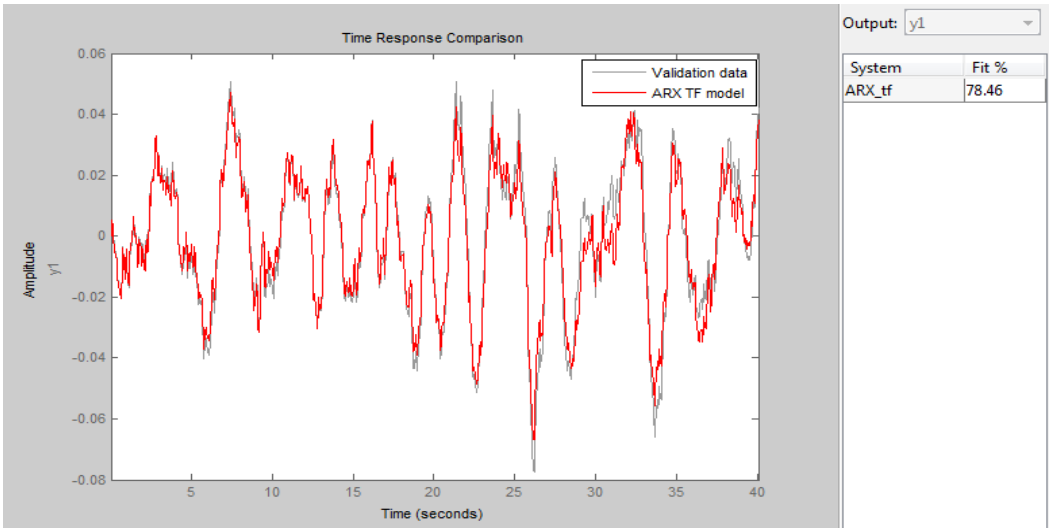

Figure 7.5: Comparison and Fitness between the output of the original and the ARX transfer function model.

7.3 Implementation of ARMAX Technique

The implementation of ARMAX does not differ significantly from that of ARX technique. The only difference between these two methods is that ARMAX contains the moving average part C(q)e(t) which describes the equation error. Consequently, that transfer function model needs also the C(q) polynomial in order to be defined.

The I/O signals for the estimation and validation of the ARMAX models that are going to be constructed are exactly the same with those that were used for ARX in order to compare and assess the efficiency of the two methods.

The next matrix is used for the construction of the ARMAX transfer function model as well as for the consideration of the appropriate model order in order to minimize the error between the estimation data and the output of the identified model:

$$NN = [n_a\ n_b\ n_c\ n_k] \quad (7.7)$$

where

- n_a is the order of the polynomial A. In our case, n_a is a vector of values between 1 and 10.
- n_b is the order of the polynomial B. In our case, n_b is a vector of values between 1 and 10.
- n_c is the order of the polynomial C In our case, n_c is a vector of values between 1 and 10.
- n_k is the input-output delay expressed as fixed leading zeros of the B polynomial. In our case, it is equal to zero.

Different sampling times varying from 0.01 sec to 0.125 sec are tested and models of all the aforementioned orders have been constructed in order to find the optimum table NN that minimizes the Fitness Criterion.

The next table displays the Fitness of the ten ARMAX models with the maximum Fit to validation data at sampling time equal to 0.05 sec:

Model Order	Fitness
$[n_a = 9\ n_b = 9\ n_c = 6\ n_k = 0]$	99.9988
$[n_a = 8\ n_b = 8\ n_c = 6\ n_k = 0]$	99.9988
$[n_a = 10\ n_b = 10\ n_c = 9\ n_k = 0]$	99.9989
$[n_a = 10\ n_b = 10\ n_c = 7\ n_k = 0]$	99.9990
$[n_a = 10\ n_b = 8\ n_c = 6\ n_k = 0]$	99.9991
$[n_a = 10\ n_b = 10\ n_c = 6\ n_k = 0]$	99.9993
$[n_a = 10\ n_b = 10\ n_c = 10\ n_k = 0]$	99.9994
$[n_a = 10\ n_b = 8\ n_c = 8\ n_k = 0]$	99.9994
$[n_a = 8\ n_b = 8\ n_c = 4\ n_k = 0]$	99.9996
$[n_a = 9\ n_b = 9\ n_c = 9\ n_k = 0]$	99.9996

Table 7.1: Model orders and the respective Fitness

From the Table 7.1 the optimum order can be set:

$$NN = [n_a = 8 \ n_b = 8 \ n_c = 4 \ n_k = 0] \quad (7.8)$$

At that point it is worth mentioning that given that the difference in Fitness between these ten models is insignificant for simplicity purposes the minimum order could be chosen to describe the system even if it doesn't correspond to the maximum Fit.

The output of the system overlaid with the validation data and their respective Fitness is shown in the next figure:

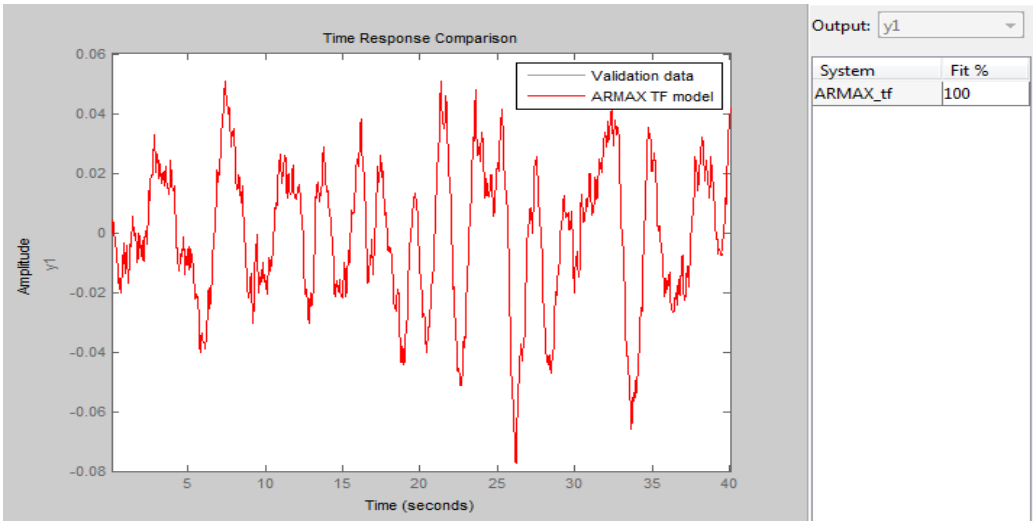

Figure 7. 6: Comparison and Fitness between the output of the original and the ARMAX transfer function model.

7.4 Comparison of the efficiency of ARMAX and ARX models

The next figure shows the eigenvalues of the original system, the armax and the arx transfer function models:

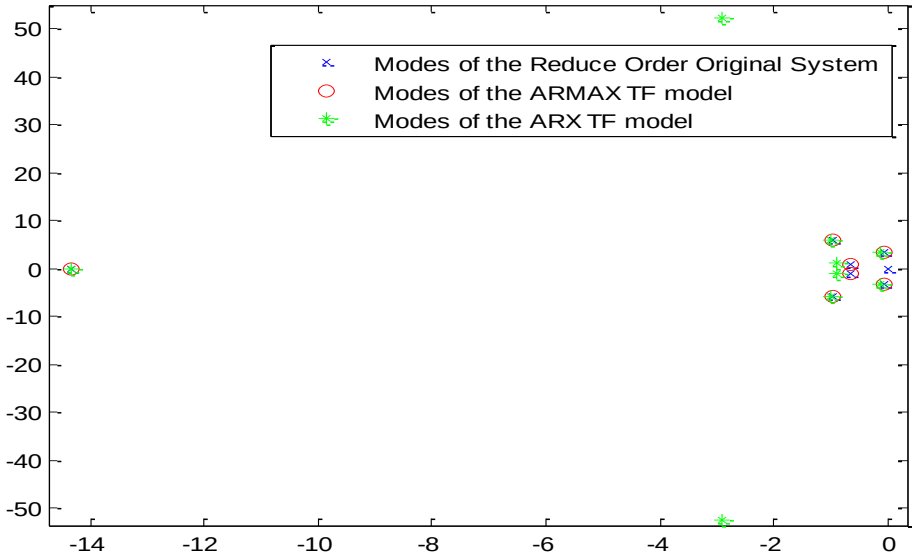

Figure 7. 7: Comparison of the the eigenvalues between the original, the ARX and the ARMAX transfer function models

The bode plots for the three models are shown below:

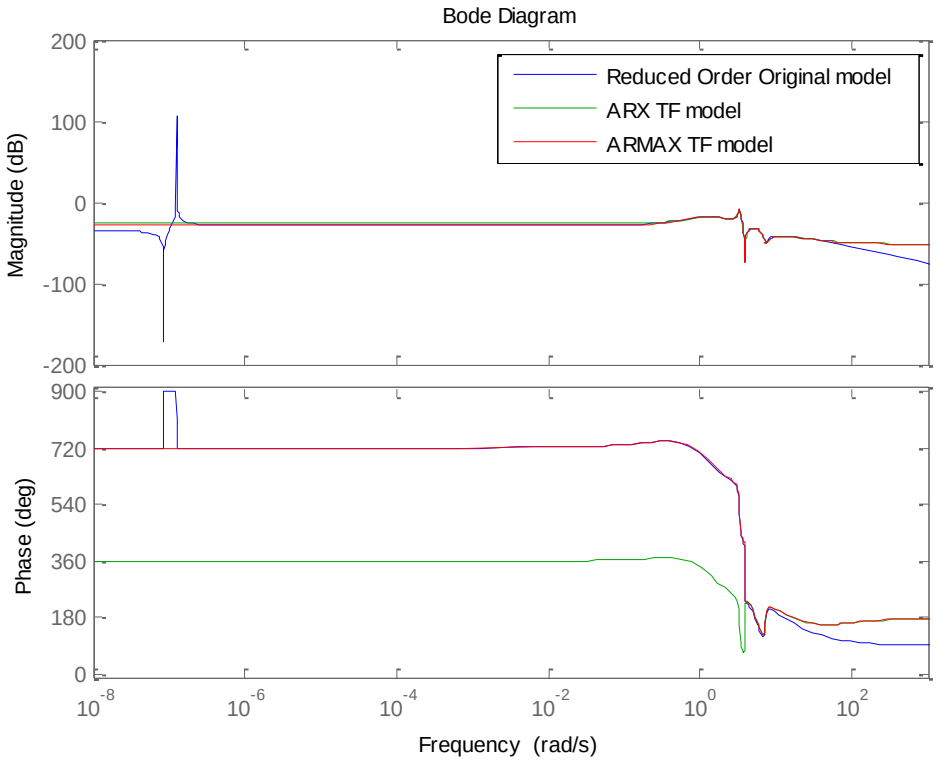

Figure 7.8: Comparison of bode diagrams between the original, ARMAX and ARX transfer function models

7.5 Implementation of Eigensystem Realization Algorithm

The system is excited by a Dirac input in order to extract the impulse response of the system (ringdown data), a mandatory requirement for the ERA.

The response of the system can be shown in the next figure:

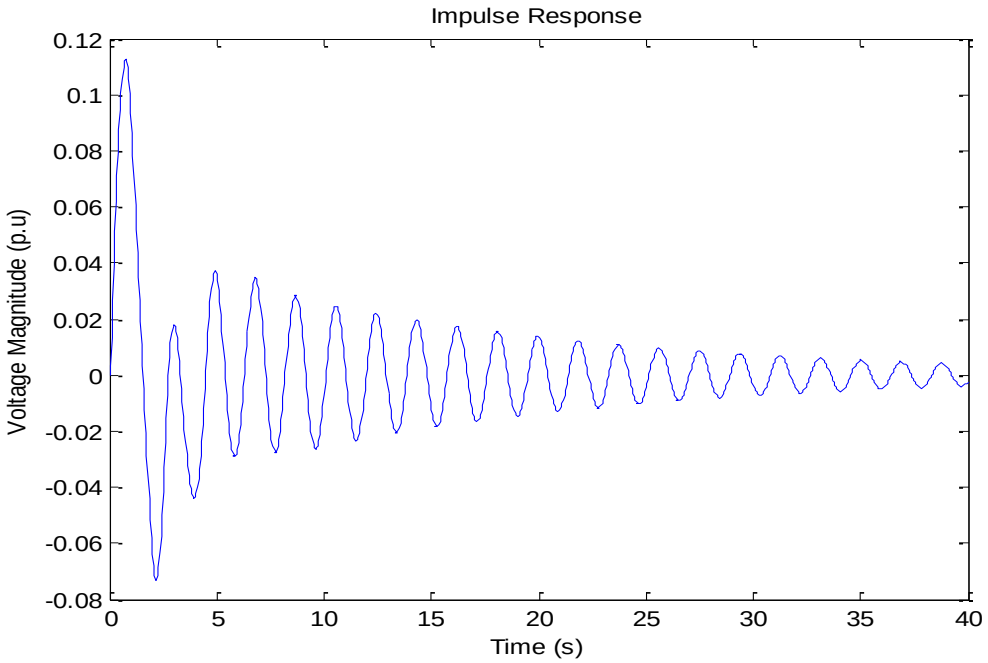

Figure 7.9: System's impulse response

mode	Nfreq(rad/s)	freq(Hz)	Damp	residue	energy
1	2.6826	0.0000	1.0000	6.7648	0.9712
2	1.1732	0.1130	0.7961	5.2504	0.9712
3	1.1732	0.1130	0.7961	5.2504	0.2068
4	6.8409	0.1418	0.9915	2.6448	0.2068
5	6.8409	0.1418	0.9915	2.6448	4.0433
6	3.3396	0.5314	0.0185	0.4772	4.0433
7	3.3396	0.5314	0.0185	0.4772	0.0969
8	16.8722	0.8688	0.9462	0.4676	0.0969
9	16.8722	0.8688	0.9462	0.4676	0.5279
10	6.0964	0.9669	0.0838	0.2867	0.5279
11	6.0964	0.9669	0.0838	0.2867	0.5800
12	29.4948	0.0000	1.0000	0.1354	0.5800
13	6.2473	0.9916	0.0737	0.1196	0.1769
14	6.2473	0.9916	0.0737	0.1196	0.1769
15	26.2628	0.0000	1.0000	0.0057	0.2222
16	0.0346	0.0000	-1.0000	0.0017	0.2222
17	119.6835	0.0000	1.0000	0.0004	0.0500
18	62.8835	10.0000	0.0405	0.0000	0.0528
19	62.8835	10.0000	0.0405	0.0000	0.0539
20	50.9031	8.0971	0.0329	0.0000	0.2125
21	50.9031	8.0971	0.0329	0.0000	215.7821

Table 7.2: Singular Values of the identified system

The eigenvalues of the system are sorted according to their respective residue and, as it can be shown from the Table 7.2, the first 9 modes are selected for the representation of the system.

The impulse response of the continuous transfer function model that has been extracted by applying ERA is compared to the original response of the system in the figures below:

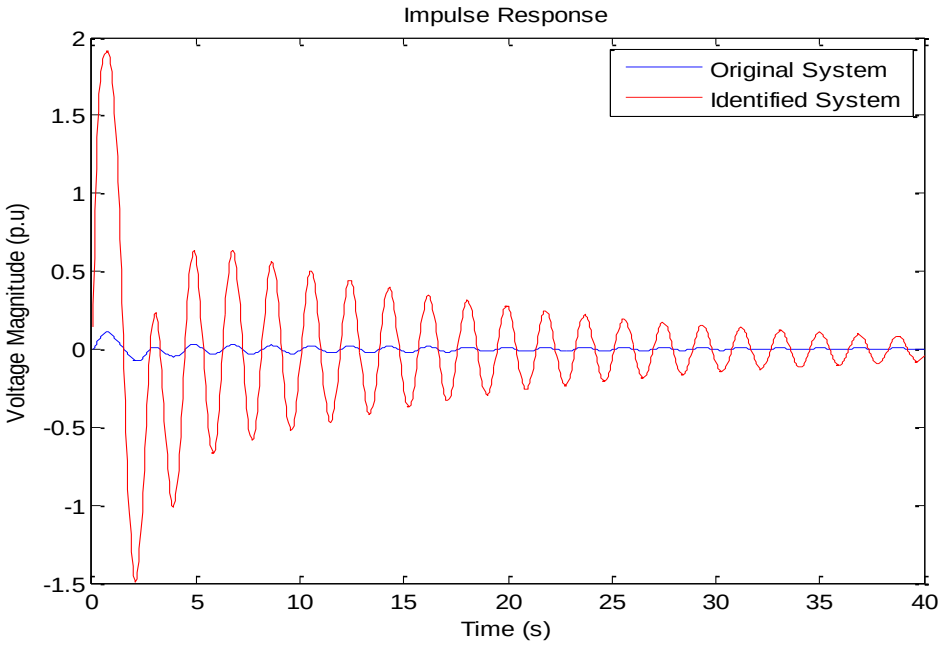

Figure 7.10: Comparison of original and identified system's impulse responses

It can be concluded from the Fig 7.10 that there is a voltage magnitude between these two signals whereas their frequencies are similar. The voltage magnitude difference is going to be computed as a constant gain in the transfer function model of the identified system.

After computations that will be described extensively in Chapter 8, the constant Gain G_a has been found:

$$G_a = 17.6376 \quad (7.11)$$

The constant gain has been contained in the identified transfer function and consequently the transfer function has been re-transformed into the state space representation.

After all these calculations and transformations, the new state space model differs from the initial one only in constant gain. That can be confirmed also from the bode diagrams of the two identified systems:

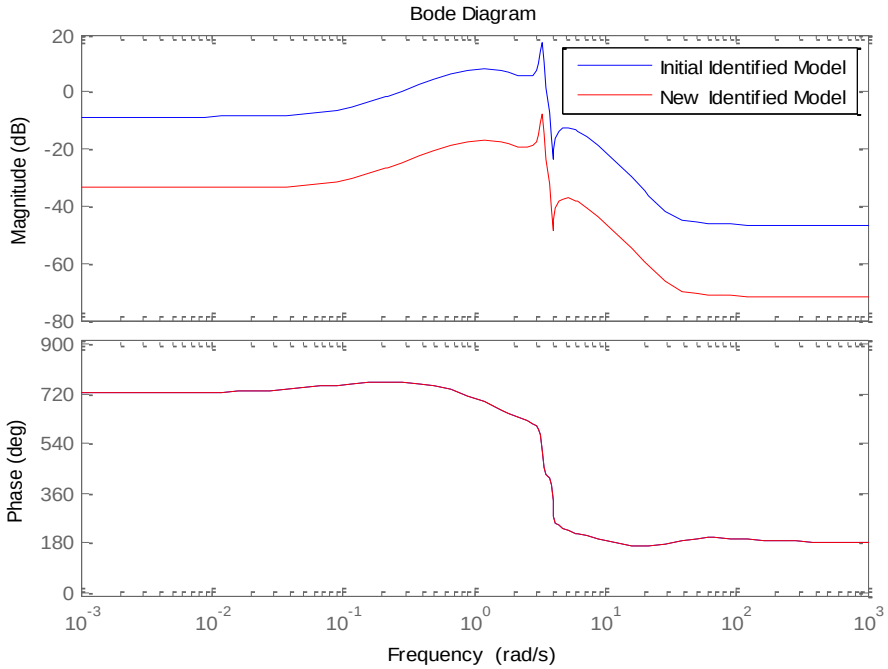

Figure 7.11: Comparison between the identified transfer function with and without G_a

The phase bode are exactly the same while the magnitude bode differ only in magnitude with the difference been equal to 24.92dB ($20 * \log_{10} G_a$) as expected.

The new impulse response of the identified system comparing to the impulse response of the original one is shown below:

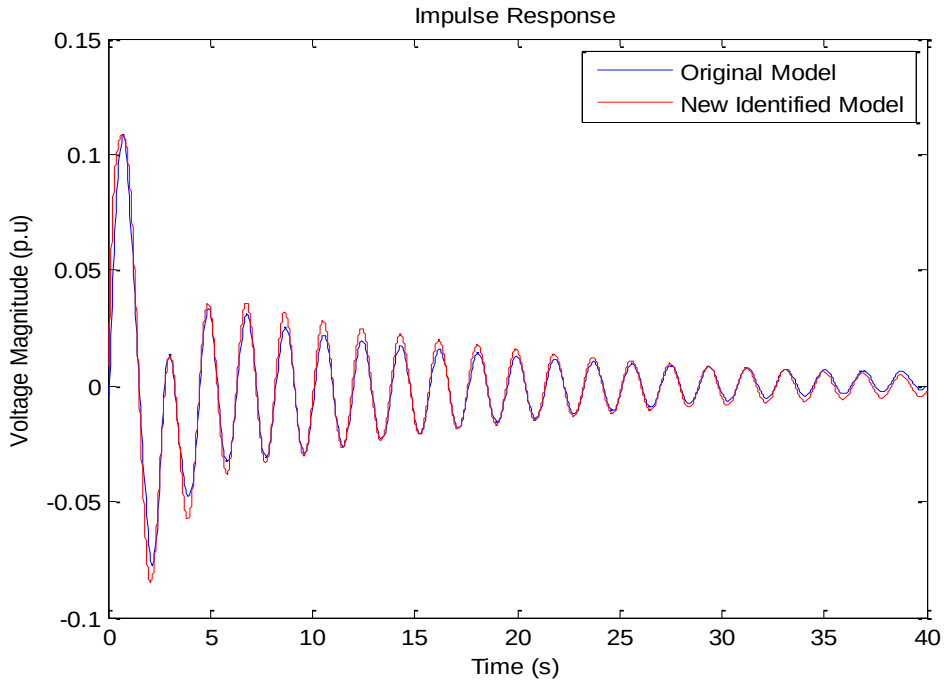

Figure 7.12: Comparison between the original and the identified models

In order to evaluate the efficiency of ERA, a signal constructed by random values drawn from a normal distribution with a zero mean value and a standard deviation of 3 is applied as input signal for the two systems. The input and output of the system are going to be used as validation data for the identification and are shown in the Figure 7.12:

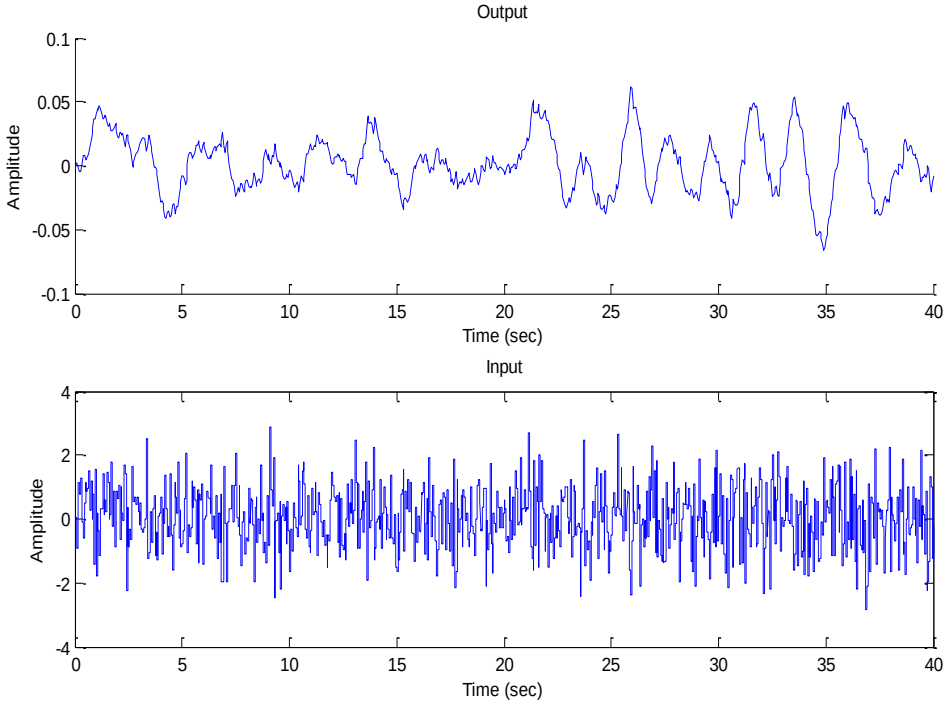

Figure 7.13: Validation data

The next step of the validation process is to simulate and compare the response of the system that is identified using ERA to the response of the original system in order to evaluate the results of the identification procedure.
The simulation results of the two systems can be shown in the next figure:

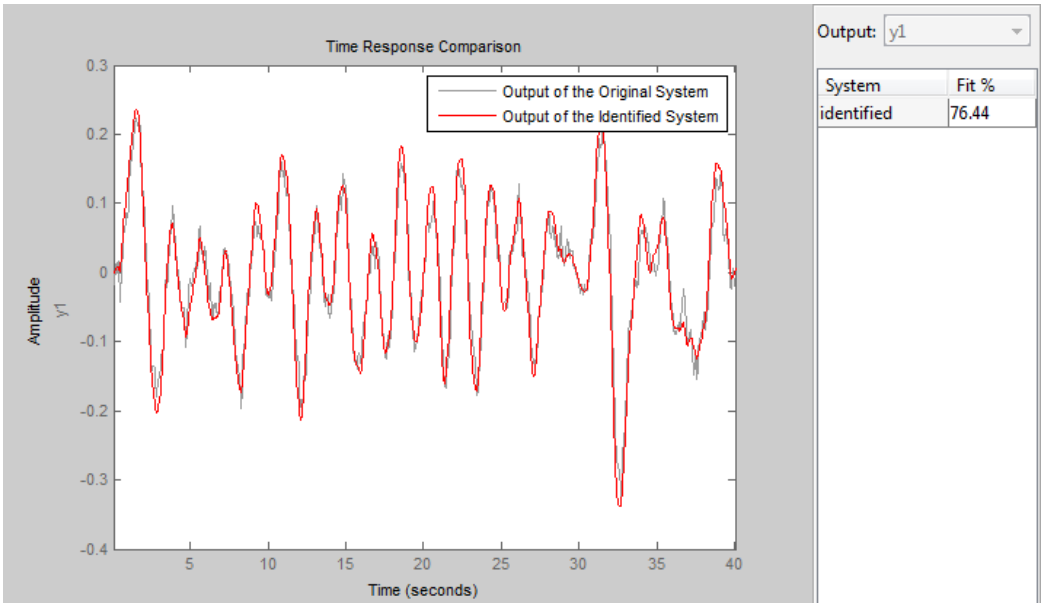

Figure 7.14: Comparison and Fitness between the output of the original and the identified model.

As an additional validation step and given that the state space representation of the original system is already known, it is feasible to compare the eigenvalues of the two systems as well as their respective bode diagram plots.

Before comparing the eigenvalues of the two systems it would be easier for practical purposes to figure out if a mode truncation technique could be applied in the original system in order to compare systems with similar model orders. The HSVD method is selected and the criterion for the mode truncation is the magnitude of the HSVs and consequently the amplitude of the state energies as they have been described in section 4.4.3.

The next figure displays the states with their respective contribution in the transfer function by using the State Energy indicator:

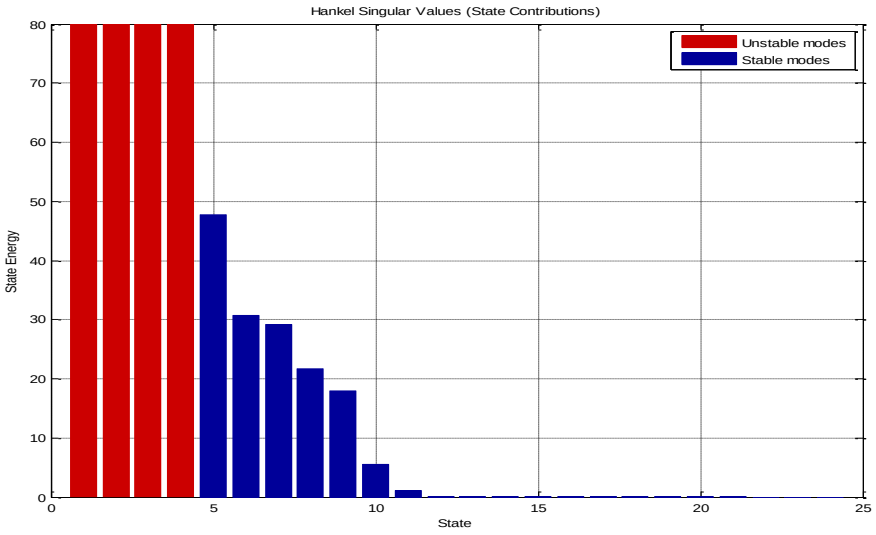

Figure 7.15: State contribution based on HSVs

As it can be seen, most of the energy is presented in the first 10 orders and consequently the higher model orders can be discarded. Proof of this is displayed below where the bode diagrams of the full order and the truncated system are overlaid at the same figure:

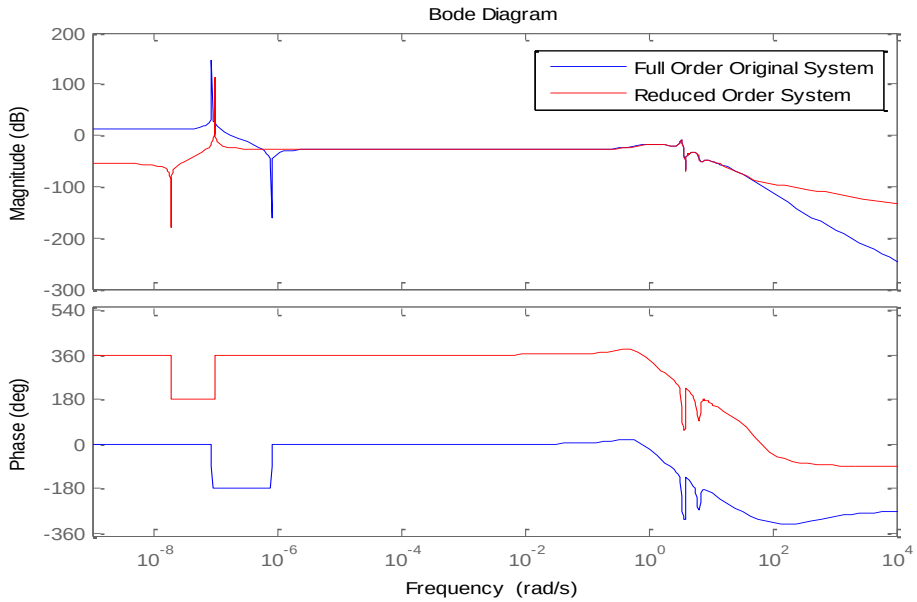

Figure 7.16: Comparison of bode diagrams between full and reduced order original system.

It can be safely deduced that the reduced order system describes the systems dynamics without losing too much information. This phase bode (blue and green) are exactly the same (a difference of 360°) while the magnitude bode of the identified naturally agrees with the magnitude bode of the full order up to 50 rad/s. After that frequency the slope of the full order system is steeper due to the existence of poles in higher frequencies.

The Fig. 7.17 shows the eigenvalues of the original and the identified system:

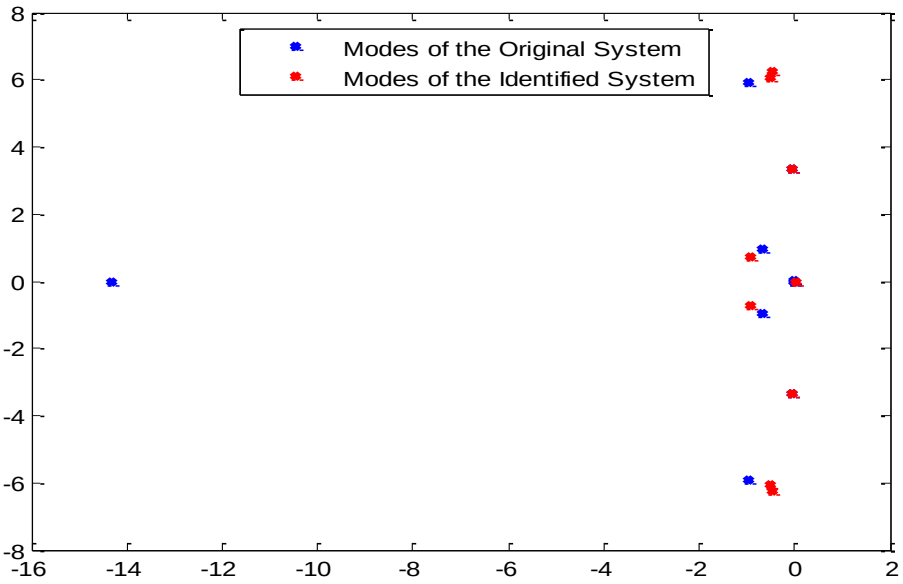

Figure 7.17: Comparison of the eigenvalues between original and identified models

The respective bode diagrams:

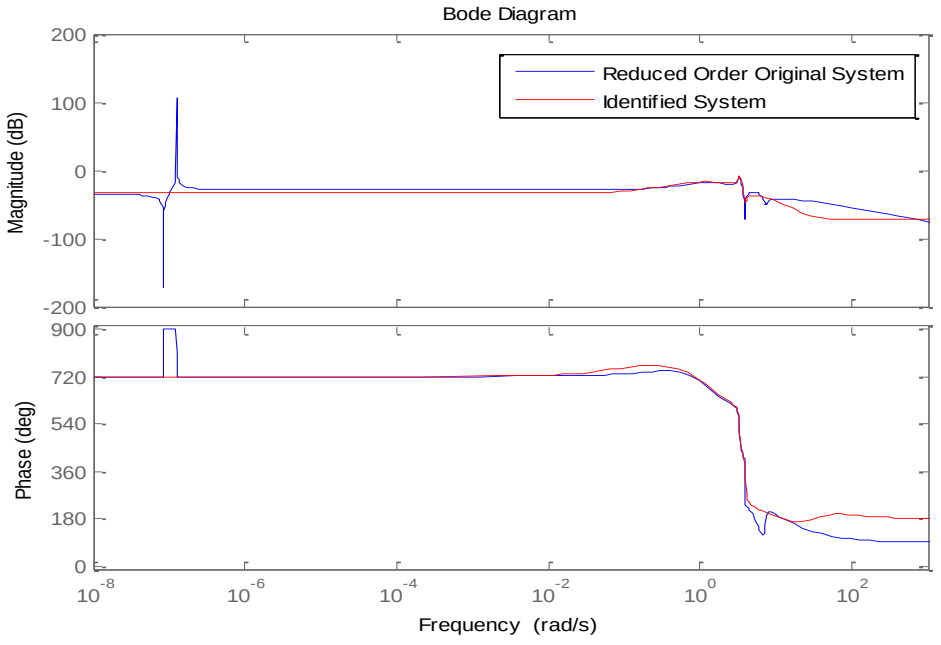

Figure 7.18: Comparison of bode diagrams between the original and the identified models

7.6 Conclusion

From the Fig. 7.5-7.9 it can be concluded that ARX and especially ARMAX can produce adequate models that preserve both the time-domain and the frequency domain information of the original model. The eigenvalues of the ARMAX transfer function and their damping rations and frequencies exactly match those of the original system with the only exception of the original's system double pole at zero, while the modes of ARX are extremely close to the modes of the original system.

On the other hand, the results of the ERA construct a model that captures the main system dynamics, and the overall fit for the estimation data as well as for the validation data is high. The eigenvalues of the two systems are very close and consequently the values of the damping ratios and frequencies of the modes are very close as well, a fact that is reverberated by the high fitness presented in Fig. 7.12 & Fig. 7.14. Finally the frequency response of the systems (Bode diagrams) confirms the aforementioned observations.

8. Identification of Wind Farm in IEEE 14 Bus Power System

8.1 Description of IEEE-14 Bus Power System

The system that is used for the implementation of the various identification processes is the IEEE 14-bus system which is a benchmark in power system analysis. This test case represents a portion of the American Electric Power System as of February, 1962. The 14 bus power system does not have line limits. Compared to recent power systems, it has low base voltages and overabundance of voltage control capability. It consists of 4 synchronous generators and a wind park of 30 DFIGs with a total capability of producing 600 MVA:

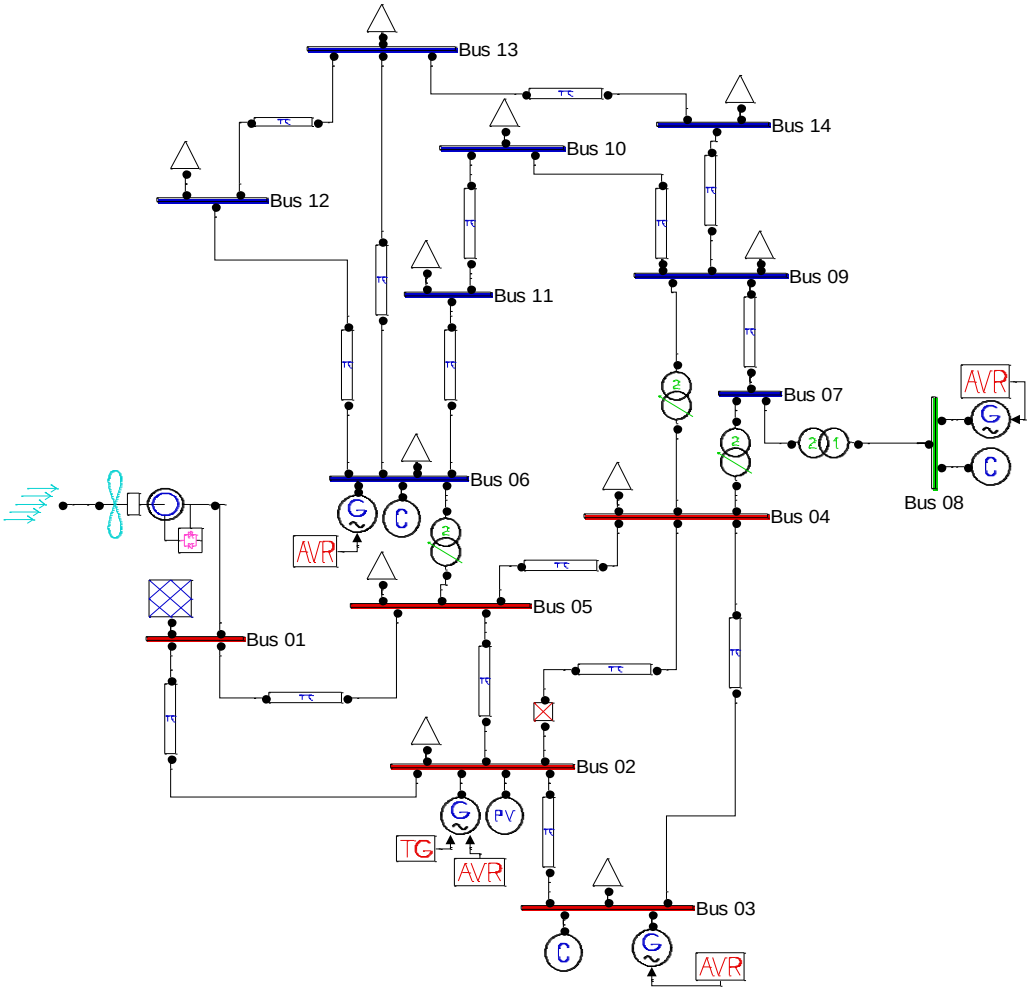

Figure 8.1: IEEE-14 Bus system with Wind Farm

8.2 Implementation of ARX Identification technique

A first step in the identification of a dynamic model is the implementation of ARX method, the simplest among the three that are going to be used in the context of this thesis. The dynamic model under identification is the wind park which is considered an aggregated model of 30 DFIG's. It is conceived as a Multi Input Multi Output (MIMO) system with two input and two output channels and ARX, which is an I/O identification technique, is going to be applied to the signals described below:

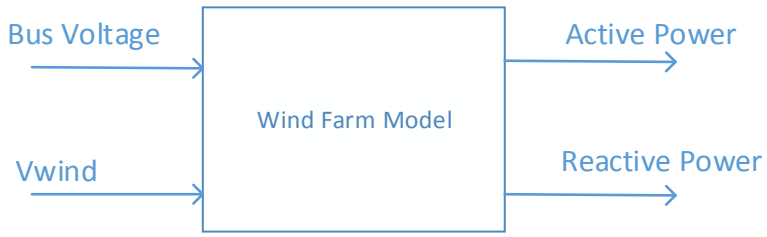

Figure 8.2: Wind Farm identification block

Input Signals:

- The signal that obviously is needed for the identification is the wind speed. Wind is the driving force of the Wind Turbine. For that reason, evidently, wind speed should be considered as an input signal for that system.
- The second signal is not as obvious as an input as the wind speed. It is known that the active and reactive power injected into the grid by a DFIG, and consequently by a wind farm consisting of DFIGs, depends on the grid side currents of the converter. It has been also mentioned that the converter is modeled as an ideal current source $\mathrm{I_{dr}}$ and is used for the control of the voltage, so one can deduce that the voltage of the bus that the wind farm is connected to can be used as an input which controls the amount of power that the wind turbines produce.

Output Signals:

- Active Power injected into the grid.
- Reactive Power injected into the grid.

The wind speed model that is used for this test case is the Weibull's distribution which is defined as follows:

$$f(v_w, c, k) = \frac{k}{c^k} {v_w}^{k-1} e^{-(\frac{v_w}{c})^k} \quad (8.1)$$

where

- v_w is the wind speed
- c and k are constants as defined in the wind model data matrix.

Time variations ξ_w of the wind speed are obtained by means of a Weibull's distribution, as follows.

$$\xi_w(t) = \left(-\frac{\ln\iota(t)}{c}\right)^k \quad (8.2)$$

where $\iota(t)$ is a generator of random numbers between zero and on ($\iota \in [0,1]$).

Finally, the wind speed is computed by setting the initial average speed ${v_w}^a$ determined as the initialization step as mean speed:

$$v_w(t) = (1 + \xi_w(t) + \widehat{\xi_w}(t)){v_w}^a \quad (8.3)$$

where $\widehat{\xi_w}$ is the mean value of ξ_w.

The wind speed time evolution generated using the Weibull's distribution with a nominal wind speed value of 15 m/s is depicted in the next figure:

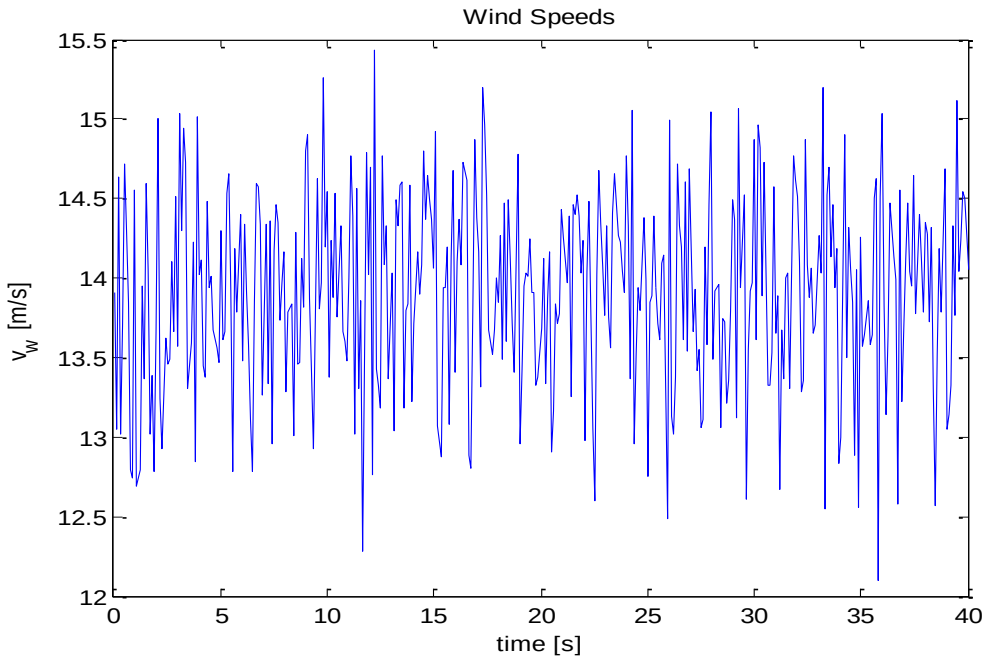

Figure 8.3: Wind speed timeseries

In order to smooth the high frequency wind speed variations over the rotor surface, a low-pass filter with a time constant τ=4 sec is applied to the signal $\hat{v}_w$. The output of the filter constitutes the input signal of the identification procedure:

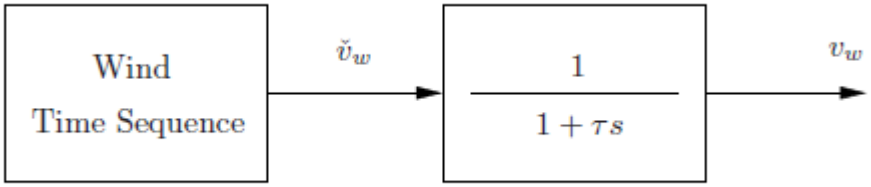

Figure 8.4: Filtering of wind time sequence

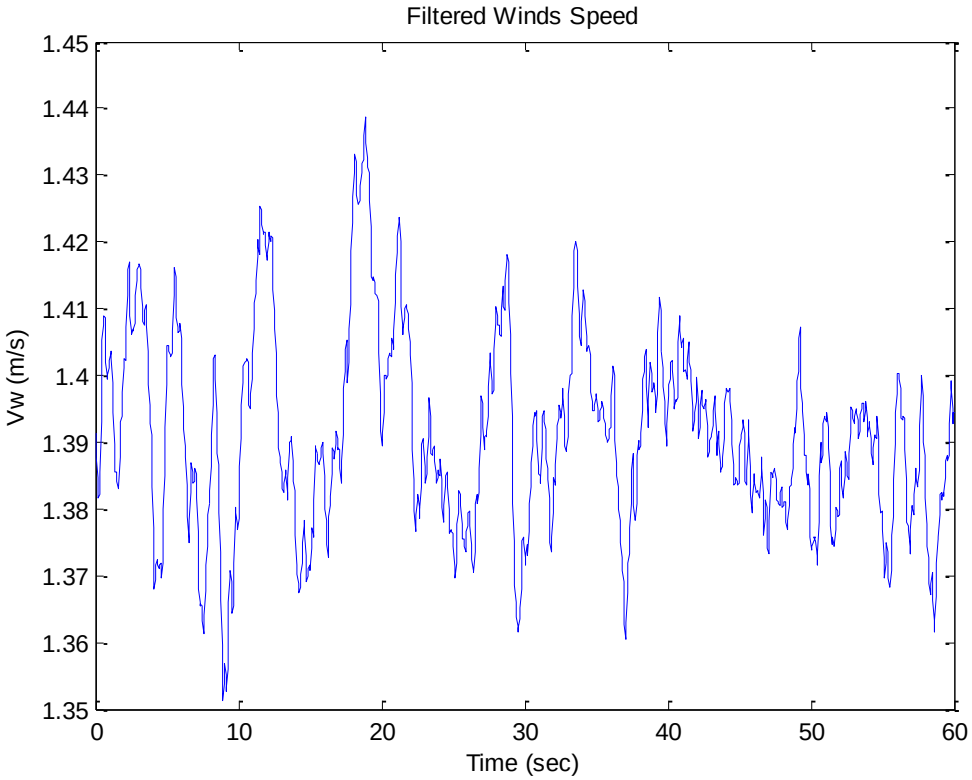

Figure 8.5: Filtered wind speed timeseries

PSAT GUI is used for the power flow analysis as well as for the time domain of the system for 60 seconds, and the injected active and reactive powers are measured in the Bus 01. Before applying ARX and ARMAX, the input and output signals need to be pre-processed:

- Firstly, the data are detrended by computing and subtracting the mean of each measurement from each corresponding value of the bus voltage, wind speed active and reactive power.
- Secondly, a data window that contains ambient data is selected. This window should be "large" enough in order to secure that the estimation will be based on enough data and consequently the identification results will be more reliable. It is important to mention at that point that the selection of the data window lies on the analyst's experience and intuition and that there are no norms or rules for the successful

selection of a "proper" window. For that reason, different windows of data are tested for a specific data set in order to choose the one that produces good estimates.

- Lastly, all the measurements are per unit. The power base is selected at $S_A = 100$ MVA, the bus voltage base is 69 kV (the voltage rating value at that Bus) and the base of wind speed is 15 m/s, equal to the nominal wind speed.

Finally, the sampling interval has been set up to 0.05 seconds and the data window that produces the best estimates lies between 0.4 sec and 60 sec ($0.4 \leq t_w \leq 60$ sec) consisting of 638 samples.

The signals that are used for the identification are shown in the next figure:

Input:

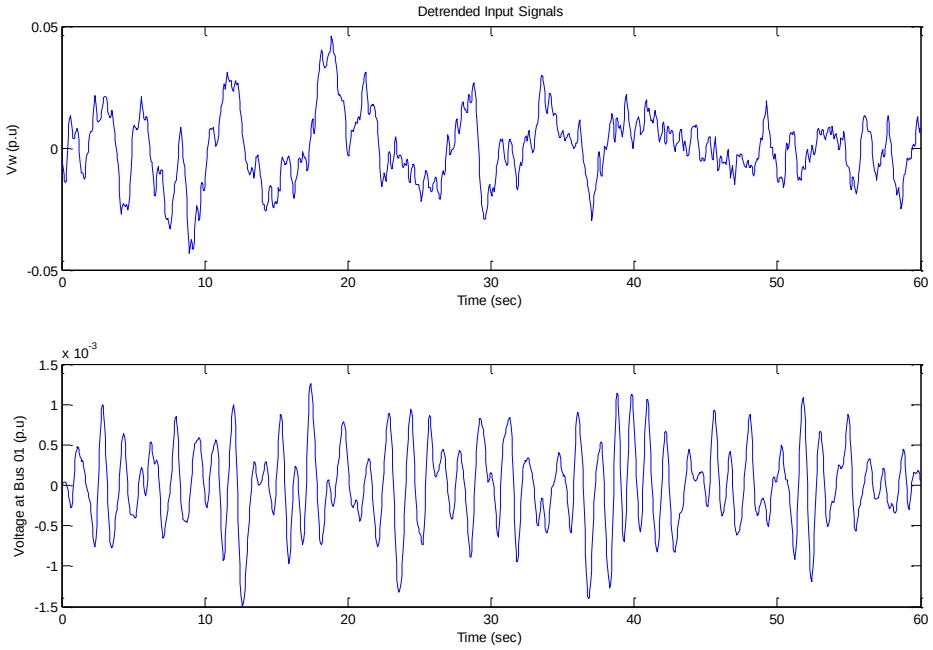

Figure 8.6: Detrended input signals

Output:

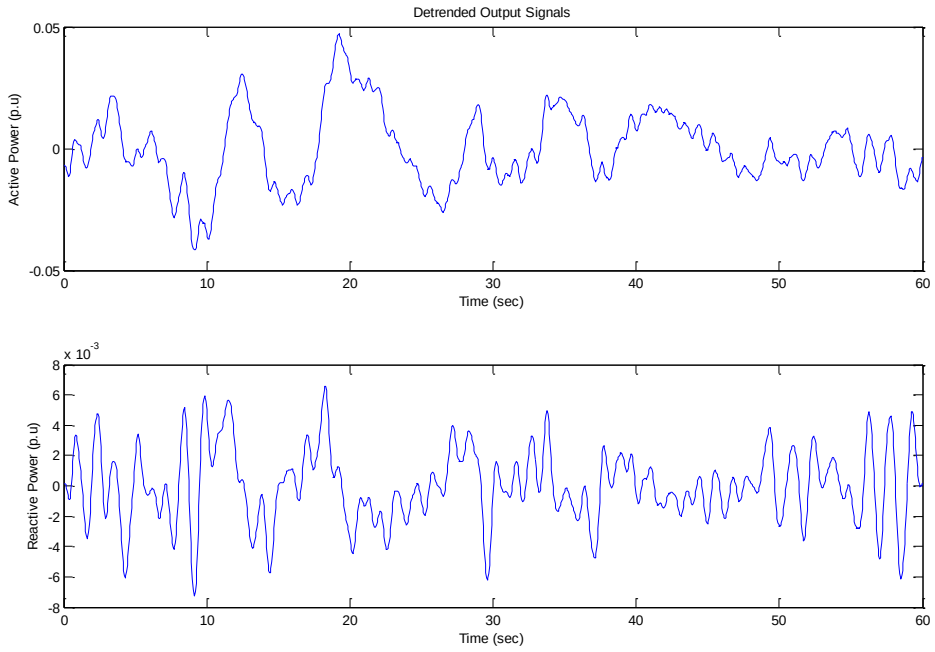

Figure 8.7: Detrended output signals

It is of significant importance to mention that in order to estimate a model and validate it according to a data set, a typical way is to divide the series into two subgroups. The first subgroup is called estimation data group and is used to apply each identification procedure and construct the identified model. The second subgroup is called validation data group and is used to evaluate the performance of the model that was built according to the estimation data.

In this chapter of the thesis as it has been already described, the PSAT simulation tool is used in order to extract the signals that compose the input and output of the wind farm. Consequently, given that simulation tools enable user to re-simulate the power grid under the same conditions (with the wind speed series as the only difference) and extract new data sets, it is decided to use the data of the first simulation as estimation data, and the data derived from the second and last simulation as validation data. For the last simulation, the power flow and the time domain simulation of the system run one more time additionally.

The Wind Farm of the IEEE 14-Bus power system is a MIMO system and in order to compute the ARX function, the delay between input and output as well as the polynomials A and B are conceived as matrices instead of integers in case of a SISO model. The construction of the ARX function uses the table that is shown below:

$$\text{table} = [\text{varying\_order} * \text{n}_\text{a}, \text{varying\_order} * \text{n}_\text{b}, \text{varying\_order} * \text{n}_\text{k}] \quad (8.4)$$

- $\mathrm{n_a}$ is the order of the polynomial A (5.10) and it is specified as a N_y-by-N_y matrix where $N_y$is the number of outputs of the system. In our case, it is a 2-by-2 matrix.
- $\mathrm{n_b}$ is the order of the polynomial $B + 1$ and it is specified as a N_y-by-$N_u$matrix where $N_y$is the number of outputs and $N_u$the number of inputs of the system. In our case, it is a 2-by-2 matrix.
- $\mathrm{n_k}$ is the input-output delayed expressed as fixed leading zeros of the B polynomial and it is specified as a N_y-by-$N_u$matrix. In our case, it is a 2-by-2 matrix.

The comparison between the validation data and the output of the identified model is realized with the use of the Fitness Criterion as is already described in eq. (7.4).

It is already stated that the nominal sampling time from PSAT is set up to 0.05 sec. This sampling rate is being changed in each iteration of the program using anti-aliasing (lowpass) FIR filter to the signals. Furthermore, the model orders that are tested are limited to six in order to secure that the identified system will retain its simplicity. Finally the following table summarizes the results of the experiments that maximize the Fit Criterion for the ARX method:

n_a	n_b	n_k	Sampling Time	Fit Criterion for Active Power	Fit Criterion for Reactive Power
$\begin{bmatrix} 6 & 6 \\ 6 & 6 \end{bmatrix}$	$\begin{bmatrix} 2 & 0 \\ 0 & 2 \end{bmatrix}$	$\begin{bmatrix} 0 & 0 \\ 0 & 0 \end{bmatrix}$	0.1 sec	86.8924	94.4224
$\begin{bmatrix} 4 & 4 \\ 4 & 4 \end{bmatrix}$	$\begin{bmatrix} 2 & 2 \\ 2 & 2 \end{bmatrix}$	$\begin{bmatrix} 0 & 0 \\ 0 & 0 \end{bmatrix}$	0.056 sec	87.6629	97.2513
$\begin{bmatrix} 4 & 4 \\ 4 & 4 \end{bmatrix}$	$\begin{bmatrix} 2 & 2 \\ 2 & 2 \end{bmatrix}$	$\begin{bmatrix} 0 & 0 \\ 0 & 0 \end{bmatrix}$	0.0833 sec	87.9016	96.4017
$\begin{bmatrix} 3 & 3 \\ 3 & 3 \end{bmatrix}$	$\begin{bmatrix} 2 & 2 \\ 2 & 2 \end{bmatrix}$	$\begin{bmatrix} 0 & 0 \\ 0 & 0 \end{bmatrix}$	0.071 sec	88.2499	97.0945
$\begin{bmatrix} 6 & 6 \\ 6 & 6 \end{bmatrix}$	$\begin{bmatrix} 5 & 0 \\ 0 & 5 \end{bmatrix}$	$\begin{bmatrix} 0 & 0 \\ 0 & 0 \end{bmatrix}$	0.1 sec	92.2852	99.2410

Table 8.1: Fit Criterion for different ARX model orders

The grey shaded row reveals the optimum combination of order and sampling frequencies among the ones that have been tested. The graphs for the comparison between the validation data and the identified ARX output are the following:

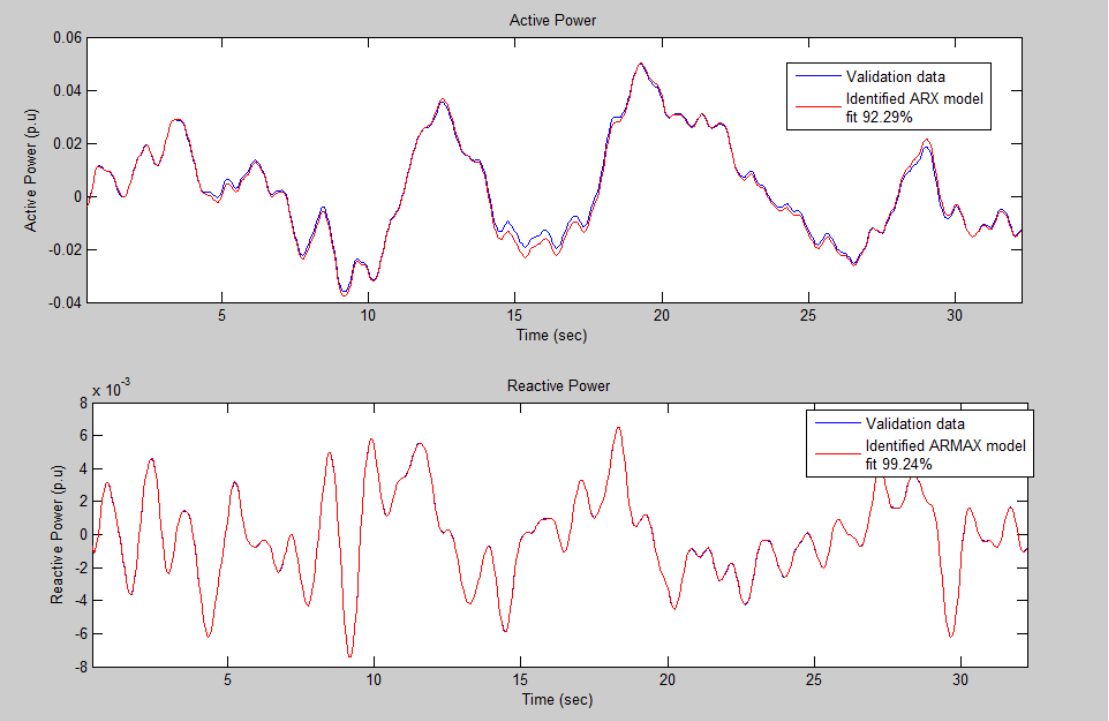

Figure 8.8: Comparison between the output of the original model and the ARX transfer function model

8.3 Implementation of ARMAX Identification technique

The table that is used for the construction of the ARMAX transfer function is similar to the table defined in eq. (8.4):

$$\text{table} = [\text{varying}_{\text{order}} * \text{n}_\text{a}, \text{varying}_{\text{order}} * \text{n}_\text{b}, \text{varying}_{\text{order}} * \text{n}_\text{c}, \text{varying\_order} * \text{n}_\text{k}]$$

where

$\text{n}_\text{a}, \text{n}_\text{b}, \text{n}_\text{k}$ have been described in the Chapter 8.3

and

n_c is the order of the polynomial $C(q)$, specified as a column vector of nonnegative integers of length N_y.

The model orders that are tested here are limited to six as they have been set in the ARX implementation in order to simplify the model. Finally, the next table summarizes the results of the experiments that maximize the Fit Criterion for the ARMAX method:

n_a	n_b	n_c	n_k	Sampling Time	Fit Criterion for Active Power	Fit Criterion for Reactive Power
$\begin{bmatrix}6 & 6\\ 6 & 6\end{bmatrix}$	$\begin{bmatrix}6 & 6\\ 6 & 6\end{bmatrix}$	$\begin{bmatrix}6 & 6\\ 6 & 6\end{bmatrix}$	$\begin{bmatrix}0 & 0\\ 0 & 0\end{bmatrix}$	0.05 sec	92.2488	99.1362

$\begin{bmatrix}5 & 5\\5 & 5\end{bmatrix}$	$\begin{bmatrix}5 & 5\\5 & 5\end{bmatrix}$	$\begin{bmatrix}5 & 0\\0 & 5\end{bmatrix}$	$\begin{bmatrix}0 & 0\\0 & 0\end{bmatrix}$	0.05 sec	92.4884	99.0476
$\begin{bmatrix}4 & 4\\4 & 4\end{bmatrix}$	$\begin{bmatrix}2 & 2\\2 & 2\end{bmatrix}$	$\begin{bmatrix}0 & 0\\0 & 0\end{bmatrix}$	$\begin{bmatrix}0 & 0\\0 & 0\end{bmatrix}$	0.05 sec	92.6442	99.4545
$\begin{bmatrix}3 & 3\\3 & 3\end{bmatrix}$	$\begin{bmatrix}2 & 2\\2 & 2\end{bmatrix}$	$\begin{bmatrix}0 & 0\\0 & 0\end{bmatrix}$	$\begin{bmatrix}0 & 0\\0 & 0\end{bmatrix}$	0.05 sec	94.8145	98.6062
$\begin{bmatrix}6 & 6\\6 & 6\end{bmatrix}$	$\begin{bmatrix}5 & 5\\5 & 5\end{bmatrix}$	$\begin{bmatrix}5 & 5\\5 & 5\end{bmatrix}$	$\begin{bmatrix}0 & 0\\0 & 0\end{bmatrix}$	0.05 sec	95.2740	98.6837

Table 8.2: Fit Criterion for different ARMAX model orders

The grey shaded row reveals the optimum combination of the order and the sampling frequency among the ones that have been tested. The graphs for the comparison between the validation data and the identified ARMAX output are the following:

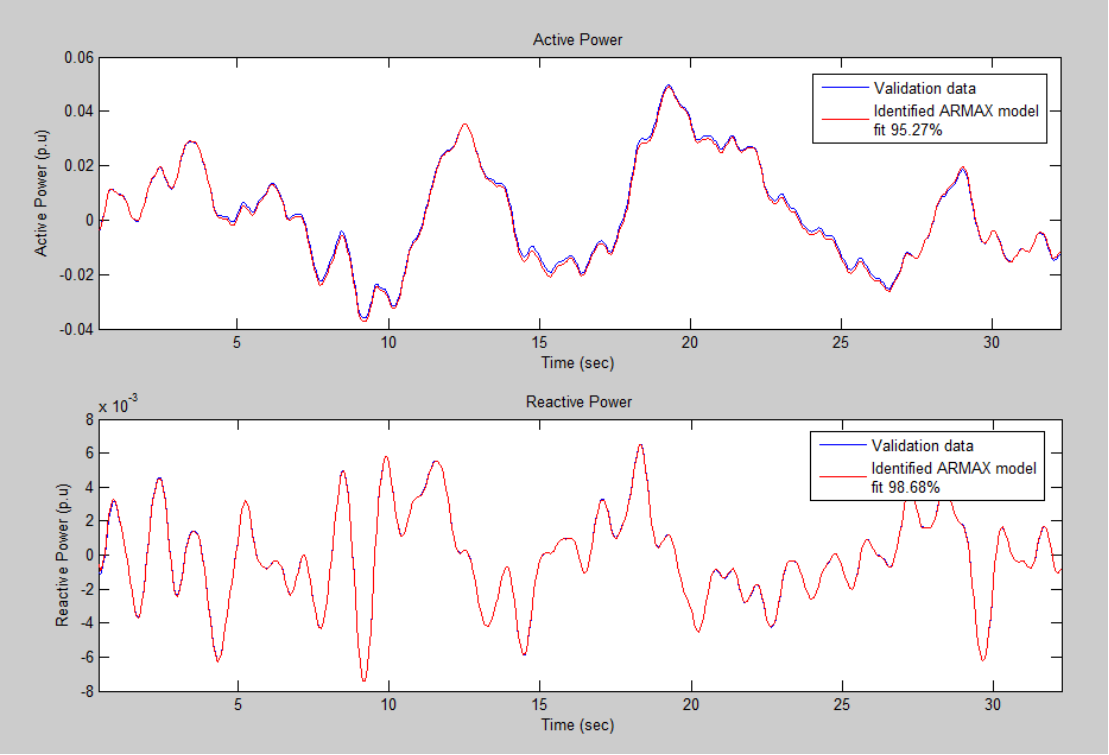

Figure 8.9: Comparison between the output of the original model and the ARMAX transfer function model

8.4 Implementation of ARX and ARMAX for Data with Measurement Noise

White Gaussian noise is added to the output signals as measurement noise with a Signal to Noise Ratio equal to 15 dB.

$$SNR = 20 * \log_{10}(mean(y^2)/mean(redidual_{noise}{}^2)) \quad (8.5)$$

where

$$residual_{noise} = signal - signal_{with\_noise} \quad (8.6)$$

The output signals with 15 dB SNR are shown in Fig.

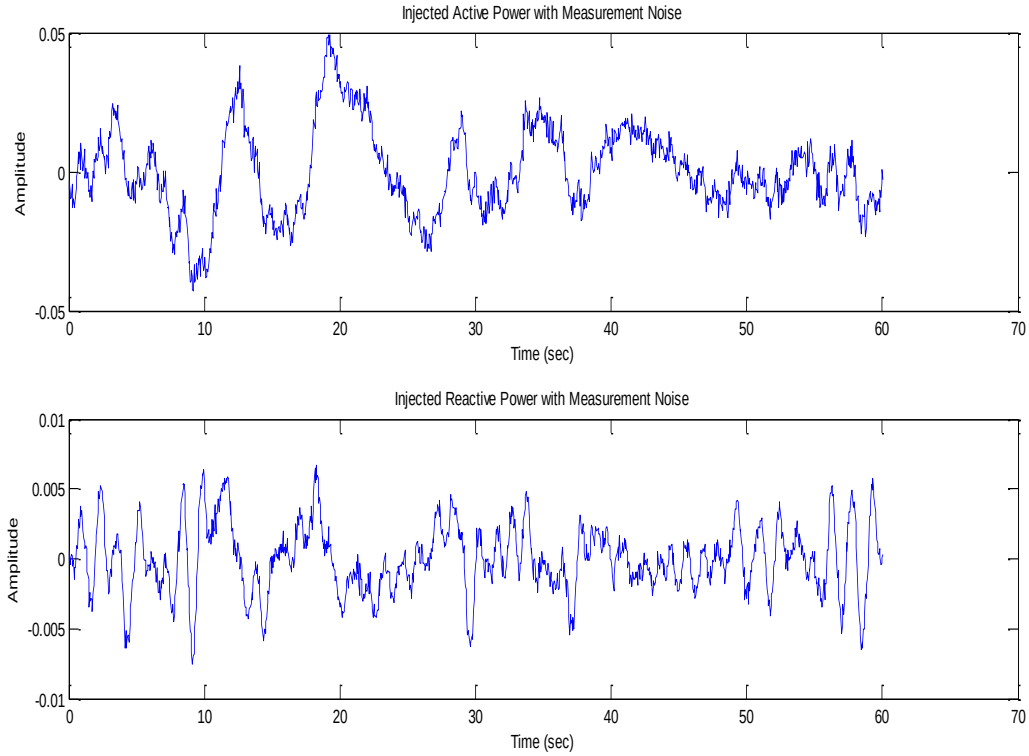

Figure 8.10: Detrended Output Signals with Measurement Noise

ARMAX and ARX are applied and the optimum combination of orders and sampling frequencies for ARX and ARMAX are summarized in Tables and respectively:

n_a	n_b	n_k	Sampling Time	Fit Criterion for Active Power	Fit Criterion for Reactive Power
$\begin{bmatrix} 6 & 6 \\ 6 & 6 \end{bmatrix}$	$\begin{bmatrix} 3 & 0 \\ 0 & 3 \end{bmatrix}$	$\begin{bmatrix} 0 & 0 \\ 0 & 0 \end{bmatrix}$	0.056 sec	83.2588	82.5115
$\begin{bmatrix} 6 & 0 \\ 0 & 6 \end{bmatrix}$	$\begin{bmatrix} 6 & 6 \\ 6 & 6 \end{bmatrix}$	$\begin{bmatrix} 0 & 0 \\ 0 & 0 \end{bmatrix}$	0.056 sec	83.1136	82.5115
$\begin{bmatrix} 6 & 6 \\ 6 & 6 \end{bmatrix}$	$\begin{bmatrix} 4 & 4 \\ 4 & 4 \end{bmatrix}$	$\begin{bmatrix} 0 & 0 \\ 0 & 0 \end{bmatrix}$	0.05 sec	84.3401	82.1431
$\begin{bmatrix} 6 & 6 \\ 6 & 6 \end{bmatrix}$	$\begin{bmatrix} 5 & 5 \\ 5 & 5 \end{bmatrix}$	$\begin{bmatrix} 0 & 0 \\ 0 & 0 \end{bmatrix}$	0.05 sec	84.0271	82.5755
$\begin{bmatrix} 6 & 6 \\ 6 & 6 \end{bmatrix}$	$\begin{bmatrix} 4 & 4 \\ 4 & 4 \end{bmatrix}$	$\begin{bmatrix} 0 & 0 \\ 0 & 0 \end{bmatrix}$	0.056 sec	84.9843	83.2941

Table 8.3: Fit Criterion for different ARX model orders with Measurement Noise

n_a	n_b	n_c	n_k	Sampling Time	Fit Criterion for Active Power	Fit Criterion for Reactive Power
$\begin{bmatrix}6 & 0\\0 & 6\end{bmatrix}$	$\begin{bmatrix}5 & 0\\0 & 5\end{bmatrix}$	$\begin{bmatrix}2 & 2\\2 & 2\end{bmatrix}$	$\begin{bmatrix}0 & 0\\0 & 0\end{bmatrix}$	0.056 sec	84.8426	89.8360
$\begin{bmatrix}6 & 6\\6 & 6\end{bmatrix}$	$\begin{bmatrix}4 & 4\\4 & 4\end{bmatrix}$	$\begin{bmatrix}5 & 5\\5 & 5\end{bmatrix}$	$\begin{bmatrix}0 & 0\\0 & 0\end{bmatrix}$	0.056 sec	84.9048	88.9627
$\begin{bmatrix}5 & 0\\0 & 5\end{bmatrix}$	$\begin{bmatrix}2 & 2\\2 & 2\end{bmatrix}$	$\begin{bmatrix}4 & 4\\4 & 4\end{bmatrix}$	$\begin{bmatrix}0 & 0\\0 & 0\end{bmatrix}$	0.056 sec	84.1069	90.4236
$\begin{bmatrix}5 & 0\\0 & 5\end{bmatrix}$	$\begin{bmatrix}2 & 2\\2 & 2\end{bmatrix}$	$\begin{bmatrix}4 & 4\\4 & 4\end{bmatrix}$	$\begin{bmatrix}0 & 0\\0 & 0\end{bmatrix}$	0.05 sec	84.9240	89.7526
$\begin{bmatrix}6 & 6\\6 & 6\end{bmatrix}$	$\begin{bmatrix}4 & 4\\4 & 4\end{bmatrix}$	$\begin{bmatrix}4 & 4\\4 & 4\end{bmatrix}$	$\begin{bmatrix}0 & 0\\0 & 0\end{bmatrix}$	0.05 sec	85.7396	88.9619

Table 8.4: Fit Criterion for different ARMAX model orders with Measurement Noise

The results of the experiments that maximized the Fit Criterion for ARX method are shown below:

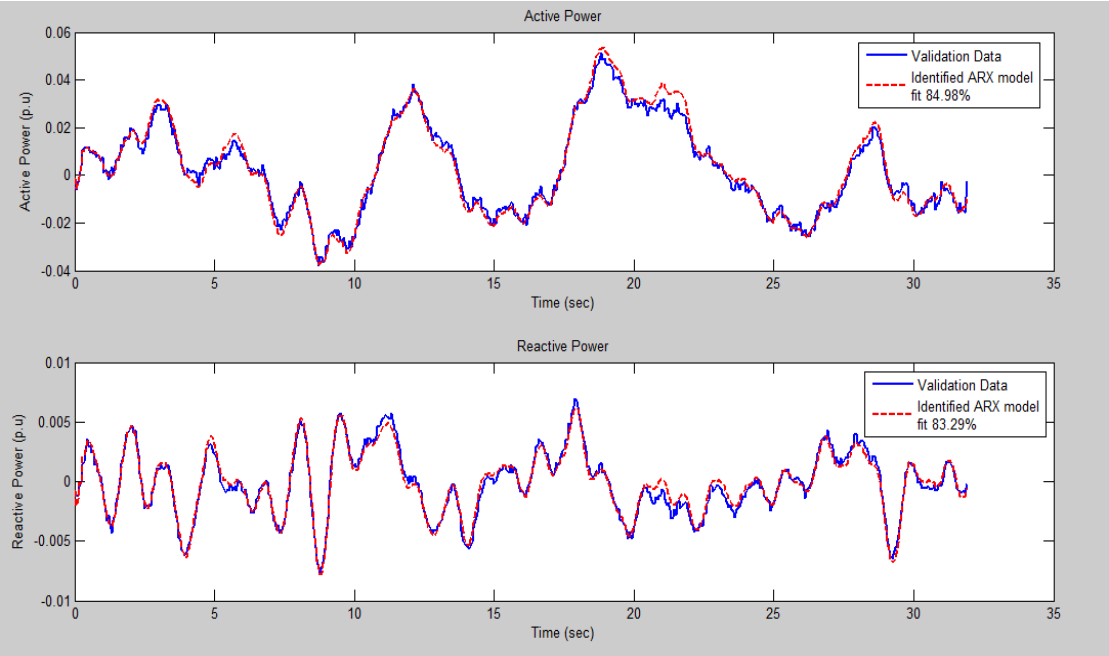

Figure 8.11: Comparison between model with noise and the ARX transfer function model

The results of the experiments that maximized the Fit Criterion for ARMAX method are shown in Fig:

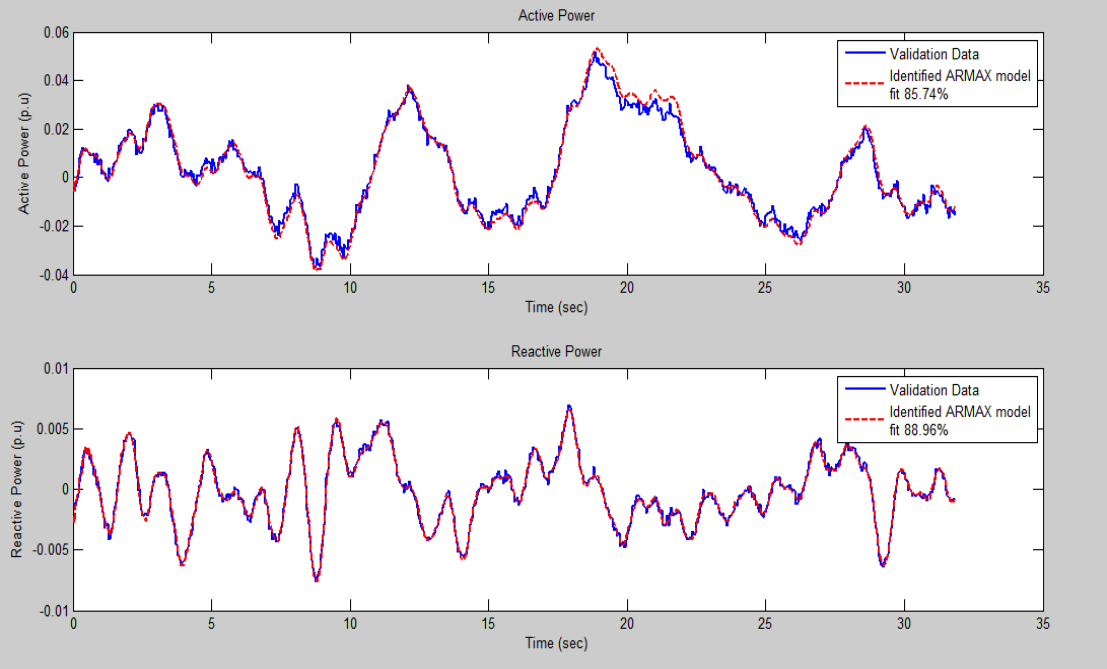

Figure 8.12: Comparison between model with noise and the ARMAX transfer function model

Except for Fitness Criterion in that case an additional indicator of the model quality is going to be applied as a final step of validation process. This indicator is known as residual test.

A residual i.e. prediction error is defined as the difference between measured data and the estimation of the identification algorithm:

$$residual = y - \hat{y} \quad (8.7)$$

The residuals correspond to the portion of the measurement data that could not be explained by the identified model. According to the residual analysis [18], an identified model is characterized as good when:

- The residuals are relatively small compared to the measurement data.
- The residuals are close to white noise signal. At that point it is important to mention that the white noise has a flat power spectrum and therefore one possible way to check the "whiteness" of the residuals is to observe their power spectrum.

The residuals for active and reactive powers overlaid with the measurements for both ARX and ARMAX methods are shown in the next Fig:

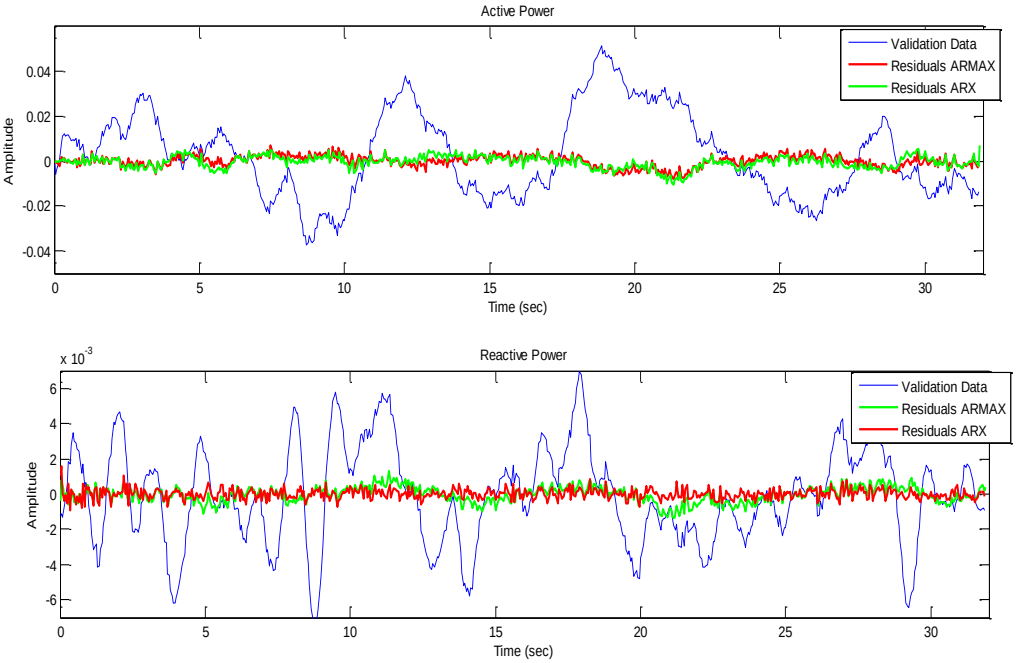

Figure 8.13:Comparison between ARX, ARMAX residuals and Validation Data

The power spectrum for residuals derived from the application of ARX and ARMAX methods are shown in Fig. (8.14):

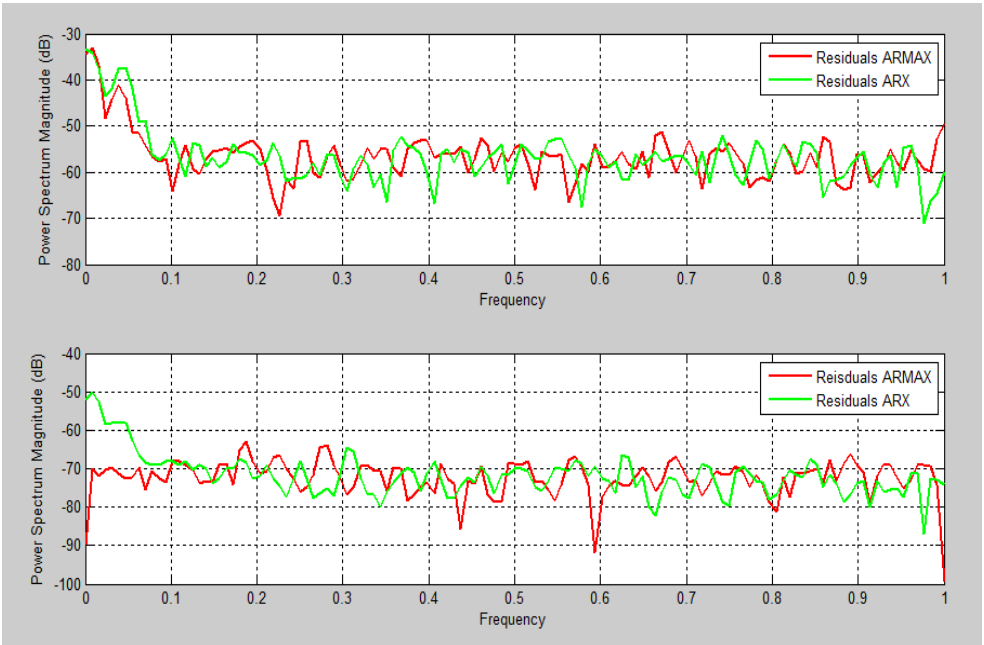

Figure 8.14: Residuals of ARX and ARMAX methods for active and reactive powers

8.5 Implementation of Eigensystem Realization Algorithm

8.5.1 Data without Measurement Noise

As it has been mentioned in previous chapters, the ERA method is applicable on transient data, therefore in order to receive the suitable response, a three-phase fault is being introduced at 13.8kV at the Bus 11. This fault occurs at $t_f = 1$ sec and is cleared at $t_c = 1.2$ sec.

The injected active and reactive power at Bus 01 is being conceptualized as the impulse response of the MIMO Output Wind Farm system in order to extract the A, B, C, D matrices of the state space representation by using the markov parameters.

The signals that are used as input for the identification process are shown below:

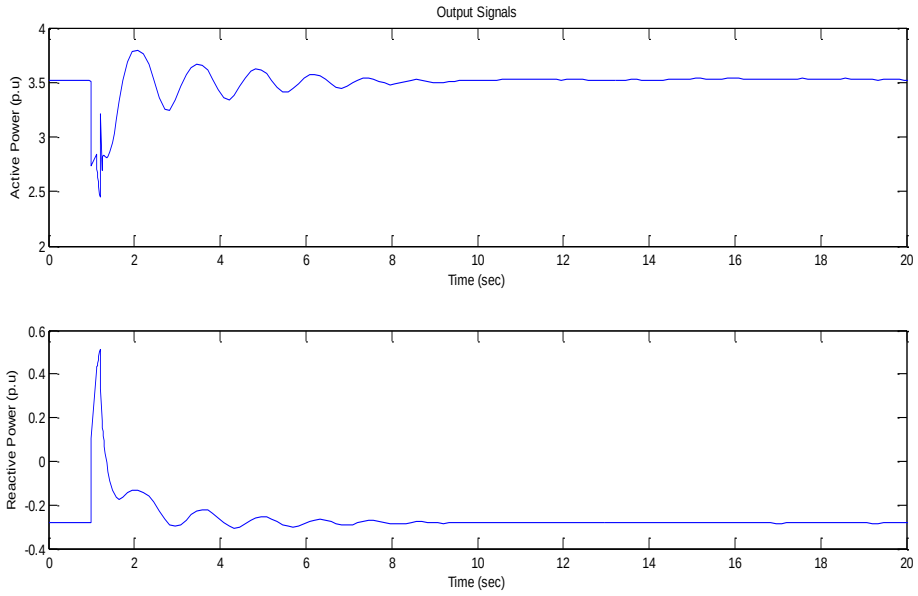

Figure 8.15: Injected Active and Reactive Power at Bus 01

At that point, the output data are detrended and a proper data window that contains the transient part in order to apply ERA has to be selected. The size of the data window that produces the best estimates is $[2\,,\ 10.3\,]$ sec and as a result the pre-processed data is shown in the next figure:

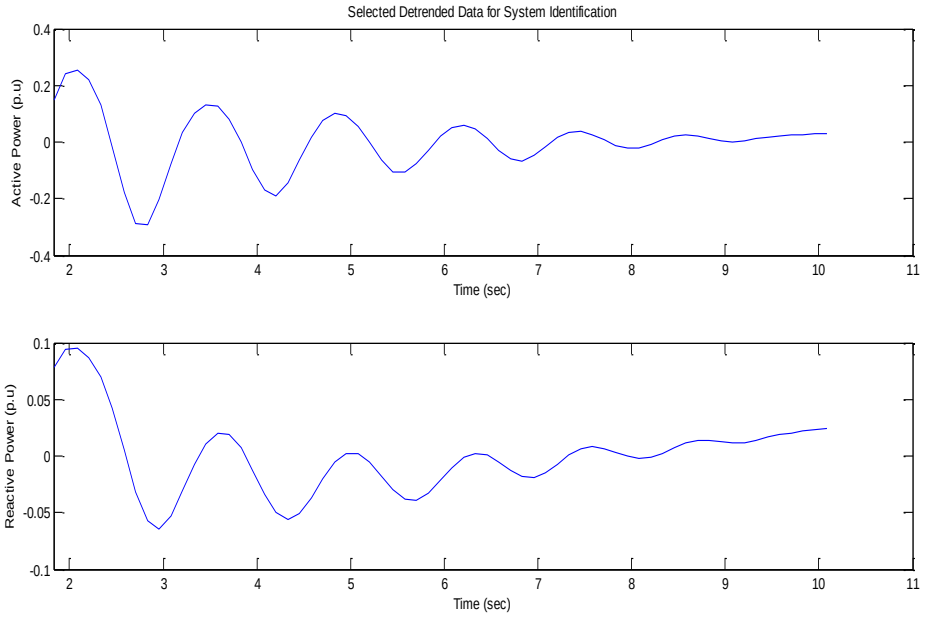

Figure 8.16: Selected detrended data for system identification

The output vector y that we use for the construction of the Hankel matrices is of size 67x2.

$$y = [(\{y_1|y_2\})] = \begin{bmatrix} 0.3121 & 0.1136 \\ 0.2720 & 0.1047 \\ \vdots & \vdots \\ 0.0058 & 0.0188 \end{bmatrix} \quad (8.8)$$

The Hankel matrices H_0, H_1 are of size 33x67 and they are computed:

$$H_0 = \begin{bmatrix} Y_1 & \cdots & Y_{33} \\ \vdots & \ddots & \vdots \\ Y_{33} & \dots & Y_{65} \end{bmatrix} = \begin{bmatrix} [0.2744 & 0.1043] & \dots & [-0.0152 & -0.0071] \\ \vdots & & \ddots & \vdots & \\ [-0.0152 & -0.0071] & \dots & [0.0140 & 0.0177] \end{bmatrix} \quad (8.9)$$

$$H_1 = \begin{bmatrix} Y_2 & \cdots & Y_{34} \\ \vdots & \ddots & \vdots \\ Y_{34} & \dots & Y_{66} \end{bmatrix} = \begin{bmatrix} [0.1614 & 0.0835] & \dots & [-0.0440 & -0.0134] \\ \vdots & & \ddots & \vdots & \\ [-0.0440 & -0.0134] & \dots & [0.0152 & 0.0190] \end{bmatrix} \quad (8.10)$$

where

$$\left.\begin{aligned} Y_0 &= [0.3117 \quad 0.1128] \\ Y_1 &= [0.2744 \quad 0.1043] \\ Y_2 &= [0.1614 \quad 0.0835] \\ &\vdots \\ Y_{66} &= [0.0152 \quad 0.0190] \end{aligned}\right\} \text{(8.11)}$$

The markov parameters can be computed from the matrices $Y_i,\ i \in [0, 66]$:

Let the Markov parameters $\beta_0^{(i)}$:

$$\left.\begin{aligned} Y_0 &= D = \beta_0 \\ Y_1 &= CB = \beta_0^{(1)} \\ Y_2 &= CAB = \beta_0^{(2)} \\ &\vdots \\ Y_{66} &= CA^{65}B = \beta_0^{(66)} \end{aligned}\right\} \text{(8.12)}$$

The computation of these parameters is really important given that they are used to form the Hankel matrices H_0, H_1. Besides that from the markov parameters and after performing the Singular Value Decomposition for H_0, the Controllability and Observability matrices can be obtained:

$$\begin{bmatrix} CB & CAB & \cdots & CA^{33}B \\ CAB & CA^2B & \cdots & CA^{34}B \\ \vdots & \ddots & \ddots & \vdots \\ CA^{33}B & CA^{34}B & \dots & CA^{65}B \end{bmatrix} = H_0 => \begin{bmatrix} C \\ CA \\ CA^2 \\ \vdots \\ CA^{33} \end{bmatrix} [B \quad AB \quad A^2B \quad \cdots \quad A^{33}B] = H_0$$

$$=>\ H_0 = O_p C_q \quad \text{(8.13)}$$

Finally, using eq. (8.10) and (5.60):

$$H_0 = O_p C_q = U_n \Sigma_n {V_n}^T => \begin{cases} O_p = U_n {\Sigma_n}^{1/2} \\ C_q = {\Sigma_n}^{1/2} {V_n}^T \end{cases} \quad \text{(8.14)}$$

Where,

Controllability matrix $\mathrm{O_p} = \begin{bmatrix} C \\ CA \\ CA^2 \\ \vdots \\ CA^{33} \end{bmatrix}$

and

Observability matrix $C_q = [B \quad AB \quad A^2B \quad \cdots \quad A^{33}B]$

These two concepts are crucial in systems theory. Controllability is concerned with whether it is possible to design a control input to steer the state to arbitrarily values, while observability is concerned with whether it is feasible to determine the state of the system without knowing its initial state.

By implementing the procedure described in Chapter 5.6 into Matlab, the matrices A, B, C, D of the discrete time model (4.2) under identification are extracted.

The modes of the system along with their natural frequency, frequency, damping ratio, residue and energy are shown in Table 8.5:

mode	Nfreq(rad/s)	freq(Hz)	Damp	residue	energy
1	4.9806	0.7832	0.1543	1.2500	0.4189
2	4.9806	0.7832	0.1543	1.2500	0.4189
3	0.7980	0.0000	1.0000	0.6487	0.6911
4	0.3132	0.0000	1.0000	0.5243	1.6509
5	5.6833	0.9023	0.0706	0.3714	0.6976
6	5.6833	0.9023	0.0706	0.3714	0.6976
7	10.2087	1.6112	0. 1291	0.1783	0.2652
8	10.2087	1.6112	0. 1291	0.1783	0.2652
9	2.1902	0.3377	0. 2483	0.0577	0.6356
10	2.1902	0.3377	0. 2483	0.0577	0.6356
11	10.9516	1.7380	0. 0758	0.0361	0.3706
12	10.9516	1.7380	0. 0758	0.0361	0.3706
13	6.8182	1.0842	0. 0408	0.0302	0.9581
14	6.8182	0.0000	0. 0408	0.0302	0.9581
15	0.2548	2.3931	-1.0000	0.0191	133.7743
16	15.1671	2.3931	0.1309	0.0191	0.1989
17	15.1671	2.1454	0.1309	0.0128	0.1989
18	13.5000	2.1454	0.0542	0.0128	0.4084
19	13.5000	1.2775	0.0542	0.0034	0.4084
20	8.0293	1.2775	0.0244	0.0034	1.2954
21	8.0293	1.9571	0.0244	0.0032	1.2954
22	12.3164	1.9571	0.0562	0.0032	0.4286
23	12.3164	2.9422	0.0562	0.0026	0.4286
24	18.5458	2.9422	0.0801	0.0026	0.2396
25	18.5458	3.4419	0.0801	0.0006	0.2396

26	21.6684	3.4419	0.0627	0.0006	0.2675
27	21.6684	3.4419	0.0627	0.0002	0.2675
28	16.4028	2.6106	0.0013	0.0002	3.5604
29	16.4028	2.6106	0.0013	0.0001	3.5604
30	19.6525	3.1277	0.0069	0.0000	1.7225
31	19.6525	3.1277	0.0069	0.0000	1.7225
32	25.1349	4.0000	0.0132	0.0000	1.5690
33	25.1349	4.0000	0.0132	0.0000	1.5690

Table 8.5: Singular Values of the Identified System

This table is of great importance because it can help in determining the order of the identified system. The estimation results (modes of the state space representation) can be sorted either by their residue or by their respective energy. In the specific example we have sorted the modes by their residue so we can select the eight first modes with the highest residue.

The impulse responses of the identified model compared with the output of the original system are shown in the next graphs:

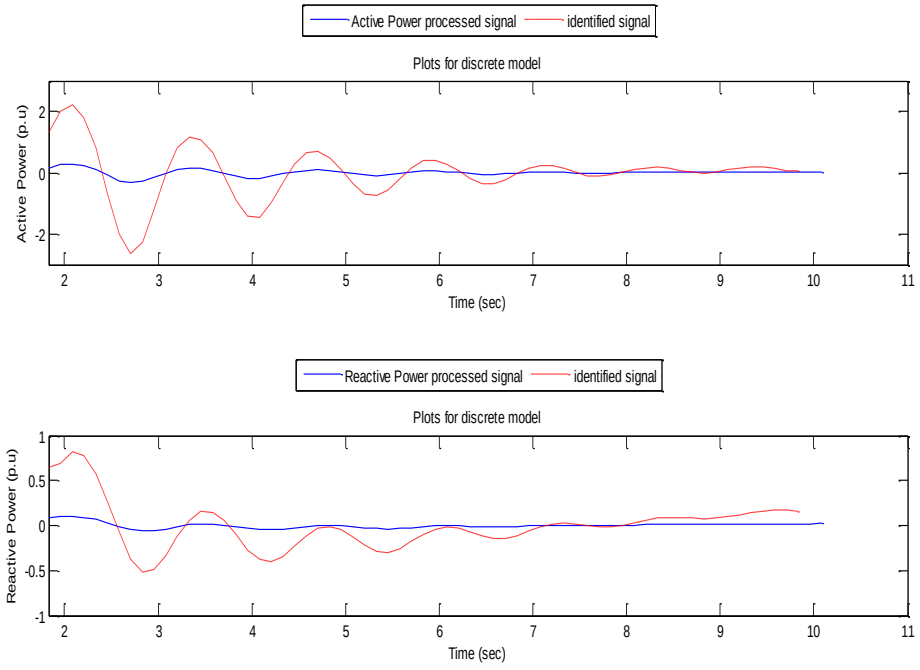

Figure 8.17: Comparison between the original and identified discrete models

The discrete time State-Space model is converted into a continuous model assuming a zero-order hold and the results are:

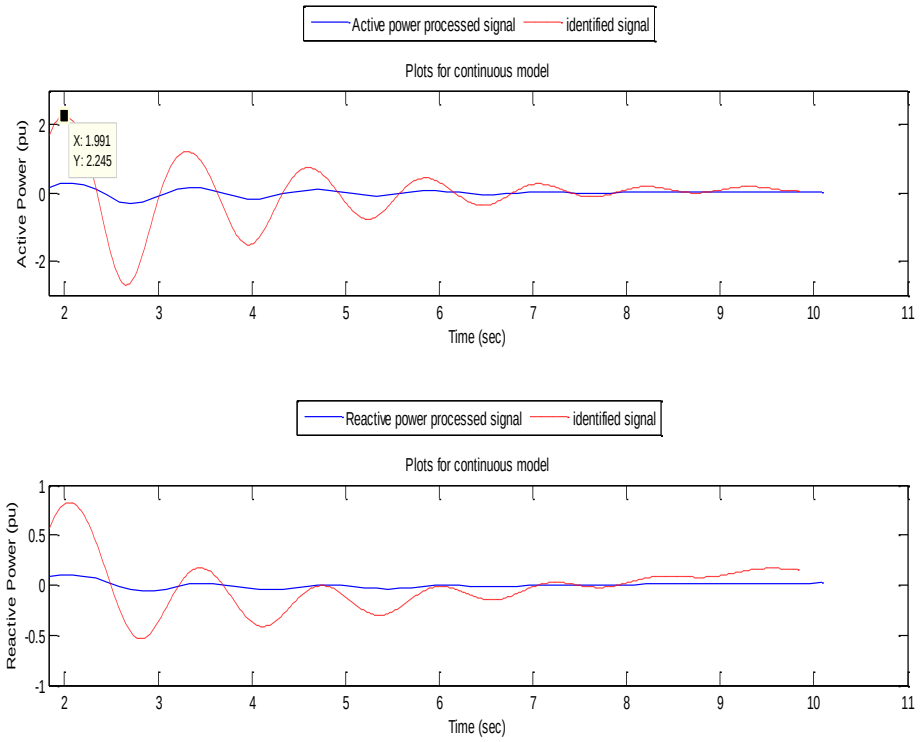

Figure 8.18: Comparison between the original and identified continuous models

From the graphs it is safe to conclude that after the conversion the new continuous identified model contains the same frequencies with the original model but obviously there is a magnitude difference between these two signals. This difference can be translated as constant Gain in the transfer function representation of the identified model. Consequently, in order to compute this gain and include it in the new continuous-time model, firstly the next steps should be followed:

- Compute the magnitude difference from the responses of the original and identified systems.
- Convert the state space identified model into a transfer function model.
- "Insert" the difference as a constant gain in the transfer function representation.
- Reconvert to state space model and plot the new responses.

The new continuous state-space model containing the constant Gain is shown in Fig. (8.19):

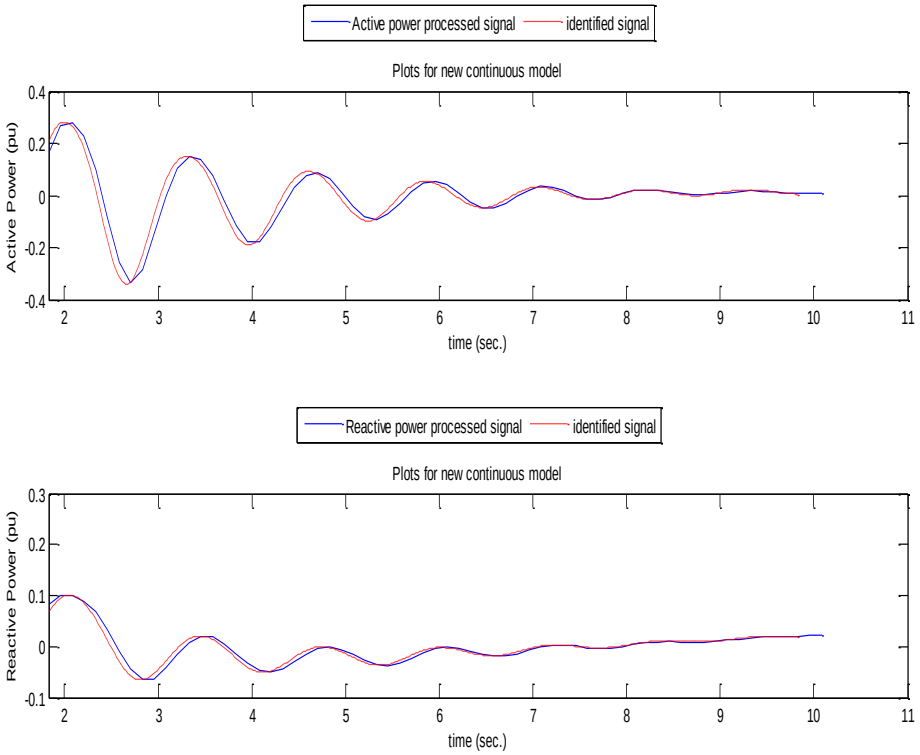

Figure 8.19: Comparison between the original and identified continuous models

After several computation of the hankel matrices, it can be safely concluded that by selecting more modes from the table above the signals under comparison tend to fit better and better. That should be totally clear given that by selecting more dominant modes (modes that decay the slowest and are closer to the imaginary axis s=0) according to their residue and/or energy from the table above the system's behavior is captured more accurately:

At this point it is important to remind that an extremely accurate model is not required in the case formulated in this thesis; instead a simplified transfer function is advisable for practical engineering purpose. A simplified transfer function renders the system easier to be understood and analyzed, and for that reason the order of the system has been chosen to be nine as a first step.

In order to double-check if there are "margins" to decrease the model order without losing much of information, the Hankel Singular Value Decomposition (HSVD) is applied.

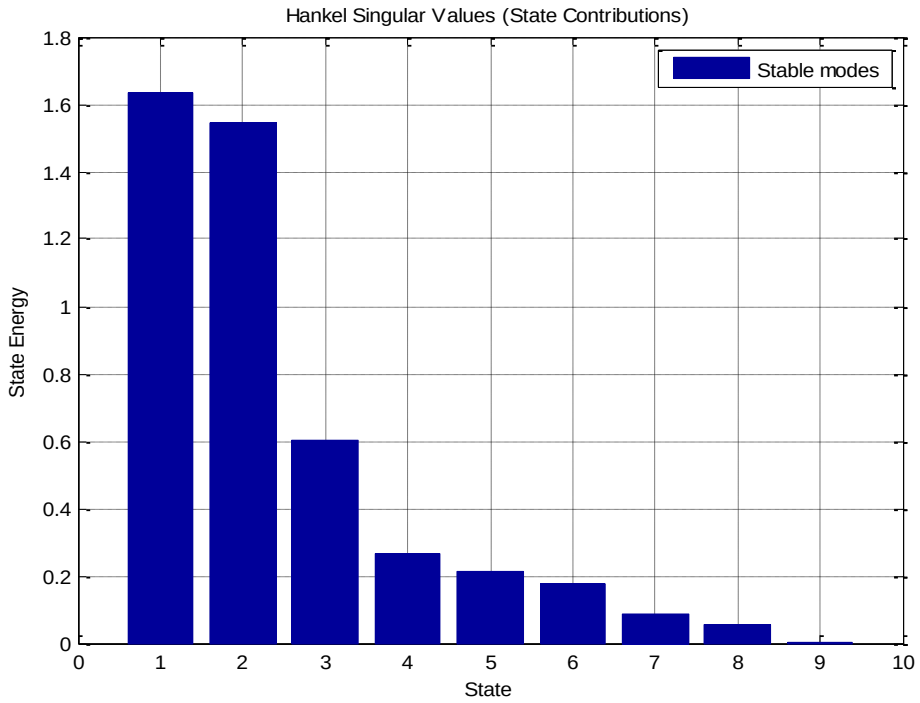

Figure 8.20: State contribution based on HSVs

In state coordinates, the hankel singular values (HSVs) measure the contribution of each state to the input/output behavior [10]. The magnitudes of the HSVs are shown above and, according to the graph, a reduction of the order of the model to six states is decided. The new plots of the output of the reduced order model comparing to the full order identified and the original model are:

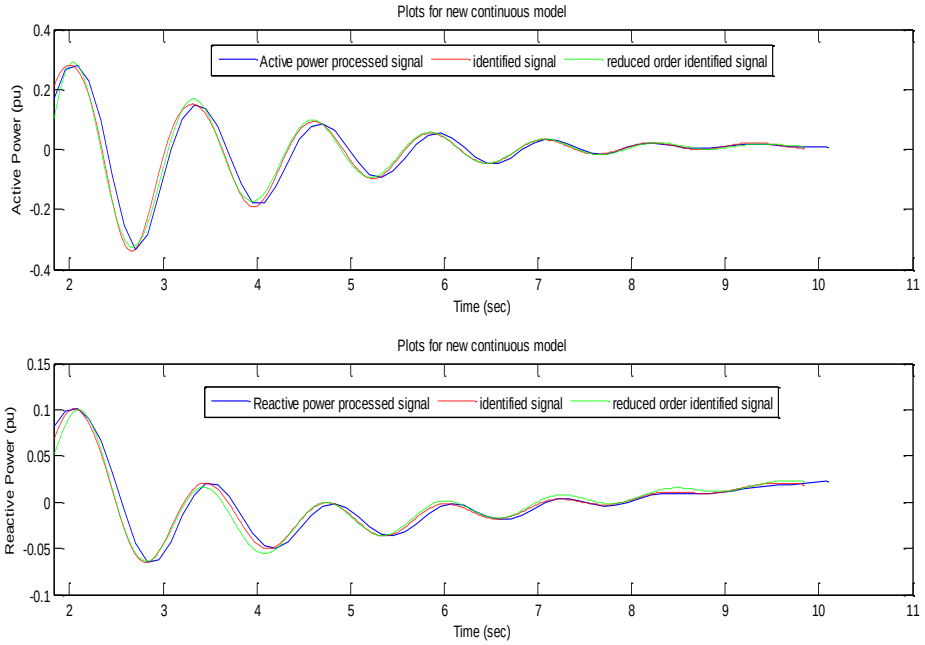

Figure 8.21: Comparison between the original, the full order and the reduced order identified continuous models.

The bode diagrams of the full order and the reduced identified are shown below:

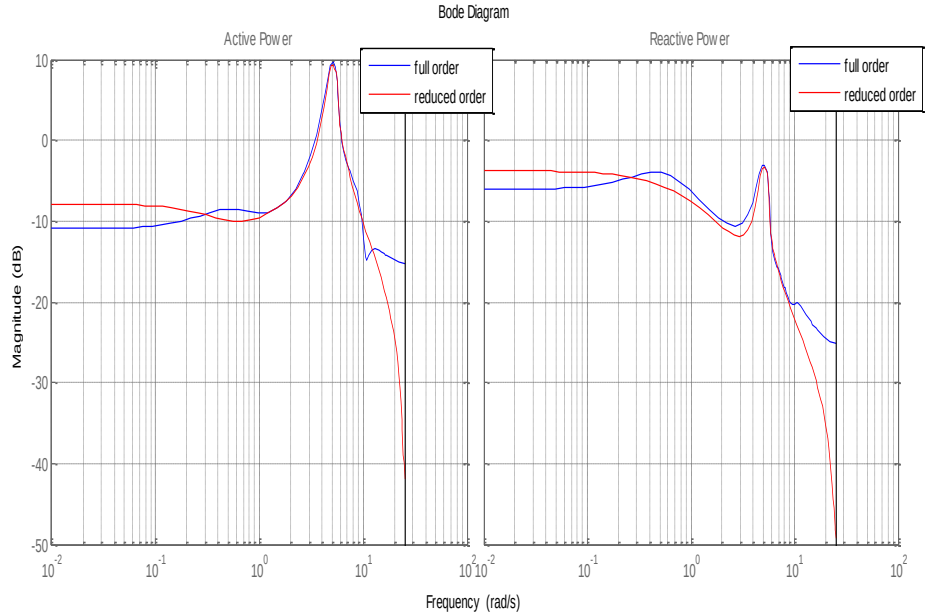

Figure 8.22: Comparison of magnitude bode diagrams between the full order identified model and the reduced order identified model.

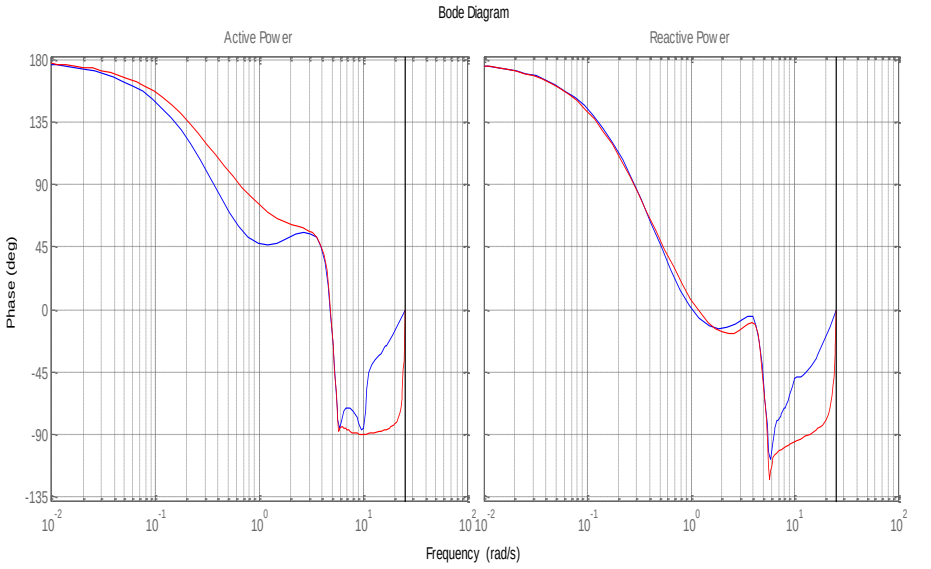

Figure 8.23: Comparison of phase bode diagrams between the full order identified model and the reduced order identified model.

An inspection on the figures regarding the system outputs as well as on the bode plot reveals that the reduction of the model did not cause significant loss of accuracy as it approximates the full order identified signal satisfactory. Therefore, the Hankel truncation can be applied to the model that is obtained from ERA.

8.5.2 Data with Measurement Noise

For that case white Gaussian noise of an SNR equal to 15 dB is added to the injected active and reactive powers measured at Bus 01 after the occurrence of the three-phase fault.

The new output signals are shown in Fig. (8.25):

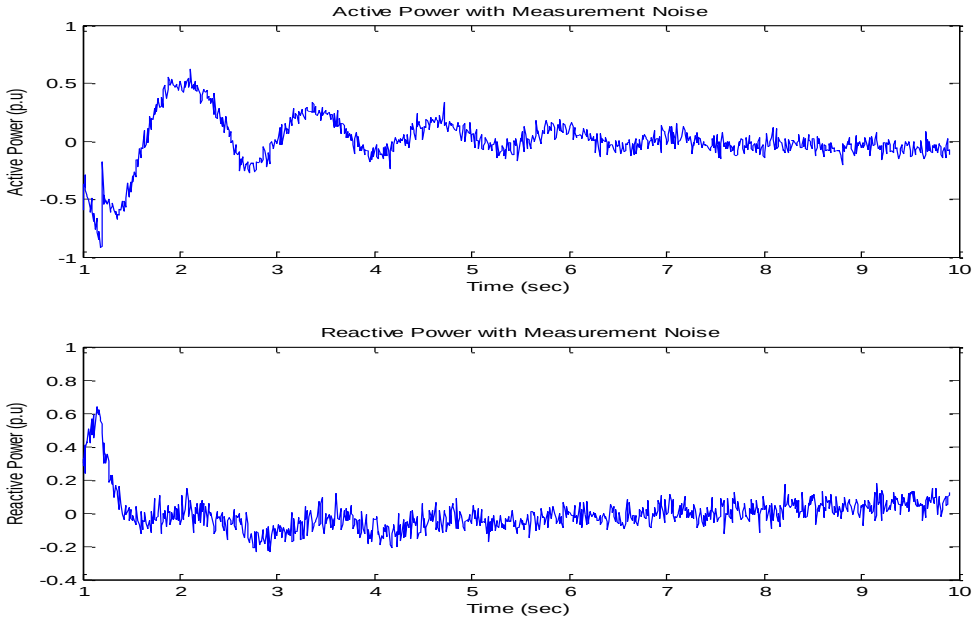

Figure 8.24: Output Signals with Measurement Noise

ERA is applied at the same way described for the case of data without noise and the new state-space model is extracted.

The same Validation data that used in ARX and ARMAX cases are going to be used for the evaluation of the efficiency of the method. The response of the identified system overlaid with the measurements present a Fitness of 66.6% for both active and reactive powers and is shown in Fig (8.25):

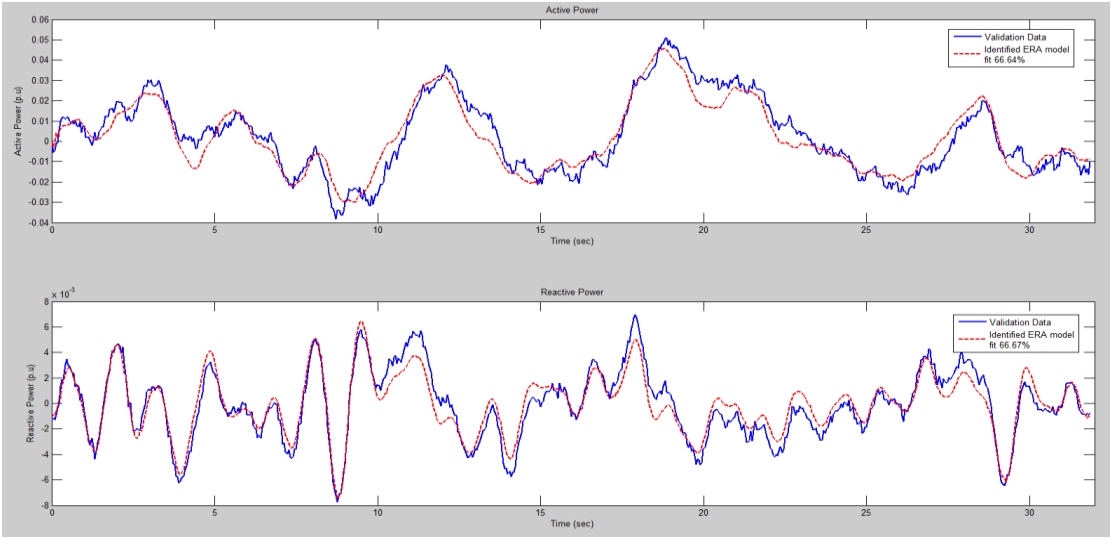

Figure 8.25: Comparison between model with noise and the ERA state-space model

The residuals of ERA compared to measurement data is shown below:

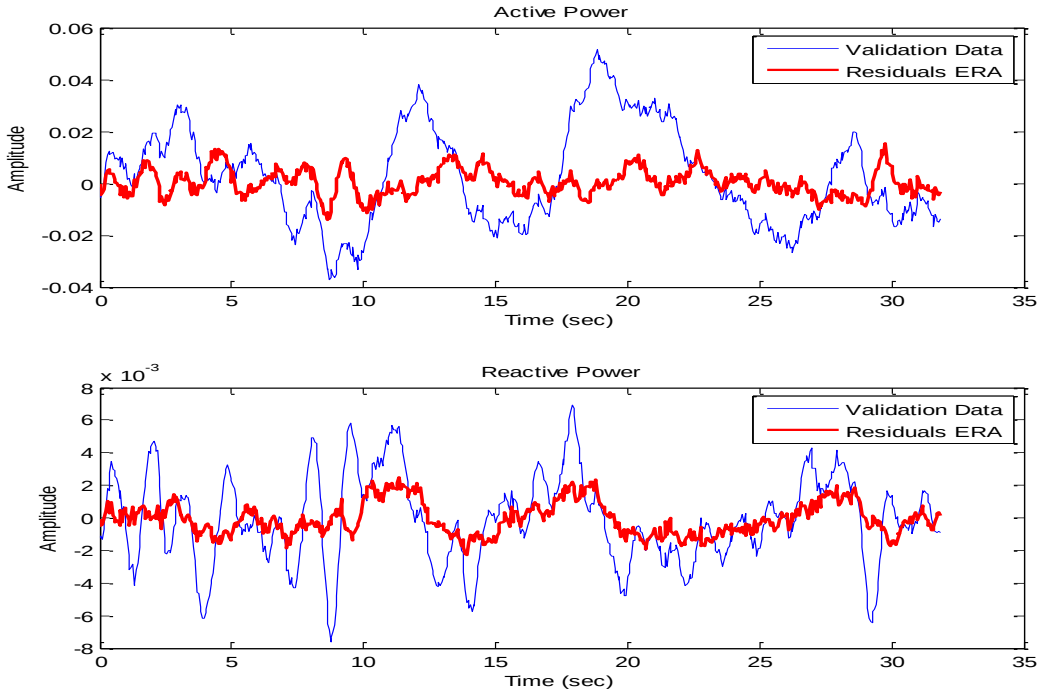

Figure 8.26: Comparison between ERA residuals and Validation Data

8.6 Conclusions

Fig. (8.8) and Fig. (8.9) reveal that the ARX and ARMAX methods capture the system dynamics very well, given that their responses to a completely new wind speed sequence present a high Fitness criterion indicator. The overall performance of ARMAX model is preferable to the ARX model in terms of fitness ability in response measured data but both modes are accurate.

On the other hand, Fig. (8.19) and Fig. (8.21) show that both the ERA full order and the reduced order state-space models encapsulate the underlying dynamics of the system.

For the case of data containing measurement noise Fig. (8.13) shows that ARMAX produces better estimates than ARX given that its residuals are smaller than those of ARX. However, the residuals for both methods are relatively small compared to measurements which is a good indicator for the efficiency of the models . Fig. (8.14) confirms the previous observation; even though the spectrum of the residuals for both ARX and ARMAX cases is not constant, it is close to white given that is reasonably flat in the band between lowest frequency and the Nyquist frequency.

Finally, from Fig. (8.26) it can be concluded that ERA produces residuals of magnitude that cannot be considered insignificant. This fact combined with the results shown in Fig. (8.25) regarding the Fit Criterion, leads to the conclusion that even though the systems main dynamics are captured, the method is not as efficient as ARX and ARMAX.

9 Conclusions and Future Work

9.1 Conclusions

Initially, a known state-space system was identified using ARX, ARMAX and ERA methods in order to illustrate in a simple and understandable way the different identification approaches and validate the efficiency of the models used. Afterwards, a wind farm consisting of 30 DFIGs was conceptualized as a MIMO model with 2 input and 2 output channels and the three aforementioned techniques were used for its identification. The black-box system identification, especially in the cases of ARX and ARMAX which use known input signals, not only identified the dominant electromechanical modes but also estimated more accurately the transfer function representation.

9.2 Future Work

Future work on the era of system identification would involve the implementation of the techniques used in this thesis for measurements collected by Phasor Measurement Units (PMUs) placed in a power grid. Modal estimation of wind farms in real power grids is significant for various reasons. First of all, it can provide valuable information regarding system security and the determination of 'at risk' conditions. Measurements are going to be selected from PMUs placed at PCC and the results of the identification will help to determine if it is necessary to design a Power System Stabilizer (PSS) for the wind farm for the system to remain in a state of operating equilibrium under normal operating conditions [17].

Besides that, the identification based on PMUs measurements will be used for the validation, calibration and at some cases replacement of the existing small signal models that are used for system planning. Simulation results must be modified and adjusted in order to account important differences between measured and simulated behavior.

9.3 Future Challenges

The implementation of the various identification methods on actual field measurements is really challenging and great emphasis should be given to the pre-processing of the time domain data for the following reasons:

- A PMU typically measures a signal at a rate of 50 samples per second (sps). In offline estimation of the models the signals have to be re-sampled at a lower rate in order to be feasible to be processed by the identification algorithms.
- Real measurements contain noise, consequently low pass-filters have to be applied in the signals in order to cut-off the high frequency components and the aliasing effect.
- Handling potential missing data. Depending on the duration of missing data, different processing methods should be applied.
- Handling potential outliers. Outliers are data that deviate significantly from normal measurements and are commonly generated by a sensor failure. These abnormalities

are more complicated than the missing data due to the fact that they are not easily detected. Model prediction errors or residual analysis has to be conducted (i.e. the difference between an observed value and the estimated value) in order to detect and handle them.

After pre-processing the measurements, the procedures can be applied in the same way as in synthetic data (data obtained from simulation software tools). Finally, MOR techniques can be used and reduced order models that represent the dynamics of interest of the renewable resources are expected to be extracted.

References

1.S Ghosh, N Senroy, "Balanced truncation based reduced order modeling of wind farm", May 2013.

2. H.A Pulgar-Painemal, P.W Sauer, "Towards a wind farm reduced-order model", March 2013.

3. L.Ljung, "System identification Theory for User", 1999.

4. IEEE Task force Report, "Identification of Electromechanical Modes in Power Systems", June 2012.

5. L.N Trefethen, D. Bau, "Numerical Linear Algebra", 1997.

6. K. Baker, "Singular Value Decomposition Tutorial", March 2005.

7. A. Hashmani,"Damping of Electromechanical Oscillation in Power Systems using Wide Area Control ", July 15 2010.

8 Aivar Soota," Model order reduction based on semidifinite programming".

9.Prabha Kundur, " Power System Stability and Control".

10. L.Shah, J.MacGregor, "Dynamics and Control of Process Sytems",5 July 2004.

11. A.Hashmani, "Damping of Electromechanical Oscillation in Power Systems using WIde Area Control",15 July 2010

12. P. Benner, E. Quintana, "Model Reduction Based on Spectral Projection Methods", April 8 2005.

13. P. Skoufanis, "Singular Value Decomposition Theory and Example", March 11 2010.

14. IEEE Task Force Report, "Identification of Electromechanical Modes in Power Systems" June 2012.

15.A.R.Messina,"Inter-area Oscillations in Power Systems, A Nonlinear and Nonstationary Perspective", 2009.

16. F. Milano, "Power System Analysis Toolbox Documentation for PSAT version 2.1.8", January 6 2013.

17. K. Sinha, P. Tapre, "Enhancement of Power System Stability using PSS in Wind Farm Distribution Generation", October 10 2013.

18. K.M Aarts, "System Identification and Parameter Estimation", 2012